NTNU – Trondheim
Norwegian University of
Science and Technology

Earthquake Analysis of Subsea Structure on Caisson Foundation using 3D Finite Element Solution

Madeleine Brandt

Civil and Environmental Engineering
Submission date: June 2014
Supervisor: Steinar Nordal, BAT
Co-supervisor: Amir Kaynia, KT
Corneliu Athanasiu, Multiconsult

Norwegian University of Science and Technology
Department of Civil and Transport Engineering

NORWEGIAN UNIVERSITY OF SCIENCE AND TECHNOLOGY
DEPARTMENT OF CIVIL AND TRANSPORT ENGINEERING

Report Title: **Earthquake Analysis of Subsea Structure on Caisson Foundation using 3D Finite Element Solution**	Date: 10.06.2014 Number of pages (incl. appendices): 193			
	Master Thesis	X	Project Work	

Name:

Madeleine Brandt

Professor in charge/supervisor:

Professor Gudmund R. Eiksund, NTNU

Other external professional contacts/supervisors:

Professor II Amir M. Kaynia, NGI/NTNU

Abstract:
One of the challenging problems in geotechnical design of caisson foundations for offshore structures is the determination of soil-structure interaction during earthquakes. In this thesis, earthquake analyses were performed on a subsea structure resting on a caisson foundation. The objective was to evaluate the soil-structure interaction, using a direct, integrated soil-structure method and a simplified, practical multi-step method. Numerical modeling was done in Plaxis 3D 2012, using two different modeling concepts, in order to investigate influence on the result from the boundary conditions. Model 1 had free vertical boundaries without viscous dampers, whereas Model 2 had viscous dampers defined together with standard fixities.

First, linear soil-structure interaction analyses were performed, where the soil behavior was modeled with a linear-elastic material model. The analyses were done for a hypothetical case proposed by Multiconsult AS, who provided soil properties, along with the geometry of foundation and structure. In order to perform the dynamic finite element analyses, however, the soil parameters had to be altered, due to the proposed material's relatively low shear wave velocity profile. Using this profile would require too much calculation time and computer capacity, which was not available, because of the requirements for mesh refinement. With the adjusted soil profile, direct analysis yielded results showing only minor soil-structure interaction. It is likely that by using the original, softer soil profile, more significant effects from soil-structure interaction would be obtained. The multi-step method yielded 30-60% higher maximum response of the superstructure than the direct method, depending on the initial choice of modeling concept.

Model 1, with lateral boundaries free in the horizontal direction, without the use of viscous dampers, was found to be the most adequate modeling concept. These conditions will, however, not enable absorption of incoming stress waves generated by the vibrating caisson foundation. Default settings for dynamic analyses in Plaxis 3D, corresponding to Model 2, were found to yield erratic results, and are thus not recommended for seismic analyses.

A non-linear analysis using the direct method was also performed, in order to investigate possible material and geometric non-linearities. The Mohr-Coulomb material model was implemented, to allow plastic deformations in the soil. Results show that gapping will occur between the top of the foundation and the soil. The difference in response in the non-linear analysis compared to the linear analysis, is negligible for this case. It is reasonable to assume that more significant differences would be experienced using the original soil profile.

Dynamic modeling in finite element programs is not straightforward, and require sufficient knowledge about the various considerations that must be made. The computational time is very long, and the analysis requires computers with relatively high capacities, regarding both disk-space and RAM. Non-linear analysis further increase the demand for capacity and calculation time. The multi-step analysis generally takes less time; however, this depends on the selected approach in dealing with the various steps of the analysis.

Keywords:

1. Geotechnical earthquake analysis
2. Suction caisson foundation
3. Soil-structure interaction
4. PLAXIS

Preface

This report is written as a Master Thesis at the Norwegian University of Science and Technology as part of the MSc in Civil and Environmental Engineering. It is written over a period of 20 week during the spring semester of 2014, and represents the completion of a 5 year study program. The thesis is an analytical report, containing finite element analyses in Plaxis 3D.

During a course in structural dynamics in the spring of 2013, my interest for the field of dynamics grew. In a combination with geotechnical engineering, it proved even more interesting, and a course in geodynamics during the fall of 2013 further expanded my curiosity. A Master Thesis within this field, was therefore desirable.

The idea of using earthquake design of offshore caisson foundations as a subject for my thesis, was brought too me in the beginning of 2014 by Corneliu Athanasiu and Steffen Giese at Multiconsult AS.

A lot of time has been spent frustrating over Plaxis 3D, particularly because of uncooperative versions of the software. This has influenced the available time for focusing on the other tasks.

Trondheim, 2014-06-10

Madeleine Brandt

Acknowledgments

I would like to give a special thanks to the following persons for their help during the process:

Amir M. Kaynia, my main supervisor, for being a great motivator and giving valuable academic support, even outside office hours.

Gudmund R. Eiksund, my supervisor, for always having an open door and welcoming questions. He has given me very useful input on the numerical 3D model in Plaxis, and has been helpful with finding relevant literature.

Multiconsult AS, for the interesting idea to the subject, along with parameters for the case study. I am very grateful they let me borrow a powerful computer, which proved to be essential for performing numerical analyses. I would especially like to thank Steffen Giese, who has been very helpful with finding relevant sources of literature and arranging the loan of computer. Gratitude is also directed at Corneliu Athanasiu, for providing interesting literature, along with the initial idea of a subject about earthquake response of suction caissons.

Steinar Nordal, for helpful advice along the way.

Friends and family, and especially my boyfriend Vegard, who have always said the right words when I've needed help and support.

Last, but not least, huge gratitude is directed to the co-students at my office. We have shared a lot of joy, laughs and heaps of frustration. The work with this master thesis would not have been the same without them around, with the unlimited access to both hugs and invaluable academic support.

M.B.

Abstract

One of the challenging problems in geotechnical design of caisson foundations for offshore structures is the determination of soil-structure interaction during earthquakes. In this Master Thesis, earthquake analyses have been performed on a subsea structure resting on a suction caisson foundation. The objective was to evaluate soil-structure interaction using a *direct*, integrated soil-structure method and a simplified, practical *multi-step* method. Numerical modeling was done in Plaxis 3D 2012, using two different modeling concepts, in order to investigate influence on the result from the boundary conditions. Model 1 had free vertical boundaries without viscous dampers, whereas Model 2 had viscous dampers defined together with standard fixities.

The analyses were performed for a hypothetical case proposed by Multiconsult, who provided soil properties, along with the geometry of foundation and structure. In order to perform the dynamic finite element analyses, however, the soil parameters had to be altered. This was due to the proposed material's relatively low shear wave velocity profile. Using this profile would demand too much calculation time and computer capacity, which was not available, because of the requirements for mesh refinement. Using the adjusted soil profile, the direct analysis yielded results showing that the structure will accelerate with the same frequency as the free-field. However, the amplitude was slightly lower. Thus only minor soil-structure interaction was noted, where the introduction of the structure resulted in a slight *de-amplification* of the response, compared to free-field motion. The multi-step method yielded 30-60% higher maximum response of the superstructure than the direct method, depending on the initial choice of

modeling concept, indicating that the analysis might be too simplified. With a slightly more sophisticated approach to the multi-step analysis, particularly regarding Step 3, the slight de-amplification could be captured also here. However, with the low natural periods of the system, Step 3 was not able to yield a lower value for the maximum acceleration than the free-field response, with the use of a response spectrum.

Evaluation of the free-field response from Plaxis 3D was performed using the program Equivalent-linear Earthquake Response Analysis (EERA). Results from response spectrum analysis show that Model 1 corresponds well to the EERA result, and succeeds better in following the response pattern in EERA than Model 2. However, the overall response using Model 1 is overestimated compared to EERA. Model 1 amplifies more of the low frequency signals in the earthquake, corresponding to the soil layer's fundamental frequency. Model 2 does not amplify these signals as much, and rather amplifies the somewhat higher frequencies around the soil layer's $2^n d$ natural frequency. In general, the frequency content of the two model's response is relatively different. The reason for this is the boundary conditions, being the only thing separating the two. In Model 2, the boundaries seem to generate artificial stress waves, in an attempt to repress the input shear wave motion. The nature of the vertically propagating SH-wave indicates, namely, that the wave will attempt to move the particles at the boundaries horizontally. This might thus result in a counterforce from the viscous dampers, trying to resist the displacement. Stress waves might be generated and propagate back in to the system, which will distort the result. If this is the case, Model 2 is obviously not applicable for earthquake analyses.

In this thesis, the response of the structure in the multi-step analysis was found by calculating the eigenfrequencies of the structure. Certain simplifications and assumptions were made. First of all, static stiffness was used in the multi-step analysis to simplify the problem. This is an approximation, however, commonly practiced for preliminary analysis in some cases for a low frequency range. Secondly, the maximum response was found from a response spectrum approach, instead of modeling the structure on springs in a dynamic finite element analysis. The main reason for this is that Plaxis 3D is not useful for structural modeling. A different finite

element program would have to be used. This was considered unnecessary because part of the intention with the multi-step approach was to perform the various steps by simple tools.

It would be possible to implement the frequency-dependent analytical methods by considering the impedance function's variation with frequency. However, this would have to be performed in the frequency domain using the Fourier transform technique, excluding the possibility of non-linear calculations. Closed-form solutions for foundation impedance must be used with caution for foundations with intermediate embedment-to-width ratio, such as suction caissons. These solutions have their validity limits, being developed through parametric studies, and calibrated through numerical analyses for certain geometries. Simple physical models, using lumped parameters with frequency-independent stiffness (see for example Wolf (1995)), could alternatively be used in the time-domain for a more site-specific analysis.

A non-linear analysis using direct method was performed, in order to investigate the local non-linearities. The Mohr-Coulomb material model was implemented, to allow plastic deformation of the soil. Results show that gapping will occur between the top of the foundation and the soil. The difference in response in the non-linear analysis compared to the linear analysis, is negligible in this specific case. It is reasonable to assume that more significant differences would be experienced using the original, softer soil profile.

Dynamic modeling in finite element programs is not straightforward, and require sufficient knowledge about the various considerations that must be made. The computational time is very long, and the analysis requires computers with relatively high capacities, both regarding disk-space and RAM. Non-linear analysis further increase the demand for capacity and calculation time. The multi-step analysis generally takes less time; however, this depends on the selected approach in dealing with the various steps of the analysis.

An apparent next step for this thesis would, first of all, be to use the original soil profile for similar SSI analyses. It is expected that the softer soil will yield more significant SSI effects. Next, it would be interesting to

use more sophisticated methods in the multi-step analysis. This includes accounting for the frequency-dependence of the foundation impedances, for example through the use of approximate, calibrated lumped-parameter models.

Contents

Chapter 1

Introduction

1.1 Background and Previous Research

A suction caisson is a type of embedded, offshore foundation. It is a hollow, open-ended cylindrical structure with a closed top, like a bucket turned up-side-down (see Figure 1.1). The foundation is penetrated into the soil by a combination of self-weight and suction induced by pumping water out of the caisson (see Figure 1.2). First, the caisson is lowered down onto the seabed (1), and partially penetrated because of gravity (2). Secondly, the water inside the caisson is pumped out through valves to create a differential pressure (3) which will lead to further penetration of the caisson (4) (see for example Aubeny et al. (2001)).

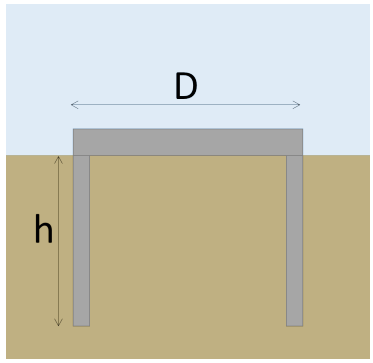

Figure 1.1: *Example of Suction caisson geometry.*

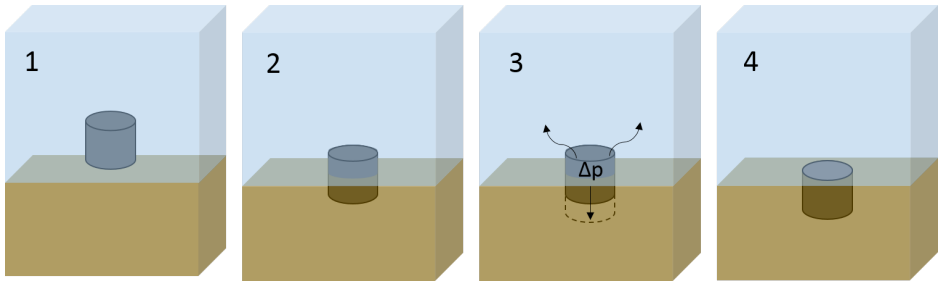

Figure 1.2: *Installation of suction caisson.*

Applications

For a complete history of the suction caisson foundation concept, the reader is referred to Tjelta (2001), who mention that the foundation type was introduced to the offshore industry in the early 1980's. After a somewhat bad first impression, the concept was first given a real chance in the 1990's. With the development of gravity-base structures (GBS) for soft soils, the suction caisson was shown to be a feasible foundation alternative. The concept was soon extended to other areas of application as anchoring of floating production, storage and offloading (FPSO) units, seabed manifolds and jack-up platforms NGI (2011).

Tjelta (2001) emphasizes the suction caisson's significant position in todays offshore oil industry, being the preferred foundation concept in some of the biggest development areas. The adaptability of the caisson foundation to various soil conditions and water depths, along with the relatively low costs and high efficiency regarding installation makes it a preferable choice in many projects. In the last decade, a lot of focus has been directed at using suction caissons as foundations for offshore wind turbines. Relevant research consist of Byrne et al. (2001), Ibsen et al. (2006), Houlsby et al. (2005) and Houlsby & Byrne (2000), to mention a few.

One of the challenging problems in geotechnical design of suction caisson foundations for offshore structures is the determination of earthquake loads that the structure and the foundation-soil system must carry with the required safety and displacements within allowable limits. Depending on the soil conditions and properties and also on site seismicity, the

stiffness of the soil response to caisson movements must sometimes be included in the analyses for a realistic design. The database of suction caisson performance under seismic loading is small, and the knowledge about the dynamic behavior of such foundations is limited.

Previous Research

A lot of focus has been directed at developing methods for considering seismic response of foundations. However, most of the research is not related to developing solutions for suction caissons in particular. As discussed in Varun et al. (2009), common design methods for evaluating the dynamic behavior of suction caissons have been based on either using solutions for shallow foundations or flexible piles, or on three-dimensional numerical analyses. Using numerical methods requires a lot of computational capacity and long calculation time. The designer must have expert knowledge on idealizing continuous physical problems as discrete elements, in addition to great insight in dynamic considerations for numerical modeling.

Rigorous numerical methods, being limited to projects with good economy and vast time-schedules, are not applicable in most engineering projects. In addition, using numerical models will not necessarily contribute to the understanding of the actual physical behavior. As a response to this, Wolf (1995) presents a whole range of simple physical models, meant to be a useful tool in practical engineering. They are aimed to increase the *"conceptual clarity and physical insight"* of foundation response to vibrations. The simple models can be used for describing dynamics of foundations and soil-structure interaction. Solutions for dynamic stiffness and foundation input motion can be obtained for various foundation geometries and soil conditions. The simple physical models can be especially helpful in preliminary study of the dynamic problem, and for verification of more rigorous numerical results. The book's foreword, written by Jose M. Roësset, summarizes a lot of research and development done within the field of foundation dynamics. Wolf (1995) further extends some of the presented concepts in his simple physical models. These are the *truncated semi-infinite cone* models, *wave pattern in the horizontal plane* and *lumped-parameter* models. The latter can be constructed by a parallel as-

sembly of the exact discrete-element models based on the truncated cone models.

As an example of two of the simple physical model concepts that Wolf (1995) presents, the surface foundation overlying homogeneous half-space in Figure 1.3 can be used. The unbounded soil underlying the foundation can be modeled as truncated cones. Figure 1.4a and 1.4b show the cones for translation and rotation, respectively. The discrete element model for the vertical translation cone is shown in Figure 1.5a, with the corresponding standard lumped-parameter model in Figure 1.5b. Two equivalent discrete element models for the rotational cone are indicated in Figure 1.6a and 1.6b. The corresponding fundamental lumped-parameter models for translational motion in such systems are indicated in Figure 1.6c and 1.6d.

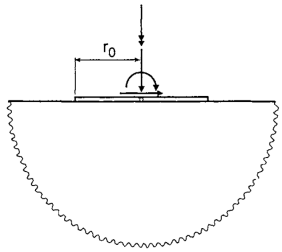

Figure 1.3: *Disk on homogeneous halfspace. Figure from Wolf (1995).*

(a) *Translational cone* ***(b)*** *Rotational cone*

Figure 1.4: *Truncated cone models. Figure from Wolf (1995)*

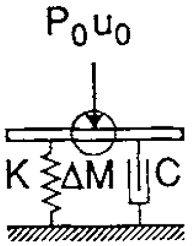

(a) Discrete element model

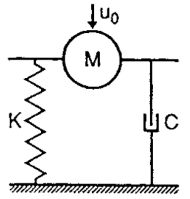

(b) Standard lumped-parameter model

Figure 1.5: *Discrete model and corresponding lumped-parameter model for vertical translation. Figure from Wolf (1995)*

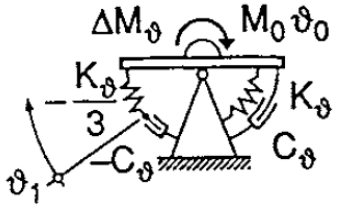

(a) Discrete element model (1)

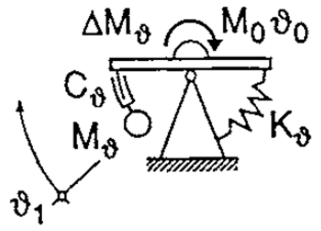

(b) Discrete element model (2)

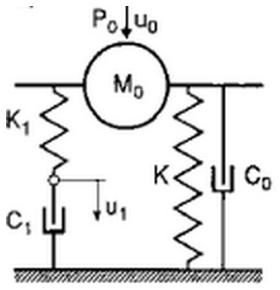

(c) Lumped-parameter model (1)

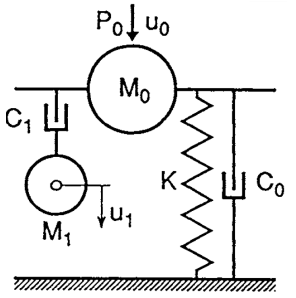

(d) Lumped-parameter model (2)

Figure 1.6: *Discrete models and corresponding lumped-parameter models for translational motion. Figure from Wolf (1995)*

As an example of application of these simple physical models, regarding suction caissons, the work by Liingaard (2006) can be mentioned. He presents extensive research on the frequency-dependence of foundation stiffness in relation to application of suction caissons as foundations for wind turbines. Lumped-parameter models with frequency-independent coefficients are suggested to represent the dynamic stiffnesses in the suction caisson foundation-soil system. The developed lumped-parameter model for a suction caisson's vertical dynamic stiffness is presented in Figure 1.7.

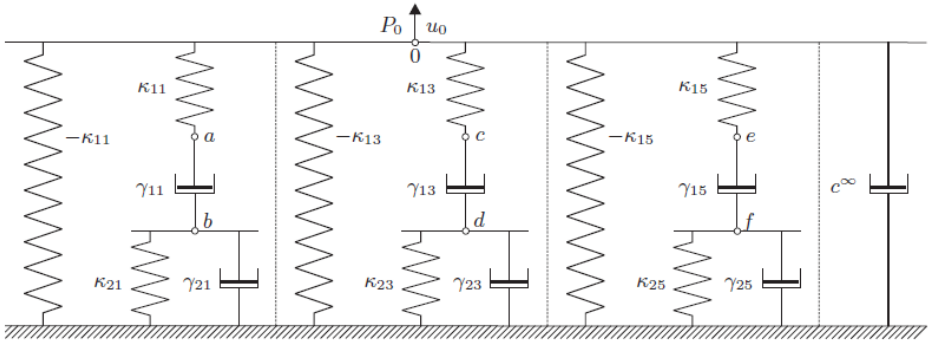

Figure 1.7: *Lumped-parameter model for vertical impedance of suction caisson developed by Liingaard (2006).*

Another good source on the historical developments within the field of foundation vibration is Gazetas (1983). In this state-of-the-art paper, the author presents previous and current methods of analysis, at the time of publication. Analogue concepts, using frequency independent springs and dashpots in lumped-parameter models, are discussed. Additionally, the development in dynamic finite element modeling and computer programs are mentioned, together with analytical solutions, accurate and approximate. The latter includes closed-form expressions for dynamic foundation stiffness. The paper gives a thorough outline on definitions and physical interpretation of impedance functions, together with an introduction to the various ways of computing them. An introduction to the most important analytical, semi-analytical and discrete computational procedures is given. Following the thorough history and physics lesson, is a vast

compilation of some of the aforementioned closed-form solutions. Graphs and expressions for dynamic stiffness and damping, calibrated through numerical modeling, are presented for various foundation geometries and idealized soil profiles. Gazetas (1991) has further extended the collection of these closed-form solutions. Similar to the approximate simple physical models presented by Wolf (1995), these closed-form solutions are meant to be easily implemented in practical study of the problem, and for validation of numerical results.

As mentioned by Gazetas (1983), the dynamic behavior of pile foundations have been researched in numerous publications. He divides the developed methods into three categories: the *Winkler* approach, where the pile is considered founded on springs and dashpots, *analytical continuum* formulations and *finite-element* methods. The former can be used to develop *p-y curves*, yielding a stiffness relation based on the correlation between lateral force (p) and deflection (y). Matlock (1970) derived such correlations for slender piles through extensive field and laboratory testing. Simple expressions for predicting the pile behavior was presented, and are currently used in several design guidelines for piles, e.g. in Norway (The Norwegian Pile Commitee 2012) and the USA (American Petroleum Institute 2010). However, the proposed solutions by Matlock (1970) will in many cases yield overestimated lateral deflections, which is reported by numerous publications through numerical and experimental studies (e.g. Stevens & Audibert (1979), Jeanjean (2009)).

As an example on implementing the aforementioned Winkler approach for suction caissons, the work by Gerolymos & Gazetas (2006*c*) can be mentioned. The article presents a simplified Winkler model for evaluating linear soil-caisson interaction under seismic loading. As shown in Figure 1.8, the soil-caisson interface is modeled as distributed springs and dashpots, whose properties are derived from mathematical expressions for the stress distribution on the foundation.

An extension of this model, accounting for soil-caisson interface nonlinearities, is presented by a companion paper by Gerolymos & Gazetas (2006*a*). The soil nonlinearities, including gapping, and the uplift at the base of the caisson, are modeled by nonlinear springs and dashpots, as indicated in Figure 1.9. The prediction of the model is validated through experimental

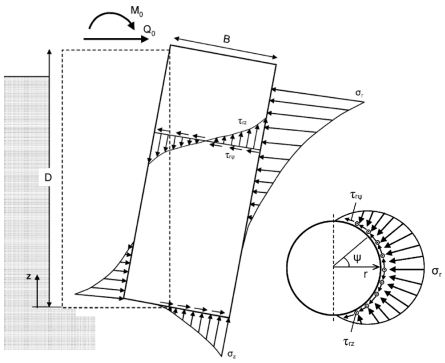

(a) *Stress distribution on caisson-soil interface*

(b) *Rotational cone*

Figure 1.8: *Winkler model for caisson foundation response proposed by Gerolymos & Gazetas (2006*c*)*

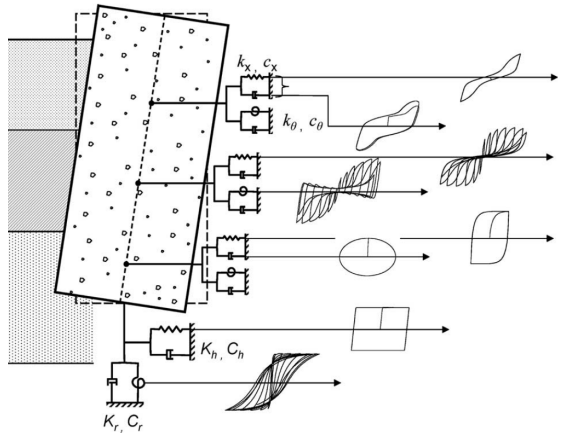

Figure 1.9: *Winkler model for nonlinear caisson foundation response proposed by Gerolymos & Gazetas (2006*a*).*

results and 3D analyses in a third companion paper (Gerolymos & Gazetas 2006*b*).

In summary, closed-form solutions for rigid embedded foundations can be used to assess suction caisson performance. Simple physical models can be developed on a case-to-case basis. Considering the caisson a pile, the design can be based on the concept of *py-curves*, or closed-form expressions for flexible piles calibrated through numerical models. Solutions for piles socketed in rock are presented by Carter & Kulhawy (1988). However, the caissons are sometimes of an intermediate geometry with regards to the embedment-to-width ratio, which exceeds validation limits for solutions for shallow, embedded foundations. As mentioned by Gerolymos & Gazetas (2006*c*), design approaches for piles will in some cases not be adequate for the stubby geometry of some suction caissons due to the kinematic response being fundamentally different. Although quite a lot of research has been performed the last decades, to develop simple design methods for seismic loading of suction caissons, nothing has yet been established as THE recognized practice.

1.2 Objectives

The objectives of this thesis are summarized in the following points:

1. Establish 3D finite element model in Plaxis 3D comprising soil, suction caisson and superstructure. Evaluate the possibilities of dynamic 3D modeling in Plaxis.
2. Evaluate soil-structure interaction by performing a dynamic earthquake analysis on the 3D finite element model.
3. Perform additional earthquake analysis on soil-caisson-structure system using a practical multi-step approach
4. Evaluation of results through alternative analyses.

The objective of this master thesis is to evaluate if simplified finite element modeling of a complex physical problem is possible with adequate accuracy. It will be investigated if a multi-step method can be more effective,

without a great loss of accuracy, compared to a full finite element model for dynamic situations.

1.3 Limitations and Approach

3D finite element modeling was performed using Plaxis 3D 2012.

Equivalent-linear analyses was performed using the Excel implemented program EERA. Response spectrum analysis was performed in Matlab®.

Due to practical limitations (computer power and time) the research was limited to mainly investigating linear soil behavior, using a linear-elastic material model.

Loads, other than connected to seismic loading, such as water loads from underwater currents, connection loads from adjacent pipe-lines and so on, are not considered in this thesis. The focus will be on horizontal and rotational deformation due to ground motion. Evaluation of capacity is not included.

The thesis is not concerned with the complex issue of damping, other than explaining the phenomena. Radiation damping, in reality being frequency dependent, is simplified using a Rayleigh damping model. Material damping is neglected completely due to the use of linear-elastic material model.

The multi-step approach is performed in a simplified manner. Frequency-dependence of foundation stiffness is commented upon, however not included in the analyses.

The content of this thesis is adapted a reader with basic knowledge within the field of geodynamics.

1.4 Structure of Report

This master thesis is divided into two parts. The first part presents the theoretical background and methodology on which this thesis is based

on. The second part presents the case study, with associated calculations, results and discussion.

Part I:

- *Chapter 2* introduces seismic waves and earthquake excitation.
- *Chapter 3* describes selected subjects within cyclic soil behavior, including the equivalent-linear model.
- *Chapter 4* gives a short introduction to the Finite Element Method, along with special considerations for dynamic modeling.
- *Chapter 5* presents the concept of soil-structure interaction, giving a brief overview of the common methods of analysis

Part II:

- *Chapter 6* gives an introduction to the case study, along with a description of the programs Plaxis 3D and EERA.
- *Chapter 7* describes the case study analyses. The procedures for analyzing the case using a direct method and a multi-step approach are presented.
- *Chapter 8* presents the results from analyses, with discussion and evaluation of these.
- *Chapter 9* gives a brief note on the main observations, together with recommendations for further work.

At the end of the thesis, appendices with calculations, derivations and figures are enclosed.

Part I

Theoretical Background and Description of Methods

Chapter 2

Seismic Waves and Earthquake Excitation

This chapter is meant to give an overview of some selected topics in the field of geotechnical earthquake engineering. First, the most relevant seismic wave types are presented, followed by wave propagation and attenuation theory. Earthquake excitation is then discussed, including a short note on response spectrum analysis.

2.1 Seismic Waves

Seismic waves originates from earthquakes deep in the ground. In general there are two different types of seismic waves; *body waves* and *surface waves* (see for example Kramer (2014)). Body waves can travel through the interior of the earth, whereas surface waves only travel in the surficial layers. When an earthquake occurs, seismic body waves are sent in all directions from the origin.

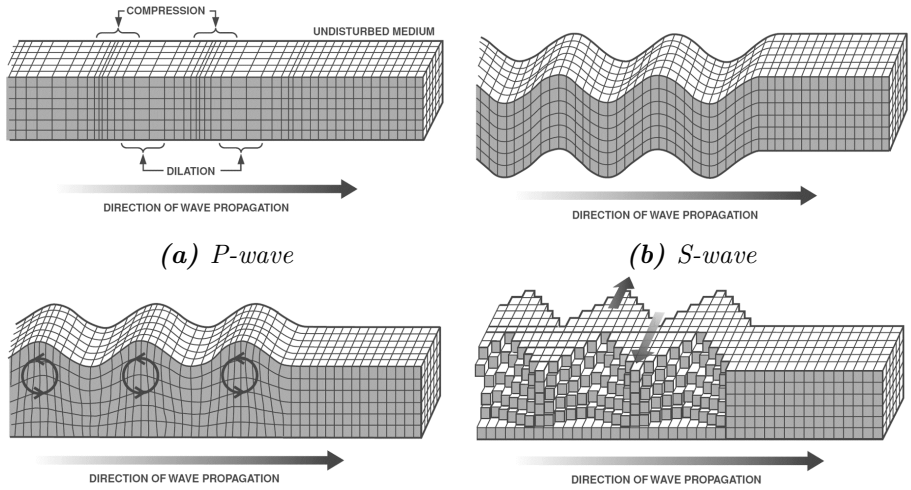

(a) *P-wave* ***(b)*** *S-wave*

(c) *R-wave* ***(d)*** *Love-waves*

Figure 2.1: *Illustrations of seismic waves from Olivadoti (2001)*

2.1.1 Body Waves

Primary waves (p-waves) are compressional body waves that are analogous to sound waves. P-waves makes the soil particles compress and extend relative to each other, like an accordion. The particles move in the direction of the wave as seen in Figure 2.1a. P-waves can pass through both fluids and solids. *Secondary waves* (s-waves) are body waves that cause shear deformations as they travel through a material. Thus they are often referred to as *shear waves*. They will make the soil particles move perpendicular to the wave direction, both horizontally and vertically (see Figure 2.1b). S-waves can only exist in solids, because fluids can not transfer shear. When the particle motion is vertical, the shear wave is often referred to as an *SV-wave*, and for horizontal particle motion, *SH-wave* is commonly used.

2.1.2 Surface Waves

Surface waves are generated when body waves hit the surficial layers of the earth. The most relevant surface waves are *Rayleigh waves* and *Love waves*. The Rayleigh wave will move the particles both vertically and horizontally, similarly to an ocean wave, in an elliptic pattern (see Figure 2.1c). It is created by a combination of P- and SV-waves. The Love wave displayed in Figure 2.1d contributes to a horizontal, snake-like particle movement, and exist in cases where there is a soft material, overlaying a stiffer material (Kramer 2014).

2.2 Wave Propagation

The wave propagation velocity through a medium depends on the stiffness and density of the material (Kramer 2014, ch. 5.2). With basis in the equation of motion of a medium, being one-dimensional or three-dimensional, the wave equations can be derived. In the following sections, the wave equation of a one-dimensional rod is derived, yielding useful relationships along the way, which are also relevant for three-dimensional wave propagation.

2.2.1 1D Wave Propagation

In Kramer (2014, p. 144-145), the equation of motion for a one-dimensional elastic rod is derived from force equilibrium of a rod element (see Figure 2.2). In the following derivations, $a_x = d^2u/dt^2$ denotes the acceleration in the longitudinal direction of the rod, m the mass and σ_x the axial stress.

$$F_x = ma_x = \rho V \frac{d^2u}{dt^2} = \rho A dx \frac{d^2u}{dt^2} \tag{2.1}$$

$$F_x = \left(\sigma_x + \frac{\delta \sigma_x}{\delta x} dx\right) A - \sigma_x A = \frac{\delta \sigma_x}{\delta x} dx A \tag{2.2}$$

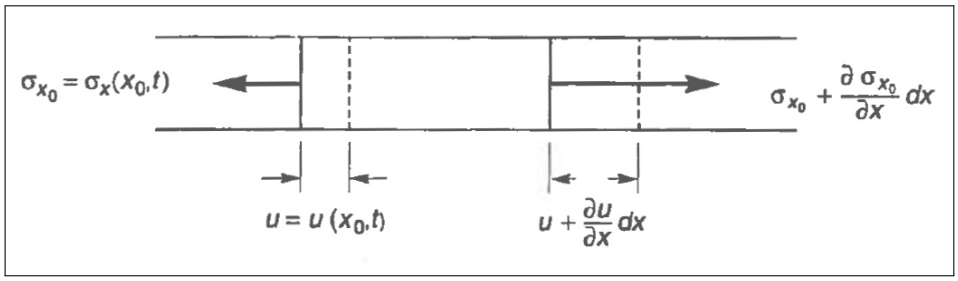

Figure 2.2: *1D rod element*

Combining Eq.(2.1) and Eq.(2.2) yields the *equation of motion* for a pressure wave propagating in the longitudinal direction of the rod:

$$\rho \frac{d^2u}{dt^2} = \frac{\delta \sigma_x}{\delta x} \tag{2.3}$$

By using the stress-strain relationship $\sigma_x = M\epsilon_x$ and $\epsilon = \delta u/\delta x$, Eq. (2.3) can be modified:

$$\frac{d^2u}{dt^2} = \frac{M}{\rho}\frac{\delta^2 u}{\delta x^2} = V_p^2 \frac{\delta^2 u}{\delta x^2} \tag{2.4}$$

where M is the constrained modulus, and V_p is the wave propagation velocity for a compression wave.

The particle velocity and the wave velocity is not equal. However, the particles in the rod will move with a speed, $\dot{u}$, proportional to the wave velocity, V_p, when the wave passes through, as shown in Eq. (2.5).

$$\dot{u} = \frac{\delta u}{\delta t} = \frac{\delta u}{\delta x}\frac{\delta x}{\delta t} = \epsilon_x \frac{\delta x}{\delta t} = \frac{\sigma_x}{M}\frac{\delta x}{\delta t} = \frac{\sigma_x}{V_p^2 \rho} V_p = \frac{\sigma_x}{\rho V_p} \tag{2.5}$$

In the above equation, ρV_p denotes the material's *specific impedance*, which is a sort of resistance to movement. Specific impedance is important with regards to wave behavior at interfaces, which is discussed in Section 2.2.3

2.2.2 3D Wave Propagation

With basis in the equations of motion for three-dimensional elastic media, the wave velocities of body waves can be derived. The calculation procedure is not included here, being a very tedious derivation. However, the expression for the compression wave velocity can be shown to be:

$$V_p = \sqrt{\frac{G(2-2\nu)}{\rho(1-2\nu}} = \sqrt{\frac{M}{\rho}} \tag{2.6}$$

and the shear wave velocity is expressed by:

$$V_s = \sqrt{\frac{G}{\rho}} \tag{2.7}$$

In the above equations, the bulk mass density of the soil is denoted ρ. M is the constrained modulus of the soil, and G the shear modulus. As seen by the above equations, a material with a high stiffness-to-density ratio will have a high wave propagation velocity.

2.2.3 Wave Behavior at Interfaces

To illustrate what happens when a wave reaches a boundary between two materials, a solution for a one-dimensional, infinite rod can be considered (see Figure 2.3). Derivations of formulas leading to the following statements, are presented in full in Appendix B. The example is borrowed from Kramer (2014, p. 165-168) and helps to gain understanding of the boundary situation.

Derivations in Appendix B show that for a rod with a *free* end (impedance ratio = 0), the incident wave will be fully reflected at the boundary. Both the stress and the displacement will be reflected with the same amplitude as for the incident wave. The same goes for a rod with a *fixed* end (impedance ratio = ∞).

For a rod where the impedance ratio between the two boundary materials are equal to unity, no stress nor displacement wave is reflected. This is

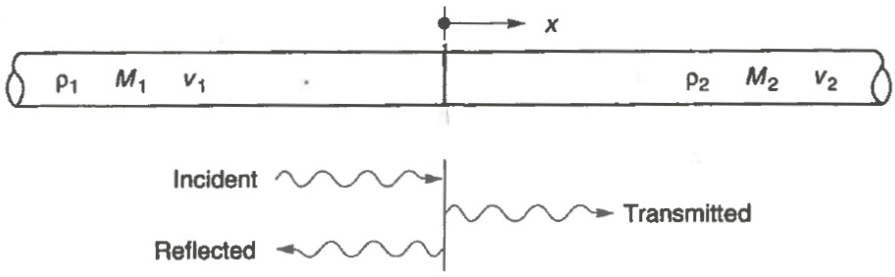

Figure 2.3: *Boundary conditions of infinite 1D rod. Figure from Kramer (2014, Ch. 5.4)*

due to the rod continuing ˝infinitely˝.

The one-dimensional rod boundary problem can be related to a situation in three dimensions as well. Stress waves induced in a 3D medium will travel in all direction from the point source (e.g. a vibrating foundation). When hitting the boundaries, these incident waves will, similarly as for the rod, be reflected and transmitted depending on the boundary conditions.

2.3 Wave Attenuation

A wave traveling in a soil material will attenuate with distance because of two main phenomena, *material damping* and *radiation damping* (Kramer 2014, ch. 5.5).

2.3.1 Material Damping

Material damping in soil is due to energy dissipation from internal soil friction and grain slippage. The phenomena is mainly hysteretic, and result in a decrease of the specific energy of a traveling wave. To account for material damping, soil is very often modeled as a *Kelvin-Voigt* solid, which is further explained in Section 3.3. It can be shown that material

damping makes the wave amplitude attenuate exponentially with distance, for the case of the Kelvin-Voigt model (Kramer 2014, Ch. 5.5.1).

2.3.2 Radiation Damping

Radiation damping, also known as geometric damping, is an energy reduction of a strictly geometric origin. This form of wave attenuation is caused by the wave spreading over a continuously increasing volume with distance (Kramer 2014, ch. 5.5.2). The energy is thus transported to ˝infinity˝, and even though the total elastic energy is conserved along the way, the system will experience attenuation of the wave amplitude because of the spreading of the wave energy. For instance, it can be shown that body waves from a point source of energy will decrease at a rate of $1/r$, where r is the distance from the energy source, while surface waves decrease at a rate of about $1/\sqrt{r}$ (Kramer 2014, Ch. 5.5.2).

2.4 Earthquake Excitation

The equations of motion for a multi-degree-of-freedom (MDOFs) system are shown in Eq. 2.8 as a set of equations in matrix form.

$$\mathbf{m\ddot{u}} + \mathbf{c\dot{u}} + \mathbf{ku} = \mathbf{q}(t) \tag{2.8}$$

where $\mathbf{m}$ is the mass matrix, $\mathbf{c}$ is the damping matrix and $\mathbf{k}$ is the stiffness matrix of the system. $\mathbf{q}$(t) is the external force vector applied on the system, while $\mathbf{u}$, $\dot{\mathbf{u}}$ and $\ddot{\mathbf{u}}$ are the displacement, velocity and acceleration vectors, respectively (e.g. Chopra (1995)).

Earthquakes will induce a motion at the base of a system. This base motion, $\mathbf{u_b}(t)$, cause an acceleration of the system mass, in addition to the acceleration caused by relative movement between ground and system, $\mathbf{u}(t)$ (Chopra 1995). Thus, the total acceleration consists of two contributions, as shown in Eq. 2.9. As a result, the equations of motion for the

system will be as shown in Eq. 2.10, where the base motion induced mass acceleration is considered an external force.

$$\ddot{\mathbf{u}}_\mathbf{t}(t) = \ddot{\mathbf{u}}(t) + \ddot{\mathbf{u}}_\mathbf{b}(t) \tag{2.9}$$

$$\mathbf{m}\ddot{\mathbf{u}} + \mathbf{c}\dot{\mathbf{u}} + \mathbf{k}\mathbf{u} = -\mathbf{m}\ddot{\mathbf{u}}_\mathbf{b} \tag{2.10}$$

2.4.1 Fourier Transformation

Earthquake motion is a non-periodic, transient vibration generated deep in the ground. It is necessary to represent these vibrations in a way that enables us to perform linear analysis to obtain the ground response to an earthquake. Fourier transformation is a common tool for this purpose.

The first part of Fourier transformation is converting a signal, p(t), to a series of harmonic functions which together constitute the initial signal, as illustrated in Figure 2.4.

$$\hat{p}(i\omega) = F[p(t)] = \int_{-\infty}^{\infty} e^{i\omega t} p(t) dt \tag{2.11}$$

The above equation shows the first step, where $\hat{p}(i\omega)$ is the amplitude of a harmonic signal at a given frequency.

From the $\hat{p}(i\omega)$ functions, the system response is calculated in the frequency domain for each frequency $\hat{u}(i\omega)$. By inverse integration of the response over all frequencies, the response in the time-domain is obtained as shown in Eq. 2.12.

$$u(t) = \frac{1}{2\pi} \int_{-\infty}^{\infty} H(i\omega)\hat{p}(i\omega) e^{i\omega t} p(t) d\omega \tag{2.12}$$

where $H(i\omega)$ is the system response to an excitation at a given frequency (Chopra 1995, Ch. 1.10).

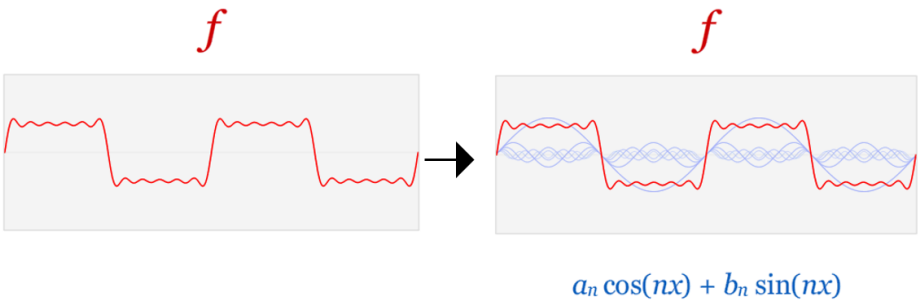

Figure 2.4: *An illustration of the first step in Fourier transformation of a vibratory motion. Figure from Barbosa (2013)*

The above equations describe a continuous Fourier transformation. In earthquake engineering, the use of discrete fourier transformation is more common, i.e. using the fast Fourier transform scheme (see Christian et al. (1977, Ch. 20-1)). In this case, the signal is defined by a series containing a finite number of harmonic functions.

Fourier transformation can only be performed on periodic functions, thus a non-periodic, transient motion such as an earthquake is ˜made″periodic by repeating the pattern after a quiet zone Kramer (2014, Ch. A.3).

2.4.2 Response Spectrum Analysis

Response spectrum analysis (RSA) is an indirect, filtered representation of a strong ground motion, and is a very useful tool in earthquake engineering.

A RSA yields the maximum response of a single-degree-of-freedom (SDOF) system to a given earthquake time history, as a function of the system's natural period. The response spectrum is dependent on damping ratio, thus different damping ratios will yield different spectra (Kramer 2014, Ch. B.7).

Figure 2.5 illustrates the concept of RSA, showing an example of an acceleration response spectrum obtained from the response analysis of five different SDOF systems.

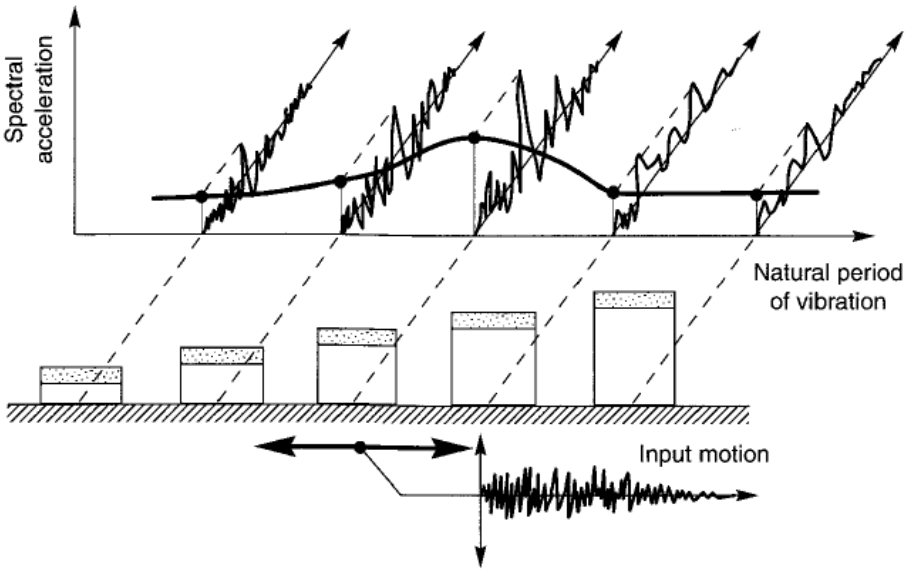

Figure 2.5: *Maximum acceleration amplitudes for different SDOF systems plotted versus natural period. Figure from Kramer (2014, Ch. B.7).*

Chapter 3

Cyclic Soil Behavior

This chapter is concerned with the aspects of cyclic and dynamic soil behavior. First, material properties of cyclically loaded soils are discussed. This is followed by a section on the soil stress-strain behavior under cyclic loading. The equivalent-linear model is presented next, followed by a short presentation of site response analysis.

3.1 Material Properties of Cyclically Loaded Soils

When cyclically loaded, soils can act non-linearly and inelastically, and the stiffness and strength of the material is influenced. The strength of cyclically loaded soils is more relevant for failure problems. In this thesis, the objective is not to evaluate failure, thus only the stress-strain behavior will be in focus.

In the following sections, the equivalent-linear model for evaluating stress-strain relationship will be discussed, including the model's assumptions regarding shear modulus reduction and damping.

3.2 Stress-Strain Behavior of Soil

Repeated loading of a soil above a certain stress level will cause plastic strains, which will increase in magnitude as the cyclic loading continues. This is due to the accumulated degradation of the soil stiffness with each cycle (Kramer 2014, Ch. 6.4). When dynamic strains are sufficiently low ($\gamma < 10^{-5}$) the material acts linear-elastic, and will have a higher stiffness moduli. The strain level for this behavior is commonly referred to as the *cyclic threshold shear strain*. In an intermediate range of strain ($10^{-5} < \gamma < 10^{-4}$), the soil exhibits non-linear elastic behavior. At higher strains, non-linear inelastic behavior kicks in with a corresponding lower stiffness and increasing degradation of the soil due to plastic deformations (Pecker 2007).

There are many models used to characterize soil behavior during cyclic loading, for example the *equivalent linear model*, the *cyclic non-linear models* and advanced constitutive models such as the *Cam Clay model* and the *small strain Hardening Soil model*. All these models have very different complexity and proper area of application (Kramer 2014, Ch. 6.4). In the following sections, the equivalent-linear model is explained, together with some important cyclic soil characteristics.

3.3 Equivalent Linear Model

The concept of the equivalent-linear model, is to represent the soil as a Kelvin-Voigt solid (Figure 3.1), i.e. as a linear, visco-elastic material. A Kelvin-Voigt solid is analogous to a system where the shear resistance consist of a spring and a dashpot. The spring's contribution to shear resistance depends on the strain, whereas the dashpot's contribution is proportional to the rate of strain, as shown in Eq. (6.5).

$$\tau = G\gamma + \eta\frac{\delta\gamma}{\delta t} \tag{3.1}$$

Here τ denotes the shear stress, $\gamma = \frac{\delta u}{\delta z}$ the shear strain, η the viscosity of

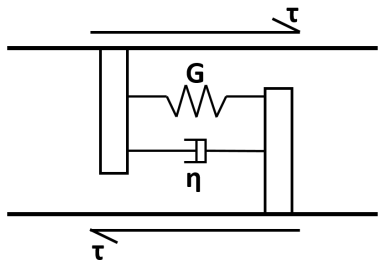

Figure 3.1: *Shear stress on an element of a Kelvin-Voigt solid. Figure after Kramer (2014, fig. 5.21).*

the material, and G the material's shear modulus.

During one cycle of symmetric loading, the stress-strain relationship can form a hysteresis loop as shown in Figure 3.2. As shown in the figure, the inclination of the loop is governed by the shear stiffness, whereas the width of the loop (and thus it's area) is related to the damping ratio.

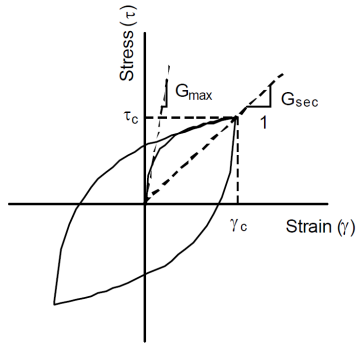

Figure 3.2: *Hysteresis stress-strain curve from Bardet et al. (2000)*

The inclination is related to the secant shear stiffness, G_{sec}:

$$G_{sec} = \frac{\tau_c}{\gamma_c} \tag{3.2}$$

And the area of the loop is related to the damping ratio, ξ, according to:

$$\xi = \frac{W_D}{4\pi W_S} \tag{3.3}$$

Here W_D is the energy dissipation during one full cycle, and W_S is the peak strain energy. It can be proved that W_D can be expressed by Eq. (3.4) and W_S by Eq. (3.5)..

$$W_D = \pi\omega\eta\gamma_c^2 = 2\pi\xi\gamma_c^2 \tag{3.4}$$

$$W_S = \frac{1}{2}G\gamma_c^2 \tag{3.5}$$

By expressing the shear stiffness and the damping ratio as functions of the shear strain level, the equivalent-linear model accounts for some of the non-linear characteristic for soils under cyclic loading. It thus mimics the soil behavior through certain assumptions about soil stiffness and energy loss.

3.3.1 Shear Modulus

The shear modulus, G, of a soil is a measure of the soil's resistance to shear deformations. A simplified illustration of the relationship between shear stress and shear deformations is shown in Figure 3.3. Stress dependency of G is given by Eq. 3.6. The shear modulus of a soil at small strains depends on the confining pressure, the overconsolidation ratio, the void ratio and the plasticity index (see for example Kramer (2014, Ch. 6.4)). Influence of the plasticity index will be briefly discussed in the following section.

$$G = \frac{\tau}{\gamma} \tag{3.6}$$

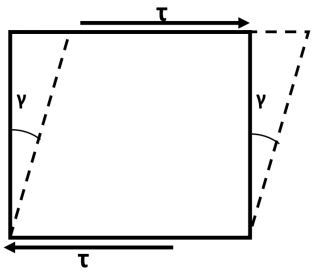

Figure 3.3: *Illustration of the shear modulus, G, as the resistance to shear deformation γ because of shear force τ.*

Backbone Curve

The backbone curve of a material illustrates how the shear modulus changes with shear strain (see Figure 3.4). The curve consists of a plot of the tip of the hysteresis loops for different strain amplitudes.

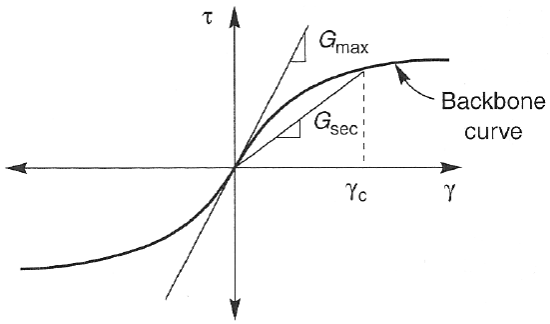

Figure 3.4: *A typical backbone curve. Figure from Kramer (2014, Fig. 6.40)*

The curve has it's greatest inclination at the origin, which is referred to as the maximum shear stiffness, G_{max}. There are multiple procedures for evaluating G_{max}: Various in-situ measurements, laboratory tests and empirical formulas (see for example Kramer (2014, Ch. 6.4)). This thesis will not go in further detail on such procedures.

Modulus reduction

To describe material behavior in equivalent-linear analyses it is common to define a *modulus reduction curve* for the material, which states how the shear modulus varies with strain (see Figure 3.5).

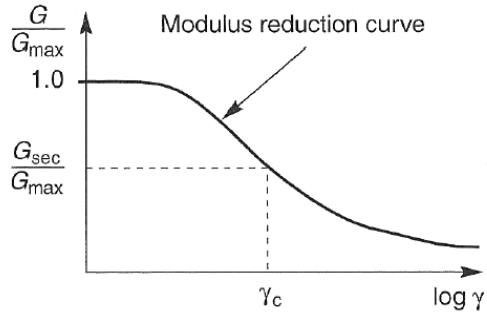

Figure 3.5: *Modulus reduction with increasing shear strain. Figure from Kramer (2014, Fig. 6.40)*

Research has shown that, amongst other factors, the soil plasticity has a significant influence on the modulus reduction curve (see for example Vucetic & Dobry (1991)). High-plasticity soils are shown to have a greater cyclic threshold strain, and a slower degradation of shear stiffness, thus indicating that high-plasticity soils will have a more linear stress-strain response. Vucetic & Dobry (1991) have presented results from various experiments graphically, reproduced in Figure 3.6.

3.3.2 Damping Ratio

Damping in a soil material is influenced by confining pressure, plasticity index and cyclic shear strain, amongst other factors (Kramer 2014, Ch. 6.4). The variation with strain level is implemented in equivalent-linear analyses by defining a damping ratio variation curve, showing the increase with shear strain. The damping ratio is, similarly to the modulus reduction, also influenced by the plasticity index as illustrated in Figure 3.7 (Vucetic & Dobry 1991).

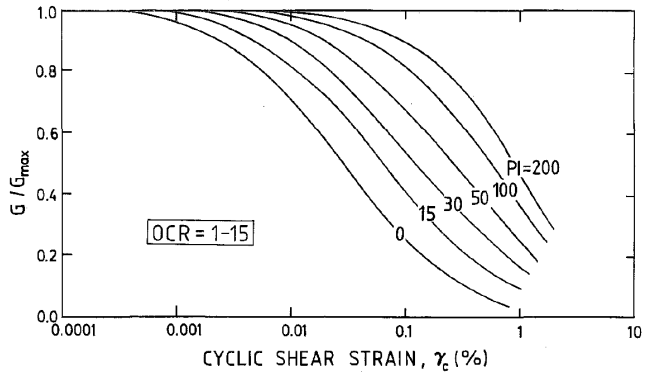

Figure 3.6: *The influence of soil plasticity on the modulus reduction curve. Figure from Vucetic & Dobry (1991)*

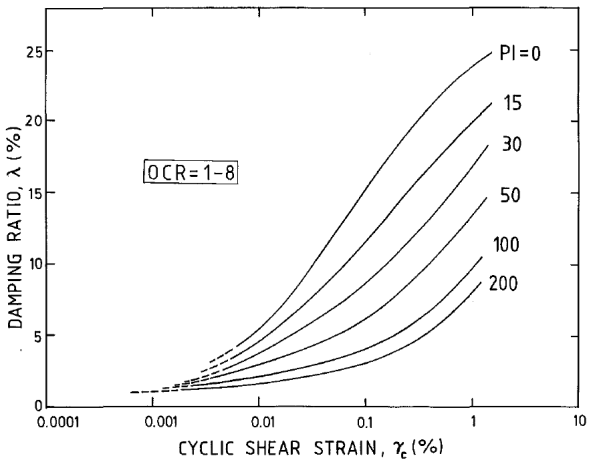

Figure 3.7: *The influence of soil plasticity on the shear strain dependent damping ratio. Figure from Vucetic & Dobry (1991)*

3.4 Site Response Analysis

A soil's stiffness and strength characteristics highly influence the dynamic response to an input motion. Generally, soft soils will have a greater response to low frequencies, whereas stiffer soils will respond more to high-frequency motions. This is due to the soil's wave velocity, which is governed by it's stiffness properties as explained in Section 2.2. In this section, some key concepts of soil amplification are presented.

3.4.1 Amplification Function for Damped Site Response

The relationship between the amplitudes of a signal in one point relative to the amplitude of the signal in another point is called the *amplification factor*. In Section 2.4.1, the amplification function $H(i\omega)$ was presented as a SDOF system's response to a frequency-dependent excitation. Similarly to the SDOF system, a soil deposit has it's own amplification function, which decides how a bedrock input motion is amplified or de-amplified through a soil layer. For uniform, damped soil on rigid rock the amplification function can be found by Eq. (3.7) (see for example Kramer (2014, Ch. 7.2)).

$$|H(\omega)| = \frac{1}{\sqrt{cos^2\left(\frac{\omega H}{V_s}\right) + \left[\xi\left(\frac{\omega H}{V_s}\right)\right]^2}} \tag{3.7}$$

This equation originates from the *transfer function* between to points, as shown in Eq. (3.8).

$$H(\omega) = \frac{u_{max}(0,t)}{u_{max}(H,t)} \tag{3.8}$$

where $u(z,t)$ is given by Eq. (3.9):

$$u(z,t) = Ae^{i(\omega t + k^* z)} + Be^{i(\omega t - k^* z)} \tag{3.9}$$

$|H(\omega)|$ is highest at the natural frequencies of the soil deposit. The natural

frequency depend on the shear wave velocity of the soil material, and the height of the soil deposit.

$$\omega = \frac{V_s}{H}\left(\frac{\pi}{2} + n\pi\right) \tag{3.10}$$

for (n=0, 1, 2, 3, ...)

Amplification through a soil layer will be greatest at the soil layers fundamental natural frequency, ω_0, with it's corresponding fundamental period, T_S.

$$\omega_0 = \frac{\pi V_S}{2H} = \frac{2\pi}{T_S} \tag{3.11}$$

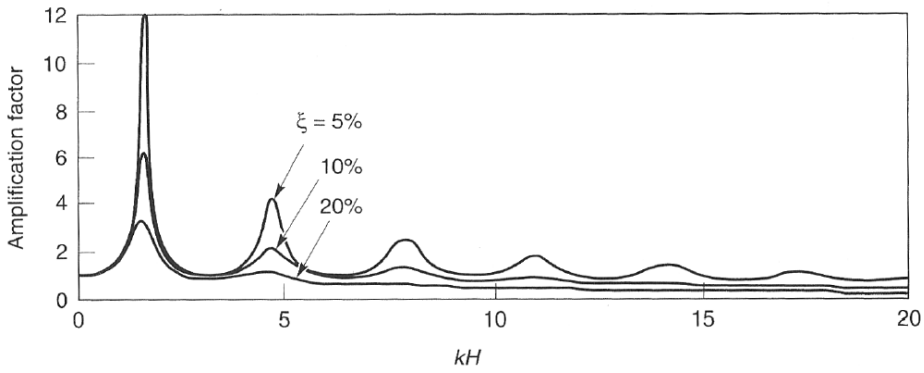

Figure 3.8: *Amplification through a damped uniform layer over rigid rock. Figure from Kramer (2014, Fig. 7.5)*

3.4.2 Natural Mode Shapes

Figure H.4 illustrates the natural movement of a medium when afflicted by a frequency corresponding to one of it's eigenfrequencies. These movement patterns are standing waves called *mode shapes*. As a rule of thumb, the number of the mode shape corresponds to the number of wave tops in the wave pattern: The 1^{st} mode shape has one wave top, the 2^{nd} shape has two wave tops and so on.

(a) 1^{st} *natural mode*

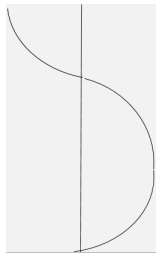

(b) 2^{nd} *natural mode*

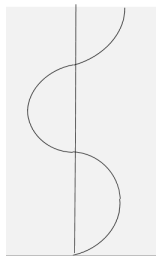

(c) 3^{rd} *natural mode*

Figure 3.9: *Mode shapes for the three first natural frequencies.*

Chapter 4

Finite Element Method

4.1 About the Finite Element Method

The finite element method (FEM) is an approach to find a numerical solution of a physical problem. The method uses the *principle of virtual displacements*, and requires that the problem can be mathematically described by differential equations or integral expressions (Cook et al. 2002). The solution is not exact, but merely an approximation of the real situation, because the principle of the method is to discrete a physical structure into a *mesh* of a finite amount of elements (small pieces of the structure). The elements are interconnected in *nodal points*, or simply *nodes*, which each has a finite number of *degrees of freedom* (DOFs). The amount of DOFs at each node depend on, among other things, the dimension of the problem. A DOF is an unknown property, commonly a nodal displacement.

As an example, a simple embankment is illustrated in Figure 4.1. This model can be divided into several elements by a mesh. One of these elements is encircled and enlarged with the nodes indicated. Each node is here shown with two translational DOFs, one lateral and one vertical.

To connect discrete elements together in a system, the elements nodal

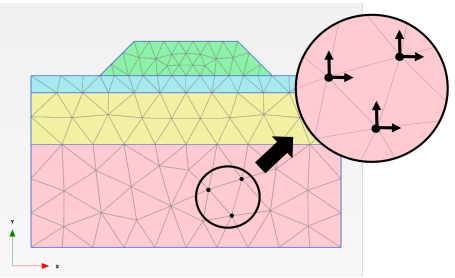

Figure 4.1: *A coarse mesh for a simple embankment modeled with triangular elements. Element and DOFs are encircled.*

forces (**S**) and displacements (**v**) must be related.

$$\mathbf{S} = \mathbf{kv} \tag{4.1}$$

k is the element *stiffness* matrix. In short, this matrix contains information about the elements' contribution to the total stiffness of the system, which describes the structure's resistance to movement (Cook et al. 2002). External forces on the system is gathered in a force vector **R**, and are related to the nodal force vector (**S**) in the following manner:

$$\mathbf{R} = \sum_{\mathbf{i=1}}^{\mathbf{m}} \mathbf{g^i S^i} = \sum_{\mathbf{i=1}}^{\mathbf{m}} \mathbf{g^i k^i v^i} = \left(\sum_{\mathbf{i=1}}^{\mathbf{m}} \mathbf{g^i k^i a^i} \right) \mathbf{r} = \mathbf{Kr} \tag{4.2}$$

i denote the element number and m the total amount of elements. Simply put, the **g** matrix describes how much of the external forces in **R** that goes into each nodal force **S**, i.e. **g** works as a sort of weighting matrix. **K** is the system stiffness matrix and **r** is the displacement vector for the system. The shape of the displacements between nodes (**u**) is a function of the nodal displacements (**v**), weighted by interpolation functions (**N**).

$$\mathbf{u} = \mathbf{Nv} \tag{4.3}$$

The displacements *between* nodes are thus merely interpolated, and accuracy of the solution will obviously depend on the amount of elements used.

4.2 Capturing Dynamic Conditions in FEM

Modeling dynamic conditions using finite elements introduces the aspect of time, and considerations must be made in order to appropriately model the problem. In the following subsections, some important issues are discussed, concerning considerations of mesh, boundary conditions and time discretization in dynamic finite element modeling.

4.2.1 Element Discretization

To ensure appropriate element discretization in dynamic modeling, it is necessary to consider the frequency of interest and what type of element to use. The selected mesh size is governed by the wave length (λ), and as suggested in Bao et al. (1998) a resolution of 8-10 nodes per wavelength is sufficient for engineering purposes. Kramer (2014, Ch. 7.3) mentions that the use of maximum element dimensions of $\frac{1}{8}-\frac{1}{5}$ of the shortest wavelength is recommended (dependent on how the mass matrix is defined). As shown in Figure 4.2, a too coarse mesh would not be able to adequately describe the propagation of the illustrated shear wave.

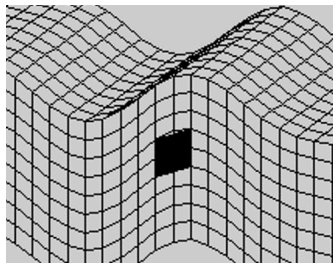

Figure 4.2: *S-wave propagating in adequate mesh. Figure adapted from Olivadoti (2001)*

4.2.2 Time Discretization

To properly capture a dynamic signal, a adequate amount of time steps must be used. The *critical time step* describes a situation where the time stepping is optimal. This time step is dependent on the mesh coarseness and the frequency of the dynamic signal (Haigh et al. 2005). As a rule of thumb, the time step could be calculated according to Eq. (4.4), i.e. small enough for the smallest element, with dimension $L_{element}$, to be able to transfer the wave, with propagation velocity V_s.

$$\delta t \leq \frac{L_{element}}{V_S} \tag{4.4}$$

The element size is again dependent on the frequency of interest, as explained in the previous section. If a signal consist of more than one frequency (e.g. earthquake time-history), the highest frequency of interest must be considered when choosing the proper time step discretization (Plaxis 2012, 4.7.2.1). In Figure 4.3 the importance of appropriate time-stepping is illustrated. Figure 4.3a shows a situation where the time steps are too few, thus the signal is not properly represented.

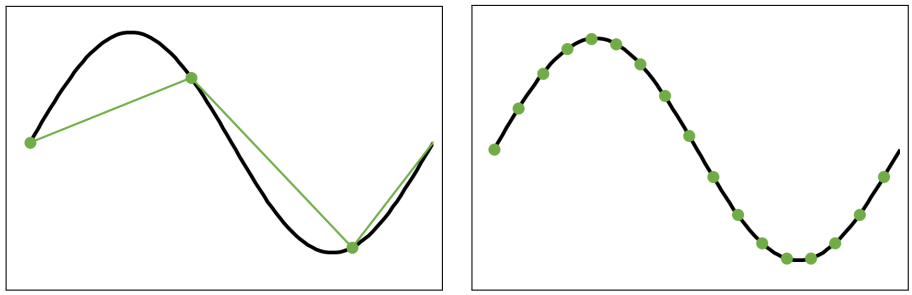

(a) *Too coarse time-stepping* ***(b)*** *Adequate time-stepping*

Figure 4.3: *The importance of appropriate time-stepping in dynamic finite element analyses.*

As a comment to the importance of time-stepping, Haigh et al. (2005) shows that the critical time step for wave propagation problems should be as small as $\frac{1}{20}$ of the time it takes for the wave in consideration to

travel through the smallest element. However, Haigh et al. (2005) are considering a certain situation with liquefaction in sand, and their results are thus not relevant for all wave propagation problems.

4.2.3 Boundary Conditions

An important issue in finite element modeling of dynamic problems, is the so-called *box-effect* which the lateral boundaries create (Christian et al. 1977). Energy propagating from a vibrating source, is "trapped"by fixed boundaries, resulting in reflection of stress waves back into the system (see Figure 4.4 for illustration). As explained in Section 2.2.3, the boundary conditions govern the reflection and transmission of an incident wave. Thus, when modeling an actual physical situation with waves propagating in a medium, the boundaries must be defined in a way that adequately simulates the real behavior. The natural lateral boundaries, which would cause reflection of stress waves, are often so far away from the area of interest, making the medium practically infinite. In these situations, an additional factor is set in play, namely radiation damping (see Section 2.3.2).

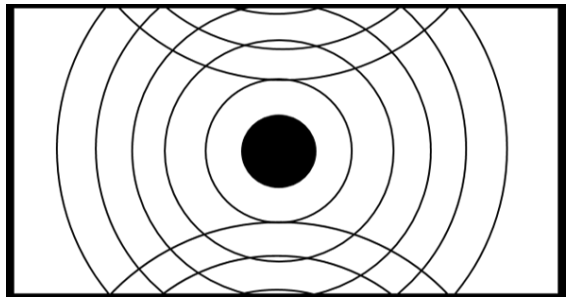

Figure 4.4: *The "box-effect" in finite element modeling*

Appropriate modeling of the boundary conditions comprise of defining *non-reflective* boundaries (Plaxis 2012). Otherwise, stress waves are reflected at the boundaries and could disturb the results of the analysis. There are multiple ways of approaching this problem described in literature (see for example Christian et al. (1977, Ch. 20-5)), some of which are

summarized here:

- Modeling the boundaries as *viscous* dampers, with dashpots designed for the specific wave problem.
- Specifying displacements or loads at the boundaries; the use of so-called *elementary boundaries*.
- Define *consistent boundaries*, which have frequency-dependent stiffness matrices which will mimic the far-field region's properties, making it seem infinite.
- Adapt material properties of boundary elements so that they have high viscosity and low stiffness in order to minimize the reflected waves.

With a wave problem being more complex than just a single train of plane waves, viscous boundaries and elementary boundaries will inevitably result in stress wave reflection to some extent. It is therefore necessary to locate the lateral boundaries far away from the region of interest, to minimize this effect. This leads to a large model, with a potentially large amount of elements and nodes, which will be quite time consuming calculation-wise.

The bottom boundary is also of great interest in dynamic FE modeling. When wanting to model a soil deposit with ˜infinite˝depth to bedrock or stiffer layer, viscous boundaries must be specified also at the bottom boundary. When dealing with a problem involving an almost rigid layer at a shallow depth, i.e. bedrock, a fixed boundary corresponds well to the physical situation (Christian et al. 1977, Ch. 20-5).

Chapter 5

Soil-Structure Interaction

5.1 Introduction to Soil-Structure Interaction

Soil-structure interaction (SSI) is a relevant issue whenever a structure is founded in or on a soil deposit affected by some type of vibration. This vibration could for example result from either a machine or an earthquake. In this thesis, the focus will primarily be on ground motions from earthquakes, though a lot of the presented formulations were developed with machine foundation vibrations in mind.

Basically, SSI denotes a situation where the presence of a structure affect the soil's ability to move, and vice versa. Without the structure, the soil would obtain a *free-field motion* as a response to an imposed vibration. The structure will restrict the soil's natural movement, as they move together in an affected motion. When the structure moves, it will again cause deformation of the neighboring soil, inducing additional soil movement. It is this intertwined phenomena which is referred to as soil-structure interaction, which is basically a result of different dynamic properties of soil and foundation (see for example Kramer (2014, Ch. 7.5)). The effect of SSI depends on the stiffness and mass of the soil, foundation and structure, with the geometry, and particularly embedment of the foundation, having considerable influence.

In general, SSI has a larger effect on heavy, stiff structures on soft soil than on light, flexible structures on stiff soil. In most cases the exclusion of SSI yields a conservative result, because the effect leads to reduction of seismic response (Wolf 1985). SSI should in all cases be considered for economical reasons, since over-conservatism leads to more expensive solutions. Research has also shown that, in some specific cases, excluding SSI is non-conservative, e.g. when dealing with relative displacements between structures (Mylonakis & Gazetas 2000).

5.2 Direct Method

A solution based on the direct method is an analysis of the full geometry of the problem in one single step. For example, this can be done with a computer program using the Finite Element Method as discussed in Section 4.1. Because the model comprises the full geometry, a large number of elements and nodes are included in the calculations. As discussed in several publications (e.g. Wolf (1995)), such a numerical analysis demands a powerful computer, and can be very time-consuming. The direct method is appropriate for non-linear analyses, because of integration of the whole system in one step.

5.3 Multi-Step Method

With a multi-step approach, the dynamic response is evaluated using several steps. There are various multi-step methods, amongst them is the *three-step method* which will be further elaborated in the following section. Common for the various multi-step approaches is to divide the soil-structure interaction into two important contributions: *kinematic interaction* and *inertial interaction*. The principle of superposition is used, thus a linear or an equivalent linear system is required (Kramer 2014, Ch.7.5.2).

5.3.1 The Three-Step Method

In the three-step method (see for example Elsabee (1973)), a fully rigid foundation is assumed. The kinematic interaction is assessed in one step, whereas the inertial interaction comprises of two steps. The method is illustrated in Figure 5.1, and can be summarized in the following steps:

1. Kinematic interaction analysis to find foundation input motion (FIM) as time history of translation and rotation.

2. First part of inertial interaction analysis: Determine dynamic stiffness (and damping) at the base of the structure, i.e. the *dynamic impedances* from foundation-soil interaction.

3. Second part of inertial interaction analysis: Modeling the structure alone with soil and foundation represented through springs (and dashpots) whose properties are found in Step 2. FIM from Step 1 is used to apply the inertial loads to the structure.

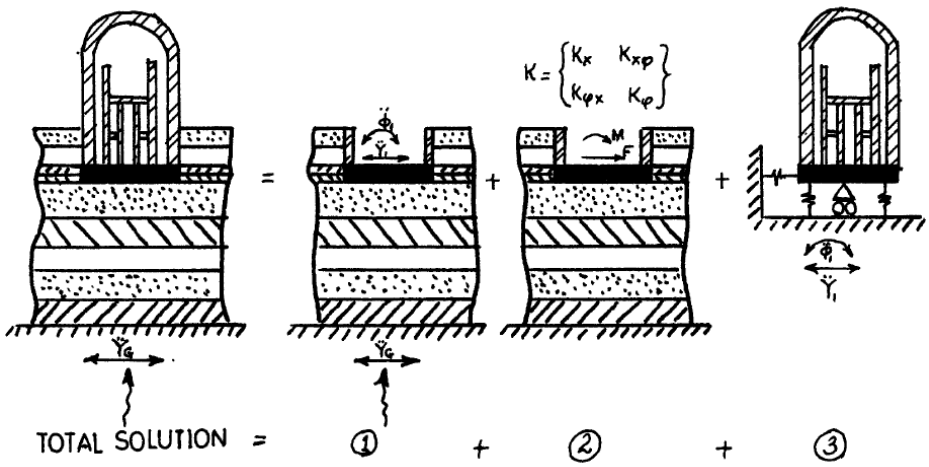

Figure 5.1: *Three-step method for SSI. Original drawing from Elsabee (1973).*

Step 1 - Kinematic Interaction Analysis

Kinematic interaction is relevant in situations where the stiffness of the foundation influences the movement of the soil, i.e. prevents the soil from attaining a free-field motion. The mass of the structure is excluded in this step of the analysis, the focus being on the stiffness of the foundation. The objective is to find the foundation movement relative to the base motion, i.e. the displacement because of kinematic interaction. This movement is often referred to as the *foundation input motion*. The interaction between soil and foundation will not always have an effect on the foundation, which is illustrated in Figure 5.2. An embedded foundation is shown for two cases of vertically propagating shear waves. Figure 5.2a show that rocking vibration might occur for certain frequencies, whereas other frequencies will suppress the rocking motion (Figure 5.2b).

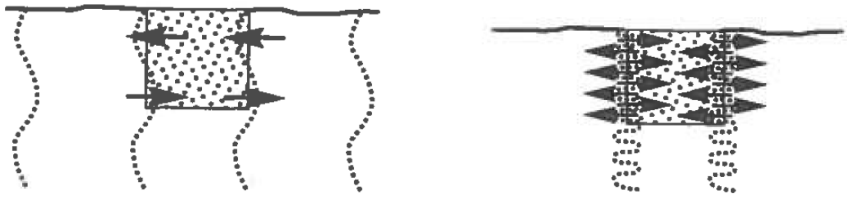

(a) *Lower frequency s-wave* ***(b)*** *Higher frequency s-wave*

Figure 5.2: *Rocking vibration of embedded foundation for s-waves of different frequencies. Figure from Kramer (2014, Ch. 7.5)*

One way of obtaining the foundation input motion, is through Fourier transformation of the input time history (see Section 2.4.1). By doing so, the time history is broken into a sum of multiple harmonic signals. This can be presented in the frequency-domain by a Fourier Amplitude Spectrum, where the amplitude of the signals are plotted versus frequency. The FIM is then obtained by multiplying the Fourier Amplitude Spectrum with *kinematic interaction transfer functions*. These functions translate an input ground motion to a foundation input motion by accounting for the kinematic interaction between foundation and soil. Transfer functions are frequency dependent, and can be defined depending on the foundation and soil properties (see for example Gazetas (1995)).

Step 2 - Obtaining Dynamic Impedances

The properties of the springs and dashpots, on which the structure will be founded on in Step 3, are obtained in Step 2. This is done by finding the dynamic impedance functions of the foundation-soil interaction.

Foundation impedance is related to the ratio between an imposed dynamic force and it's resulting displacement of the foundation (Gazetas 1983). The impedance function can be formulated in complex form by Eq. (5.1).

$$\mathbf{K_a}(\omega) = \mathbf{K_{a1}}(\omega) + i\mathbf{K_{a2}}(\omega) \tag{5.1}$$

where $a = v,\ h,\ r,\ hr,\ t,$ corresponds to vertical, horizontal, rotational, coupled horizontal/rotational and torsional impedances, respectively.

The real part of the equation refers to the stiffness and inertial effect on the impedance, and the imaginary part refers to the energy loss in the system. This energy loss is a result of radiation and material damping. Both the imaginary and real part is frequency dependent, the real part because of inertia and the imaginary part because of radiation damping. Soil stiffness and material damping are practically independent of frequency. Related to a 1-DOF system, the dynamic impedance function can be formulated as:

$$K = K(k + i\omega c_s) \tag{5.2}$$

where K is the static stiffness, ω_n is the natural frequency, $k = (1\text{-}\omega^2/\omega_n^2)$ and c_s=C/K.

As indicated by the equation, the dynamic impedance is a function of the static stiffness, and at zero frequency they are equal. The dynamic part of the impedance is related solely to inertial effects and damping. c_s and k vary with frequency, and their variation is very dependent on the mode of vibration, the soil profile, the soil properties, and the geometry of the problem (see for example Gazetas (1983) and Gazetas (1991)).

Often, Eq. (5.2) is rewritten to include the dimensionless frequency factor, $a_0 = \omega B/V_s$:

$$K = K(k + ia_0 c) \tag{5.3}$$

where $c = c_s(V_s/B)$.

To isolate the effect of material damping, Eq. (5.3) is often reformulated:

$$K = K(k + ia_0c)(1 + 2i\xi) \tag{5.4}$$

This equation is frequently used in dynamic analysis of foundation-soil interaction.

Another common term is the *dynamic flexibility* of the foundation, which is the inverse of the impedance, i.e. the ratio between displacements and imposed dynamic force. The dynamic flexibility coefficients can be found by inverting the impedance matrix, and vice versa.

Numerical results from previous research have revealed that various parameters effect the dynamic foundation response (see for example Gazetas (1983)):

- Depth-to-radius ratio
- Embedment-to-radius ratio
- Shape of foundation
- Dimensionless frequency factor
- Shear moduli ratio for upper and underlying soil layer.
- Poisson's ratio of soil layer
- Hysteretic damping ratio of soil layer
- Degree of anisotropy and inhomogeneity of soil layer
- Flexibility of foundation

The foundation impedance functions can be obtained both analytically and numerically, using continuum methods and discrete models, where the latter include finite element modeling. Closed-form solutions for various foundation geometries and soil idealizations are presented in Gazetas (1983) and Gazetas (1991), and will be discussed further in Section 5.3.3.

Step 3 - Inertial Interaction Analysis

Inertial interaction is present when the soil is compliant, i.e. when the dynamic forces from the acceleration of the structure's mass cause an additional deformation of the soil.

In Step 3 the structure is founded on frequency-dependent springs and dashpots replacing the soil, whose properties were found in Step 2. The applied base motion corresponds to the foundation input motion found in Step 1. One calculation procedure could be to apply the base motion stepwise for each frequency. Then the corresponding response at each frequency could be found. The springs and dashpots will have a different value for each frequency, resulting in different harmonic response functions for the structure. These functions could be added together, and through Fourier Transformation the total response of the structure is obtained in time domain. However, the use of frequency-dependent springs and dashpots are not always conducted in practical engineering. The use of static values for stiffnesses and damping (for certain selected frequencies representative for earthquakes) will be an effective and adequate simplification at low frequencies (Kaynia 2014).

5.3.2 Equations of Motion for Multi-step Method

A multi-step analysis can be summarized through the following sets of equations of motion. For the kinematic interaction:

$$\boldsymbol{M_{soil}\ddot{u}_{KI} + K^{*}u_{KI} = -M_{soil}\ddot{u}_{b}} \tag{5.5}$$

$\mathbf{M}_{soil}$ is the mass of the soil. Foundation and structure are, as mentioned, assumed massless for this part of the analysis. $\mathbf{u_{KI}}$ denotes the aforementioned *foundation input motion*.

The equations of motion from inertial interaction can be written:

$$\boldsymbol{M\ddot{u}_{II} + K^{*}u_{II} = -M_{(s+f)}(\ddot{u}_{KI} + \ddot{u}_{b})} \tag{5.6}$$

$\mathbf{M}_{(s+f)}$ is the mass of the foundation and structure, assuming massless

soil. $\mathbf{u_{II}}$ denotes the displacement due to inertial interaction.

The total response is the sum of the responses from kinematic interaction and the inertial interaction: $\mathbf{u}=\mathbf{u}_{KI}+\mathbf{u}_{II}$. The combination of the equations of motion for kinematic and inertial interaction can be gathered in the total equations of motion:

$$\begin{aligned} \boldsymbol{M_{soil}\ddot{u}_{KI} + M\ddot{u}_{II} + K^*(u_{KI} + u_{II}) =} \\ \boldsymbol{-(M_{soil} + M_{s+f})\ddot{u}_b - M_{(s+f)}\ddot{u}_{KI}} \end{aligned} \tag{5.7}$$

with $\mathbf{u}_{II} + \mathbf{u}_{KI} = \mathbf{u}$ and $\mathbf{M}_{(s+f)} + \mathbf{M}_{soil} = \mathbf{M}$ the above equation yields the well known equation of motion presented in Eq. (5.8):

$$\boldsymbol{M(\ddot{u}_{KI} + \ddot{u}_{II}) + K^*(u_{KI} + u_{II}) = -M\ddot{u}_b}$$

$$\Downarrow$$

$$\boldsymbol{M\ddot{u} + K^*u = -M\ddot{u}_b} \tag{5.8}$$

5.3.3 Closed-Form Solutions for Foundation Impedance

Closed-form solutions for foundation impedances are numerous, and varies for different foundation geometries and soil-idealizations. In Gazetas (1983) and Gazetas (1991), multiple closed-form solutions are presented, for surface and embedded foundations on homogeneous half-space, soil layer over bedrock, inhomogeneous soil profiles, to mention a few. To obtain stiffnesses of deep foundations, solutions for piles are used. In the following section, some relevant closed-form solutions for obtaining stiffnesses are presented.

Fully Embedded Foundation in Homogeneous Stratum-over-Bedrock

Solutions for a rigid, embedded, circular foundation in a homogeneous soil layer overlaying a bedrock (see Figure 5.3) are presented in Gazetas (1991). The solutions are based on the formulas for surface foundations overlying

an elastic half space, originally proposed by Veletsos & Wei (1971). The effect of embedment and stratum depth were derived by Elsabee (1973) and Kausel (1974) from these solutions, through parametric studies using numerical methods. Some unrealistic assumptions are laid to ground for the development of the solutions for the embedded foundation, which are emphasized in the report by Kausel (1974):

1. Sidewalls are assumed completely rigid

2. Walls are assumed perfectly welded to the surrounding soil, allowing no relative movement

3. Backfill soil properties and strength are assumed equal to the soil beneath the foundation.

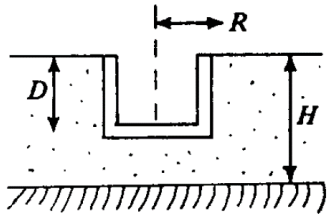

Figure 5.3: *Rigid embedded circular foundation profile as basis for theoretical foundation stiffness. Figure from Gazetas (1983).*

Static, horizontal stiffness of such a foundation is proposed calculated from Eq. (5.9).

$$K_{HH} = \frac{8GR}{2-\nu}\left(1+\frac{1}{2}\frac{R}{H}\right)\left(1+\frac{2}{3}\frac{D}{R}\right)\left(1+\frac{5}{4}\frac{D}{H}\right) \tag{5.9}$$

where G is the soil shear modulus, R is the radius of the foundation, D is the depth of embedment and H is the depth to rock, as indicated in Figure 5.3. The rotational stiffness is proposed calculated from Eq. (5.10).

$$K_{\theta\theta} = \frac{8GR^3}{3(1-\nu)}\left(1+\frac{1}{6}\frac{R}{H}\right)\left(1+2\frac{D}{R}\right)\left(1+0,7\frac{D}{H}\right) \tag{5.10}$$

Coupled rotational-horizontal stiffness is given by:

$$K_{H\theta} = 0,4K_{HH}D \tag{5.11}$$

The range of validity of these functions is $\frac{D}{R} < 2$ and $\frac{D}{H} \leq 0,5$.

As presented in Gazetas (1983), foundation impedance is dependent on frequency. Figure 5.4 illustrate the variation of stiffness and damping coefficients, with frequency and embedment.

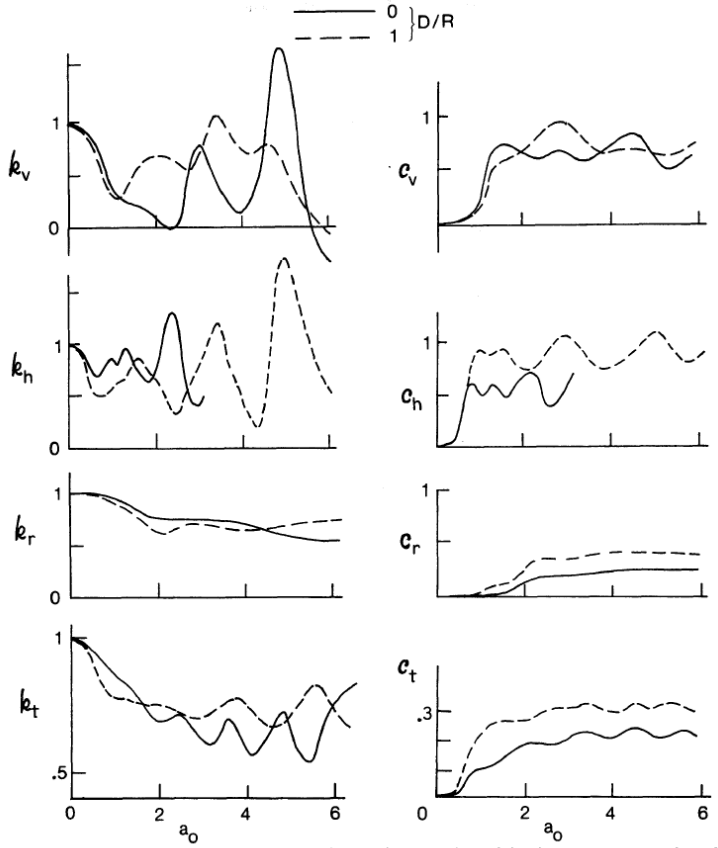

Figure 19. Effect of embedment on dynamic coefficients of a rigid cylindrical foundation on stratum-over-bedrock (H/R = 3, ν = 1/3, ξ = 0.05)[33, 88, 90]

Figure 5.4: *Frequency dependence of stiffness coefficients. Figure from Gazetas (1983).*

Surface Foundation on Inhomogeneous Soil Deposit

The closed-form solution described in the previous section assumes a homogeneous soil layer over bedrock, i.e. a soil layer with constant shear modulus. In most cases, this assumption is somewhat inaccurate, because the stiffness usually increase with depth (Gazetas 1991). As mentioned previously in Section 3.3.1, the shear modulus of a soil at small strains is dependent on the confining pressure. In Gazetas (1991) a deposit with a shear modulus function as Eq. (5.12) is proposed as a suitable representation for saturated normally and slightly overconsolidated clays.

$$G = G_0 \left(1 + \frac{z}{B}\right) \tag{5.12}$$

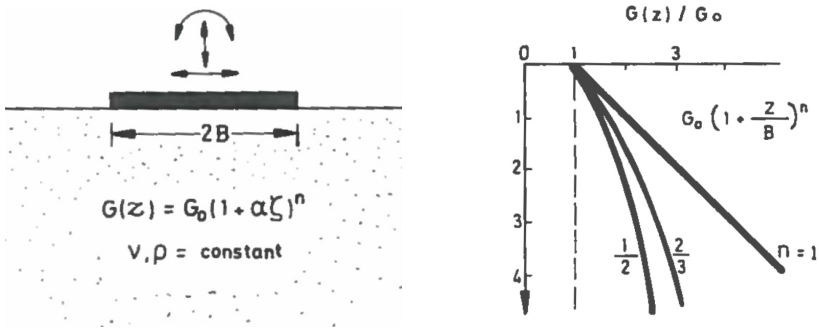

(a) *Geometry of foundation* ***(b)*** *Increasing shear modulus with depth*

Figure 5.5: *Square surface foundation on deep inhomogeneous deposit. Figure from Gazetas (1991)*

Further, the article presents closed-form solutions for the stiffnesses of square, surface foundations for various vibration modes (see Figure 5.5a). However, Gazetas (1991) emphasizes that the following solutions are merely crude estimates:

$$K_x \simeq \frac{9}{2-\nu} G_0 B \left(1 + \frac{1}{2}\alpha\right)^n \tag{5.13}$$

$$K_{ry} \simeq \frac{3,6}{1-\nu} G_0 B^3 \left(1 + \frac{1}{3}\alpha\right)^n \tag{5.14}$$

α and n are inhomogeneity parameters, the former being the slope of the shear modulus curve and the latter being the power controlling the type of curve. For example, given a linearly increasing shear modulus profile, n = 1.

Short, Rigid Pile in Weaker Rock

Carter & Kulhawy (1992) have developed closed-form expressions for predicting the behavior of shafts in rock. Amongst their research, solutions for surface translational and rotational displacement of short, rigid shafts socketed into weaker rock are presented (see Figure 5.6).

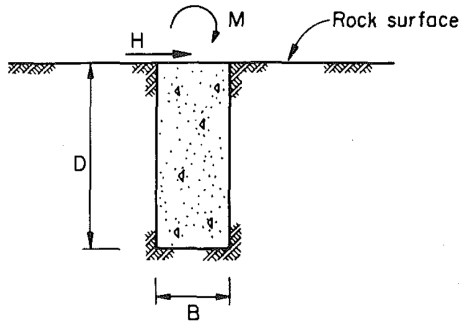

Figure 5.6: *Geometry for rock-socketed shaft*

Solutions were derived from finite element analyses presented in Carter & Kulhawy (1988). Their results show that when the shaft is relatively rigid compared to the rock, the displacements will depend solely on the ratio between embedment-to-diameter (slenderness ratio) and the Poisson's ratio of the rock. The shaft is assumed rigid when:

$$\frac{D}{B} \leq 0,05 \left(\frac{E_e}{G^*}\right)^{1/2} \tag{5.15}$$

where D is the embedment, B is the diameter of the shaft, E_e is the

effective Young's modulus of the shaft and G^* is the rock's equivalent shear modulus.

The translational and rotational displacements are proposed calculated from Eq. (H.8) and Eq. (5.17), respectively.

$$u = 0,4\left(\frac{H}{GB}\right)\left(\frac{2D}{B}\right)^{-1/3} + 0,3\left(\frac{M}{GB^2}\right)\left(\frac{2D}{B}\right)^{-7/8} \tag{5.16}$$

$$\theta = 0,3\left(\frac{H}{GB^2}\right)\left(\frac{2D}{B}\right)^{-7/8} + 0,8\left(\frac{M}{GB^3}\right)\left(\frac{2D}{B}\right)^{-5/3} \tag{5.17}$$

This indicates that the shaft top flexibilities can be calculated from:

$$f_{xx} = \left(\frac{0,4}{GB}\right)\left(\frac{2D}{B}\right)^{-1/3} \tag{5.18}$$

$$f_{x\theta} = f_{\theta x} = \left(\frac{0,3}{GB^2}\right)\left(\frac{2D}{B}\right)^{-7/8} \tag{5.19}$$

$$f_{\theta\theta} = \left(\frac{0,8}{GB^3}\right)\left(\frac{2D}{B}\right)^{-5/3} \tag{5.20}$$

The above equations are validated for:

$$1 \leq \frac{D}{B} \leq 10$$

and

$$\frac{E_e}{E_r} \geq 1$$

Part II

Analyses, Results and Discussion

Chapter 6

Introduction of Case Study

This chapter presents a hypothetical case study of a single suction caisson foundation provided by Multiconsult AS. First, the background material for the case study is presented. The next section is dedicated to the finite element program Plaxis 3D 2012, used for numerical analyses. Then, the Excel implemented program EERA is introduced, followed by a brief presentation of selected material models.

6.1 Background Material

A hypothetic case study of a single suction caisson foundation was provided by Multiconsult AS. Soil parameters and geometry of the problem is given. The objective with the case study is to analyze the response of a superstructure supported by a single suction caisson foundation, with regards to earthquake loading. The superstructure consists of a manifold with pipe connections supported by a frame construction, similar to the one in Figure 6.1. An illustration of the simplified geometry is shown in Figure 6.2. Design soil parameters is provided by Multiconsult AS, and are summarized in Table 6.1. For input to the earthquake analysis, Professor Amir Kaynia kindly provided a time history (see Figure 6.3),

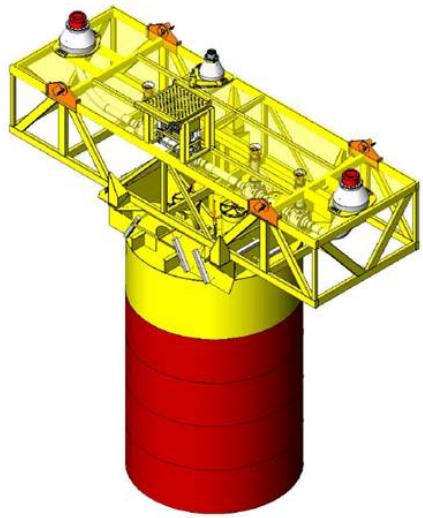

Figure 6.1: *Example of a manifold structure with a single suction caisson foundation. Figure borrowed from Aker Solutions.*

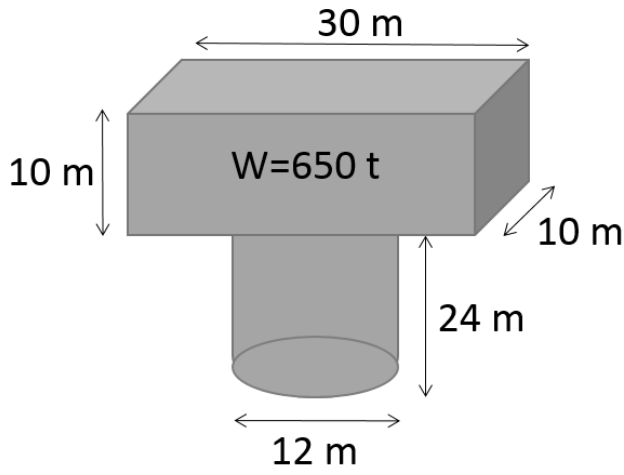

Figure 6.2: *Simplified geometry of single suction caisson and manifold superstructure*

representative for an earthquake with a return period of 500 years in the Bengal Bay area.

6.1.1 Comments on Provided Material Properties

Preliminary numerical analyses with provided geometry and material properties presented in Section 6.1 was performed. The result revealed that the given shear wave velocity profile required a very high degree of element discretization. Combined with the relatively large dimensions of the problem, the finite element analysis would demand a huge computational effort regarding disk space and time. In order to complete the analysis in due time, the shear wave velocity was increased for the whole soil layer. The altered profile is illustrated in Appendix C.

6.2 Plaxis 3D 2012

Plaxis 3D 2012 is a three-dimensional finite element program developed specifically for use in geotechnical engineering and design. It is possible to choose from a range of predefined material models, developed for describing soil behavior.

6.2.1 Interfaces

In order to model the interaction between soil and structural units, it is necessary to define interfaces. This is done to specify a lower strength between a structure surface and the soil. Without interface elements, no slipping or gapping is allowed, which in most cases is a non-physical assumption for the interaction between structure and soil. A strength and stiffness reduction is introduced through the use of interfaces, by the parameter R_{inter}. The interface material model is elastic-plastic and based on the Coulomb failure criterion (Plaxis 2013a).

Table 6.1: *Material properties (Athanasiu 2014)*

PROVIDED MATERIAL PROPERTIES		
Property	Unit	Design value
γ'_{sub}	kN/m^3	0m < z < 12m: 4.5
		12m < z < 20m: 5.5
s_u	kPa	z < 2m: 1 + 1.3z
		2m < z: 3.6 + 1.7(z-2)
G_{max}	MPa	1.54z
PI	%	80-85
OCR	–	0m < z < 4m: 1.4
		4m < z < 10m: 1.2
		10m < z < 20m: 1.0
c	kPa	1.0
ϕ'	°	28
R_{inter}	–	0.5

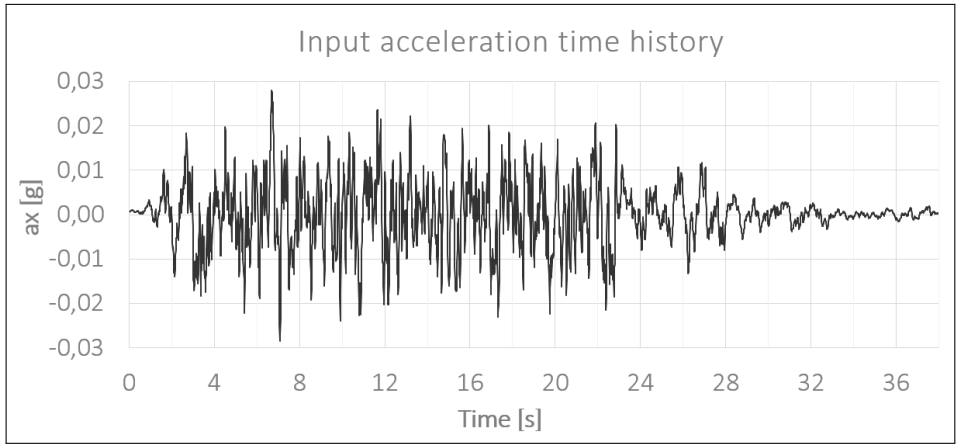

Figure 6.3: *Time history of acceleration for return period of 500 years*

6.2.2 Standard Boundary Conditions

Plaxis assigns general fixities to the boundaries of the model, illustrated in Figure 6.4. As shown, the vertical boundaries are by default free in the z-direction (vertical) and the lateral direction parallel to the boundary plane, while fixed in the normal direction to the boundary. The top surface is by default free in all directions, while the bottom surface is completely fixed. The standard fixities may be overruled by user-defined boundary conditions, and can be turned off completely if wanted. User-defined boundary conditions can be implemented by defining surface prescribed displacements (Plaxis 2013*a*, Ch. 7).

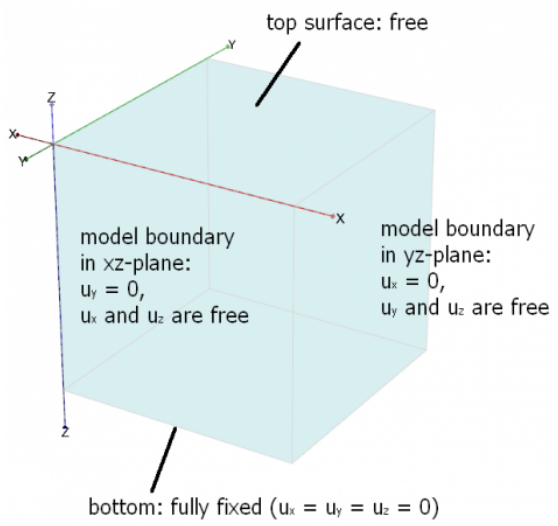

Figure 6.4: *Default Fixities in Plaxis 3D. Figure from (Plaxis 2013*a*).*

6.2.3 Elements used in Plaxis 3D

The soil body is modeled by 10-noded tetrahedral elements with 4 integration points (Gauss points). For plates 6-noded triangular elements are used, with 3 Gauss points. Interfaces are modeled with 12-noded triangular elements, where 2-and-2 nodes are in pairs. The paired nodes are in

zero distance from each other. Interface elements consist of 3 Gauss-points, and are similar to the plate elements except for the double nodes. Beams are discretized in 3-noded line elements, with 6 DOFs per node (Plaxis 2013*a*). Some of the element types used in Plaxis 3D are illustrated in Figure 6.5.

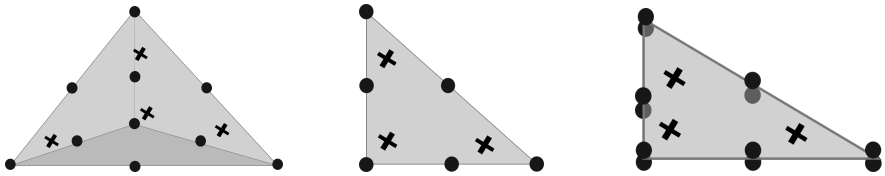

(a) *Soil element* ***(b)*** *Plate element* ***(c)*** *Interface element*

Figure 6.5: *Elements used in the FE program Plaxis 3D. Nodes are indicated as dots, while crosses represent Gauss points. Figures inspired by Plaxis (2012)*

6.2.4 Dynamic Modeling in Plaxis 3D

As discussed in Section 4.2, certain considerations must be made when modeling a dynamic problem with the finite element method. In the following subsections, these considerations are discussed for the application in Plaxis 3D.

Boundary Conditions

Default settings in Plaxis for dynamic modeling is the use of viscous dampers on vertical boundaries. These dampers are modeled as dashpots, introduced in order to absorb the stress waves hitting the boundary. Figure 6.6 is an illustration of the default settings, indicating the dampers connected to shear- and normal stress absorption. Plaxis (2013*b*, Ch. 7.4) define the viscous dampers as follows:

$$\sigma_n = -C_1 \rho V_p \dot{u}_x \tag{6.1a}$$

$$\tau = -C_2 \rho V_s \dot{u}_y \tag{6.1b}$$

This corresponds to the viscous boundary dampers originally proposed by Lysmer & Kuhlemeyer (1969). The coefficients C_1 and C_2 can be manually defined, and determine the amount of absorption. As a default, $C_1 = C_2 = 1$.

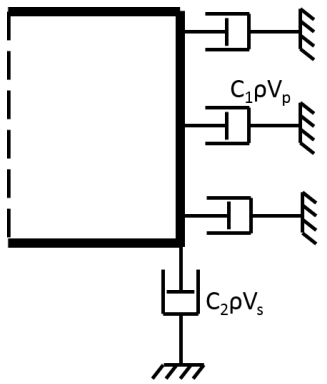

Figure 6.6: *Simplified illustration of the viscous boundary dashpots implemented in Plaxis.*

Element Discretization

The discretization of the mesh is highly dependent on the given problem, as discussed in Section 4.2. In Plaxis, the mass matrix is lumped, thus it is recommended that the maximum element dimension is less than $\lambda/8$, where λ is the shortest wave length of interest. The element dimensions can be adjusted when generating the mesh.

Time Discretization

Plaxis 3D uses implicit time integration based on the Newmark scheme. $\alpha = 0.25$ and $\beta = 0.5$ are the default settings of the Newmark coefficients. The time step in dynamic analyses should not be larger than the *critical time step*, which depends on the frequency and element dimensions as explained in Section 4.2 (Plaxis 2012). The critical time step (δt) governs

the number of steps (m×n) necessary in dynamic calculations, as indicated in Eq. 6.2. In the equation, Δt is the total dynamic time interval.

$$m \times n = \frac{\Delta t}{\delta t} \tag{6.2}$$

Material Damping

Damping may be included in the Plaxis model by a non-linear constitutive soil model that has some sort of material damping implemented. As suggested by Plaxis (2013*a*, Ch. 6.1.1) the use of Soft Soil Creep or Hardening Soil Small model will include a viscous damping phenomena resembling material damping. In the HS Small model, hysteretic behavior is included, but damping depends on the amplitude of the strain cycles. Thus, for small amplitudes the model hardly provide any damping at all. Real soils exhibit viscous damping even at very small vibrations (Plaxis 2013*a*, Ch. 6.1.1).

Damping can be defined for each material through Rayleigh damping, independent of material model. Rayleigh damping assumes that the damping matrix ($\mathbf{C}$) of the system is proportional to the mass matrix ($\mathbf{M}$) and stiffness matrix ($\mathbf{K}$) (Chopra 1995, Ch. 11.4):

$$\mathbf{C} = \alpha\mathbf{M} + \beta\mathbf{K} \tag{6.3}$$

The Rayleigh damping model is illustrated in Figure 6.7. As shown, the mass governs the damping of low frequencies, while the stiffness contributes mostly to damping at high frequencies. Thus, α (a_0 in the figure) is the damping coefficient related to low frequencies, and β (a_1 in the figure) is related to high frequencies. The coefficients can be manually adjusted, in order to obtain a best fit for the given problem.

Geometric Damping

Geometric, or radiation, damping can be modeled using viscous boundaries.

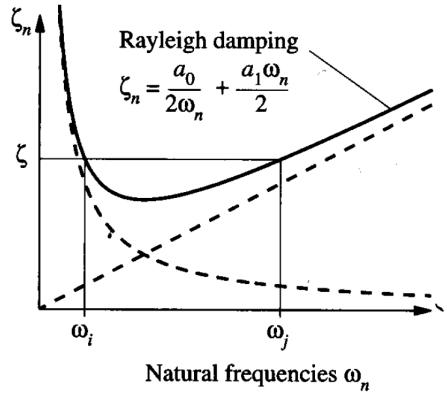

Figure 6.7: *The Rayleigh damping model as illustrated in Chopra (1995, Ch. 11.4)*

6.3 EERA - Equivalent-linear Earthquake Response Analysis

EERA is a computer program integrated in Excel, for calculation of one-dimensional, equivalent-linear earthquake response of layered soil deposits. It was developed in 1998, and is based on the same concepts as the program SHAKE; one of the first computer programs developed for simulating soil amplification of ground motions (Bardet et al. 2000). SHAKE, and EERA, is based on the assumption that non-linear cyclic soil behavior can be adequately simulated using equivalent-linear modeling concepts.

As described in Section 3.3, the equivalent-linear model describes the material behavior through defined modulus reduction curves and damping ratio curves which are dependent on shear strain. As an input to EERA, such curves must be specified for each material.

To determine values of the effective shear modulus (G) and damping ratios (ξ) for each layer, EERA uses iterative procedures. Initial values of G and ξ are found from the specified material curves. These values are used as input for calculating the ground response. From the response, the maximum shear strain amplitude is found. This amplitude is further mod-

ified with a certain factor dependent on the magnitude of the earthquake. Often a factor of 0.65 is used, to yield an effective shear strain amplitude (Christian et al. 1977, Ch.20-4). At last, the corresponding values of G and ξ are found from the effective shear strain. This procedure is repeated until the differences between the output and input G and ξ are lower than a predefined limit in all layers (Bardet et al. 2000). The procedure is illustrated in Figure 6.8.

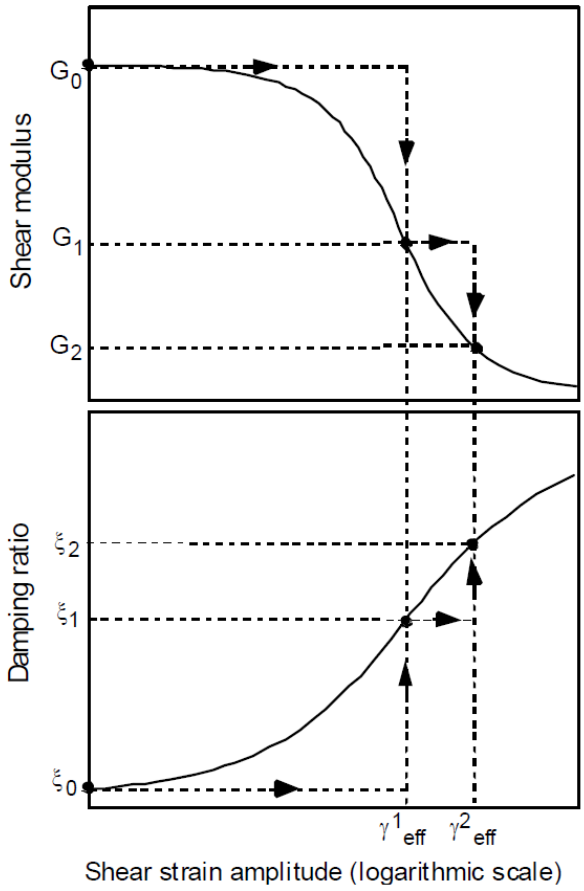

Figure 6.8: *Iteration procedure in equivalent-linear analysis implemented in EERA and SHAKE. Figure from Bardet et al. (2000).*

6.4 Material Models

To describe the behavior of a certain material in finite element modeling, material models must be defined. There are various predefined material models, developed especially for capturing the peculiar characteristics of soil. Common for the soil models is that they are described by a *yield surface*, which indicates failure in the material. In relation to material models we use the terms *elastic* and *plastic* range and strains. Elastic strains are reversible, which means the material will return to it's initial state. On the contrary, plastic strains lead to permanent deformation of the material. Real soils will experience a combination of plastic and elastic strains, at times simultaneously (Nordal 2013, Ch. 6). In the following section the Linear Elastic material model will be described, together with the Mohr-Coulomb model, which is one of the simplest material models used for soil.

6.4.1 Linear Elastic Material Model

Using a linear elastic material model, the stiffness-strength relationship is given by Hooke's law, demonstrated for one dimension in Eq. (6.4).

$$E = \frac{\sigma_y}{\varepsilon_y} \tag{6.4}$$

The material model has no yield limit defined, and all deformations are thus purely elastic.

6.4.2 Mohr-Coulomb Material Model

One of the simplest material models for soil is the Mohr-Coulomb model, which is *linear elastic perfectly-plastic*. The model assumes linear elastic behavior up to a certain stress ratio. For stress increments above this limit ratio, the soil will act perfectly-plastic (Nordal 2013). See Figure 6.9 for the stress-strain relationship in one dimension. The yield surface is given by the MC failure criterion presented in Eq. (6.5). This states that the

maximum shear stress, τ_{max} the soil can withstand depends on the normal stress level in the soil (Emdal et al. 2006):

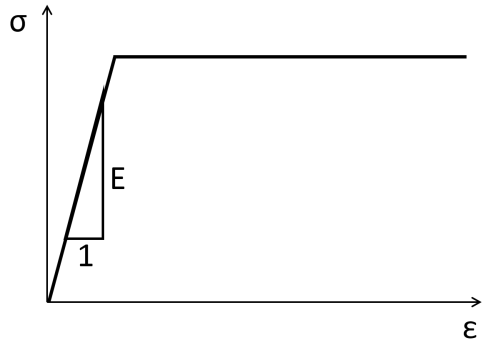

Figure 6.9: *The Mohr-Coulomb elastic-perfectly plastic stress-strain relationship illustrated for one dimension.*

$$\tau = (\sigma'_f + a) \times \tan\phi \tag{6.5}$$

where σ'_f is the normal stress, a is the attraction and $\tan\phi$ is the friction angle in the soil. The yield surface is a straight line in the τ-σ plane, with the inclination of $\tan\phi$, as demonstrated in Figure 6.10.

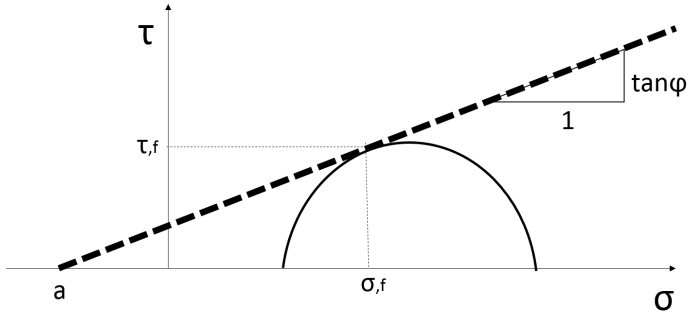

Figure 6.10: *The Mohr-Coulomb yield surface*

Chapter 7

Description of Analyses

The main objective with this chapter is to explore the differences between methods of analyzing soil-structure interaction, namely a *direct* and a *multi-step* analysis. The second objective is to investigate the influence of boundary conditions.

First, the development of two finite element models using Plaxis 3D is described, together with simple verification analyses. Material properties used in numerical analyses in the case study, are then presented. Following, is a description of each analysis performed in relation to the case study: Free-field response analysis and the direct and multi-step analysis.

To compare the SSI analyses, the maximum acceleration of the superstructure will be used.

7.1 Verification of Finite Element Models

In this section, two modeling concepts for dynamic analyses in Plaxis 3D are presented. The only thing separating these concepts is the conditions for the vertical boundaries. As presented in Section 4.2, defining proper boundary conditions is of uttermost importance in dynamic modeling,

since different wave propagation problems will have different boundary criteria.

Simple verification tests for investigation of the performance of the individual modeling concepts are described below. The soil amplification obtained from the models are compared with theory. Results are presented in Section 8.1.

7.1.1 Description of Preliminary Finite Element Models

For calculation efficiency, the model geometry used for development of the modeling concept is much smaller than what the case study implies. In addition, the soil properties have been simplified. However, the methodology is the same, regardless of geometry and material properties. The soil was modeled as a linear elastic material, using 10-noded tetrahedral elements as described in Section 6.2. Material properties are presented in Table 7.1.

Model 1

Model 1 has *elementary* vertical boundaries in the YZ-plane, as discussed in Section 4.2. A surface prescribed displacement is defined at these boundaries, with free displacement in the X-direction. Fixed displacements (=0) was defined for the Y- and Z-direction. Viscous dashpots are not defined for any of the boundaries. For the bottom boundary (XZ-plane), this setting is analogue to a situation where a rigid bedrock is present. The finite element model with Model 1 conditions is illustrated in Figure 7.1.

The hypothesis for Model 1, is that free displacements in the X-direction will allow an input shear wave (SH) to propagate undisturbed from bottom to top of the soil layer.

Model 2

Model 2 is based on the use of *viscous* boundaries, as discussed in Section 6.2.4. Viscous dampers are thus defined at the boundaries, for normal and tangential incident waves. Default values were used for the dashpot coefficients (C_1=C_2=1). As for Model 1, the bottom boundary is not prescribed viscous dashpots. The boundary conditions in Model 2 correspond to the default Plaxis settings for dynamic problems, and are suggested for seismic analyses (Plaxis 2013*c*, Plaxis Support 2014). The finite element model with Model 2 conditions is illustrated in Figure 7.2.

A reason for implementing Model 2 would be to simulate radiation damping of potential stress waves that reach the boundaries. Radiation damping of the input signal will not be necessary to model, consisting solely of vertical waves. However, if a foundation is introduced (as it will be, later in the case study), the vibration of this component will generate body and surface waves which ideally should be absorbed at the boundaries.

7.1.2 Initial Testing with Single Harmonic Signal

As an initial verification, a harmonic signal corresponding to the soil layer's 1^{st} eigenfrequency is applied both models. The signal is applied as a surface prescribed displacement in the horizontal (X) direction on the bottom boundary. Meanwhile, displacements in Y- and Z are fixed. The 1^{st} eigenfrequency is found by using Eq. (3.11).

The soil layer is discretized in the necessary amount of elements for the given frequency, according to the principles presented in Section 6.2.4. To make sure the models reach a steady-state vibration, the time interval is chosen as $15T$ (i.e. fifteen times the period of the input signal). A Rayleigh damping ratio of 5% is defined for the 1^{st} eigenfrequency.

Amplification of the signal is registered in the control point at the top of the soil layer. For comparison, the theoretical amplification factor is calculated using Eq. (3.7).

Table 7.1: *Material properties for preliminary finite element models*

SOIL PROPERTIES - PRELIMINARY MODELS					
Material Model	Behavior	γ $[kN/m^3]$	V_s [m/s]	ν [–]	ξ [%]
Linear-elastic	Drained	20	50	0,3	5

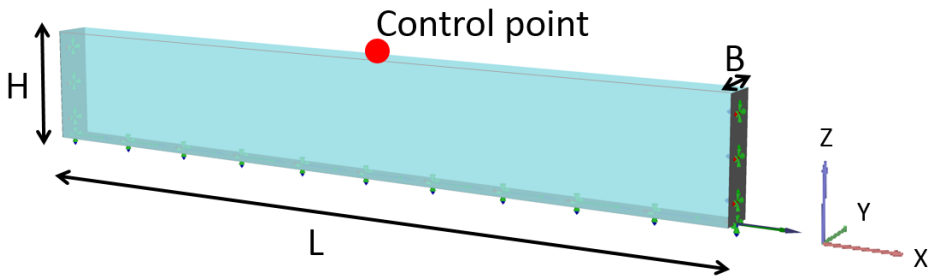

Figure 7.1: *Geometry of Model 1, with prescribed boundary conditions indicated for bottom and sides. The indicated dimensions are L=100 m, H=15 m, B=2m.*

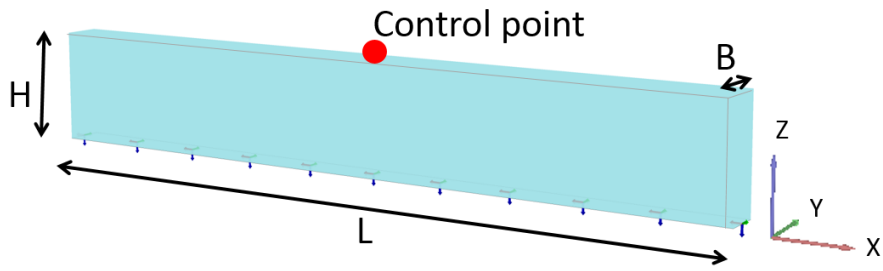

Figure 7.2: *Geometry of Model 2, with prescribed boundary condition at bottom. The indicated dimensions are L=100 m, H=15 m, B=2m.*

7.1.3 Soil Amplification Function

Only Model 1 is tested further, to verify if it can reproduce the soil layer's complete theoretical amplification function. It is necessary to find the soil amplification at various frequencies, thus a total of 10 frequencies are analyzed. For each of the 10 frequencies, the model is discretized in to the necessary amount of elements and time steps, according to the principles presented in Section 6.2.4. To make sure the model reach a steady-state, the time interval is chosen as $15T$ (i.e. fifteen times the period of the input signal). A Rayleigh damping ratio of ξ=5% is defined for each specific frequency. Amplification of the signals is registered in the control point at the top of the soil layer.

7.2 Material Properties for Case Study

In this section, the material properties for the case study are presented.

7.2.1 Soil and Interfaces

The soil is modeled as a linear-elastic material with increasing shear stiffness with depth, overlying rigid bedrock. To be able to vary the element dimension in the soil volume (for calculation efficiency), the model is divided into *four* layers, with *two* different material properties. Element discretization of the individual layers is based on a chosen "cut-off"frequency of 10 Hz. Calculations of corresponding element dimensions are shown in Appendix D. As mentioned in Section 8.1.3, it was necessary to increase the overall shear wave velocity. The resulting shear wave velocity profile is shown in Appendix C, where the aforementioned layering is indicated. Material properties for the soil are otherwise presented in Table 7.2.

A Rayleigh damping ratio of 5% is defined at 1 Hz and 10 Hz. The assumption of 5% damping is reasonable for the design earthquake, having a peak acceleration as low as 0,03g (see for example Whitman (1976)). Radiation damping is only defined for Model 2, with the use of viscous boundaries.

Interfaces are modeled on the inside, outside and bottom of the caisson, allowing relative movement between soil and foundation. The bottom interface is given a roughness equal to 1, because it ultimately describes relative movement between soil and soil. Material properties for the interfaces are displayed in Table 7.2.

Table 7.3 presents the additional soil parameters used for non-linear analysis.

7.2.2 Foundation and Structure

The caisson foundation geometry is modeled as a half cylinder with a lid and an open end, like a bucket turned up-side-down. Walls of caisson and lid are modeled as plate elements. The plates are given a unit weight corresponding to common properties of steel. For simplicity the foundation is assumed completely rigid, in order to more easily compare the numerical solution to closed-form solutions in the multi-step analysis. Due to this, the walls and lid are made extra thick (1 m), thus the unit weight is adjusted accordingly. Material properties for the suction caisson plates are shown in Table 7.4.

For a simplified representation of a manifold frame-construction, the superstructure is modeled as a completely rigid horizontal beam. The beam is given a mass distribution corresponding to half the design dry weight of the superstructure, including added hydraulic mass. The beam is placed at the assumed center of gravity (midpoint of structure), at a height h above the top of the foundation. To appropriately model inertial effects resulting from rocking of the superstructure, the wingspan, L, of the beam is set equal to the proper length of the manifold construction (L=30 m).

The caisson foundation and superstructure is given a fixed connection, using a completely rigid, massless, vertical beam. In order to distribute the load of the superstructure on the foundation top plate, multiple massless, rigid connection beams are modeled. They are placed in a fan on the caisson lid. Material properties for structure and connection beams are shown in Table 7.4.

Table 7.2: *Material properties for linear finite element analysis*

SOIL PROPERTIES FOR LINEAR ANALYSIS			
Material	Layer 1 (0-12 m)	Layer 2-4 (12-50m)	Interface
Material Model	Linear-elastic	Linear-elastic	Linear-elastic
Type of behavior	Undrained C	Undrained C	Undrained C
γ $[kN/m^3]$	14.5	15.5	15.5
E [kPa] [1]	177 000 + 4604z	232 300 + 4604z	232 300 + 4604z
ν [–]	0.495	0.495	0.495
ξ [%]	5	5	5
R [–] [2]	0.5	0.5	1.0

[1] E increases with depth. Reference depths: *Layer 1* z=0, *Layer 2-4* z=-12 m.

[2] Interfaces describing relative movement between soil and structure follows properties of adjacent soil (R=0.5).

Table 7.3: *Material properties for non-linear finite element analyses*

SOIL PROPERTIES FOR NON-LINEAR ANALYSIS				
Material	Mohr-1 (0-2 m)	Mohr-2 (2-12m)	Mohr-3 (12-38m)	Interface
Material Model	Mohr-Coloumb	Mohr-Coloumb	Mohr-Coloumb	Mohr-Coloumb
Type of behavior	Undrained C	Undrained C	Undrained C	Undrained C
γ $[kN/m^3]$	14.5	15.5	15.5	15.5
E [kPa] [1]	177 000 + 4604z	186 200 + 4604z	232 300 + 4604z	232 300 + 4604z
ν [–]	0.495	0.495	0.495	0.495
ξ [%]	5	5	5	5
R [–] [2]	0.5	0.5	0.5	1.0

[1] E increases with depth. Reference depths: *Mohr-1* z=0, *Mohr-2* z=-2 m, *Mohr-3* z=-12 m.

[2] Interfaces describing relative movement between soil and structure follows properties of adjacent soil (R=0.5).

Table 7.4: *Material properties for plates and beams in FE-model*

MATERIAL PROPERTIES - PLATES & BEAMS				
Material	Top plate	Wall plate	Structure beam	Support beams
Material Model	Linear-elastic	Linear-elastic	Linear-elastic	Linear-elastic
Type of behavior	Isotropic	Isotropic	–	–
$\gamma\ [kN/m^3]$	4.06 [1]	2.52 [1]	2.216 [2]	0
$d\ [m]$	1.0	1.0	–	–
$A\ [m^2]$ [3]	–	–	50	$10 \cdot 10^4$
$I_3 = I_2\ [m^4]$ [4]	–	–	$100 \cdot 10^9$	$100 \cdot 10^9$
$E\ [kPa]$	$210\ \cdot 10^9$	$210\ \cdot 10^9$	$210\ \cdot 10^6$	$210\ \cdot 10^6$
ν [–]	0	0	–	–

[1] Thickness adjusted to 1 meter, thus unit weight is reduced to fit total weight of plate.

[2] Unit weight is reduced to fit half the total weight of the superstructure and added mass (325 tons).

[3] Large value (for support beam) to ensure rigidity.

[4] Large value to ensure rigidity.

7.3 Free-Field Response Analysis

The free-field response was modeled using both Model 1 and Model 2 boundary conditions. A thin slice of the soil was modeled, with boundaries located far away from the control point. See Figure 7.3 for the geometry of the models used for free-field analysis. In addition, the design earthquake (Figure 6.3) was used as input in EERA, for comparison with the finite element analyses.

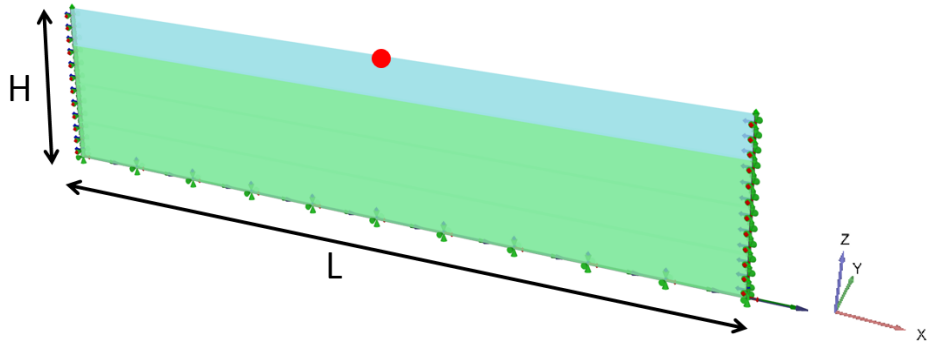

(a) *Model 1*

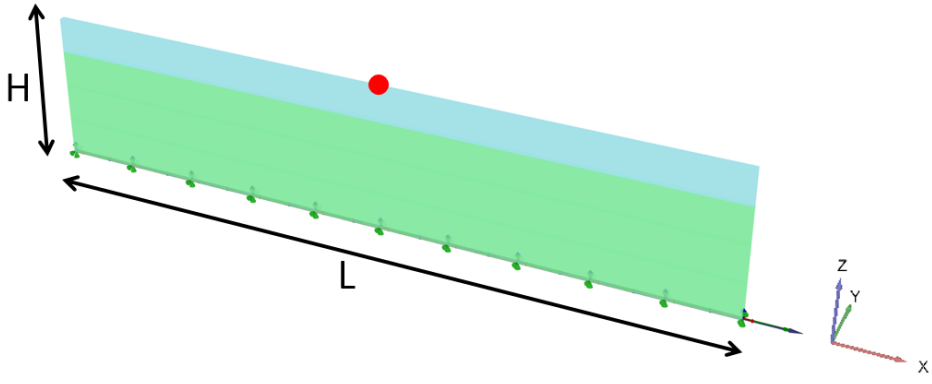

(b) *Model 2*

Figure 7.3: *Geometry of finite element models for free field response analysis. Dimensions are L=240 m, H=50 m and B=2 m. The control point is indicated as a red dot.*

7.4 Direct Analysis

Using the direct method of analysis, the whole problem (with full geometry) is analyzed in one step using a dynamic finite element model. The objective with the analysis is to obtain the acceleration response of the superstructure. Both linear and non-linear analyses are performed. The latter solely for indicating geometric non-linearities.

7.4.1 Linear Analysis

The linear analysis is performed in Plaxis 3D using both models. The calculation scheme in Plaxis is summarized in Table E.1 in Appendix E).

Geometry used in the finite element analysis is shown in Figure 7.5 and 7.6 for Model 1 and Model 2, respectively. Element discretization is indicated in Figure 7.4. Due to symmetry regarding geometry and load conditions, only half of the numerical domain is modeled, which is advantageous for calculation efficiency. Geometry of foundation and superstructure is shown in Figure 7.7. The input acceleration time history is applied on the model as prescribed displacements on the bottom boundary.

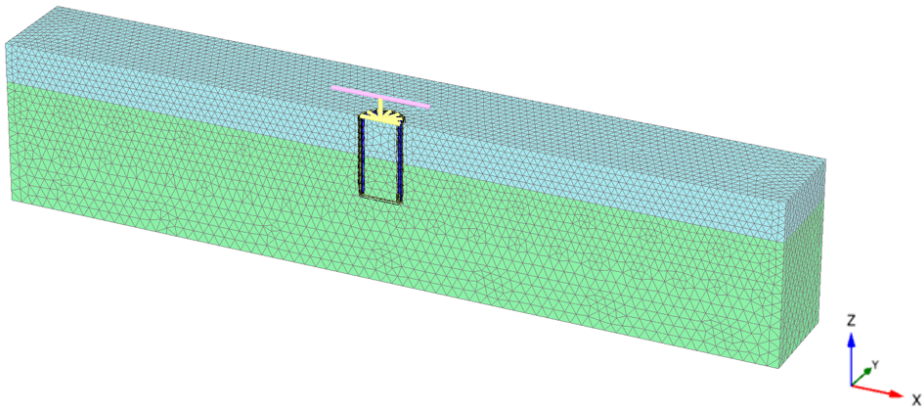

Figure 7.4: *Mesh of finite element model for direct analysis.*

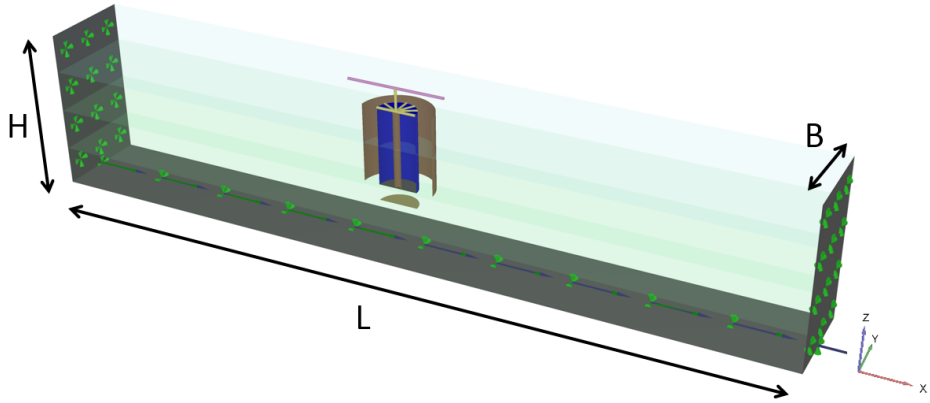

Figure 7.5: *Model 1 geometry for direct analysis. Dimensions are L=240 m, H=50 m and B=30 m.*

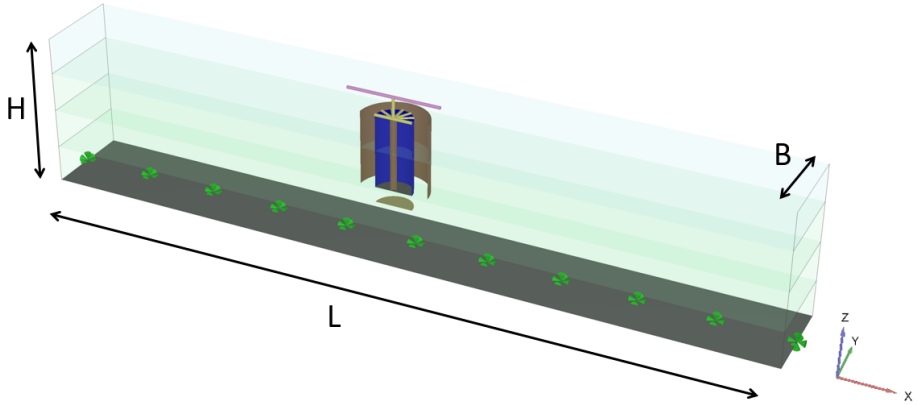

Figure 7.6: *Model 2 geometry for direct analysis. Dimensions are L=240 m, H=50 m and B=30 m.*

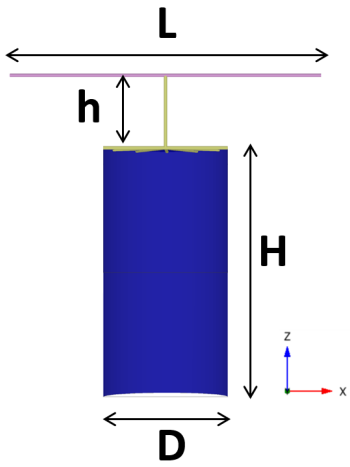

Figure 7.7: *Geometry of foundation and structure in numerical model. Dimensions are L=30 m, H=24 m, D=12 m and h=7 m.*

7.4.2 Non-linear Analysis

In most cases, real soil does not act linear, and for evaluation of a soil's capacity non-linearity must be considered. A non-linear analysis is performed to investigate the local effects around the caisson foundation. The analysis is done using the concept of Model 1. Introducing a non-linear material model using these boundary conditions, demands some adjustments to the geometry. A core of Mohr-Coulomb material is therefore placed around the suction caisson, maintaining linear-elastic material on both sides for support. This enables evaluation of non-linear behavior in the vicinity of the foundation.

Altered geometry is presented in Figure 7.8, with the mesh shown in Figure 7.9. Material properties for the foundation and structure are the same as for the linear analysis (Table 7.4). The properties used for the linear-elastic supports are also the same as before (Table 7.2), while the Mohr-Coulomb core is given the material properties presented in Table 7.3.

The calculation scheme is the same as for the linear analysis (Table E.1 in Appendix E).

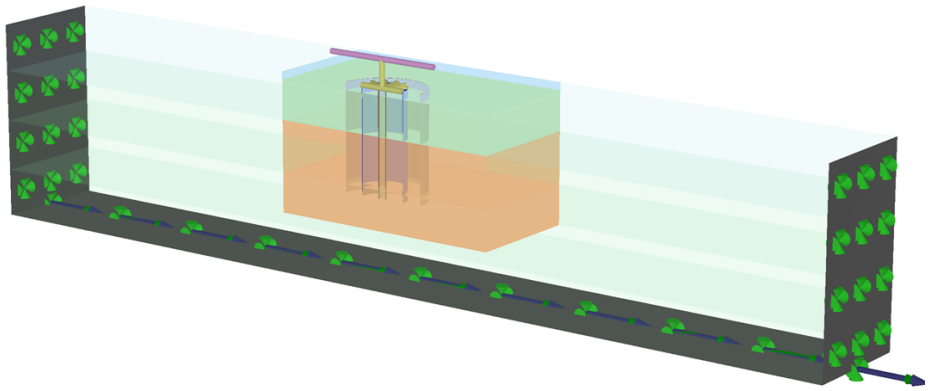

Figure 7.8: *Geometry used in nonlinear direct analysis. Dimensions are the same as for the linear analysis.*

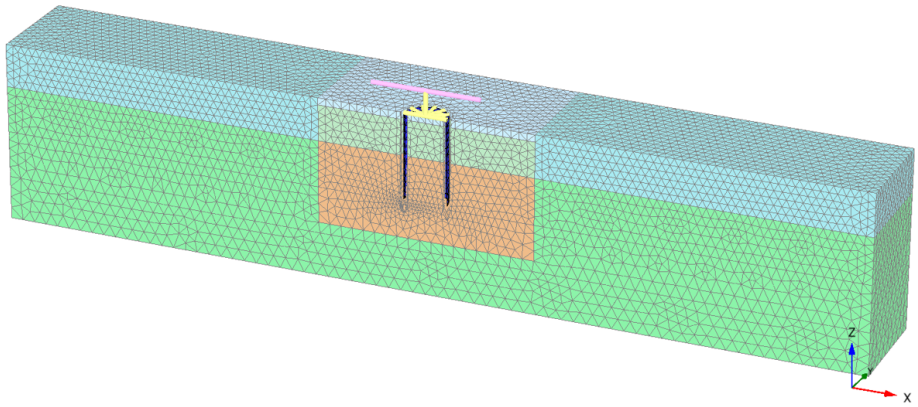

Figure 7.9: *Mesh used in nonlinear direct analysis.*

7.5 Multi-Step Analysis

Following the principles presented in Section 5.3.1, the multi-step analysis is divided into the following three steps:

- Step 1: Evaluating the kinematic interaction between soil and foundation. Obtaining foundation input motion, as the response of the suction caisson.
- Step 2: Calculating foundation stiffness.
- Step 3: Evaluating inertial interaction between soil-foundation-structure.

Each step is further elaborated in the following sections.

7.5.1 Step 1: Kinematic Interaction

The objective with this step is to evaluate the kinematic interaction between soil and foundation. The following are to be obtained through Step 1:

- Time history for horizontal acceleration of foundation
- Time history for rotational acceleration of foundation
- Response spectrum for horizontal acceleration for various damping ratios ξ=2% - 10%.

To find the response of the suction caisson, a dynamic numerical analysis is performed using the concept of Model 1. Geometry is almost identical to the one analyzed using the linear direct approach (Figure 7.5). However, the superstructure is removed, leaving the suction caisson foundation and the soil. Material properties, input signal and so on, are defined exactly as for the linear direct analysis (Table 7.2 and 7.4). The calculation scheme is basically the same, but for the *Structure*-phase being removed (see Table E.1 in Appendix E).

The response spectrum analysis of the obtained foundation response is performed in Matlab® using the script shown in Appendix K.

7.5.2 Step 2: Foundation Impedance

The objective of this step is to find the foundation stiffnesses (K_{HH}, $K_{\theta\theta}$, $K_{H\theta}$), which will be used as an input for the calculations in Step 3. The stiffness coefficient are found through a *static* finite element analysis.

The geometry of the model is shown in Figure 7.11, while the material properties are the same as before (see Table 7.2 and 7.4). Being a static analysis, default boundary conditions are used. However, boundaries are placed at a certain distance from the suction caisson foundation to avoid disturbances. The utilized mesh is shown in Figure 7.15. A sensitivity analysis regarding mesh refinement is presented in Section 7.6.

To find the resistance against rotation and translation (i.e. the stiffness coefficients), two load sets are applied to the model, shown in Figure 7.10. Load set 1 is a translational load (Figure 7.10a). Load set 2 is a moment load, induced by two vertical loads: One on each edge of the caisson top in opposite directions (Figure 7.10b). Positive translation is defined in the positive x direction, while positive rotation is defined as counterclockwise.

From the analyses, flexibility coefficients are obtained. The stiffness matrix is then calculated as the inverse of the flexibility matrix:

$$\begin{bmatrix} K_{HH} & K_{H\theta} \\ K_{H\theta} & K_{\theta\theta} \end{bmatrix} = \frac{1}{f_1 f_4 - f_2 f_3} \begin{bmatrix} f_4 & -f_2 \\ -f_3 & f_1 \end{bmatrix} \tag{7.1}$$

Foundation Stiffness from Closed-Form Solutions

For comparison with the numerical solution of foundation stiffness, two different closed-form solutions were also used:

1. Solution for a fully embedded foundation in a homogeneous soil stratum-over-bedrock, as presented in Section 5.3.3.

2. Solution for a short, rigid shaft in weaker rock, as presented in Section 5.3.3.

For simplicity, the shear modulus at the soil surface was used as representative for the soil layer, and used as input for the closed-form solutions.

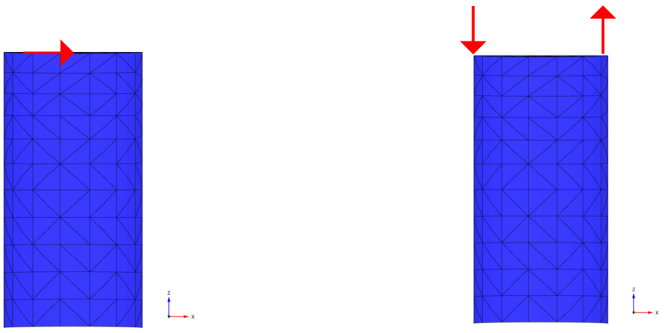

(a) Load set 1 *(b) Load set 2*

Figure 7.10: *Load sets used in static analysis*

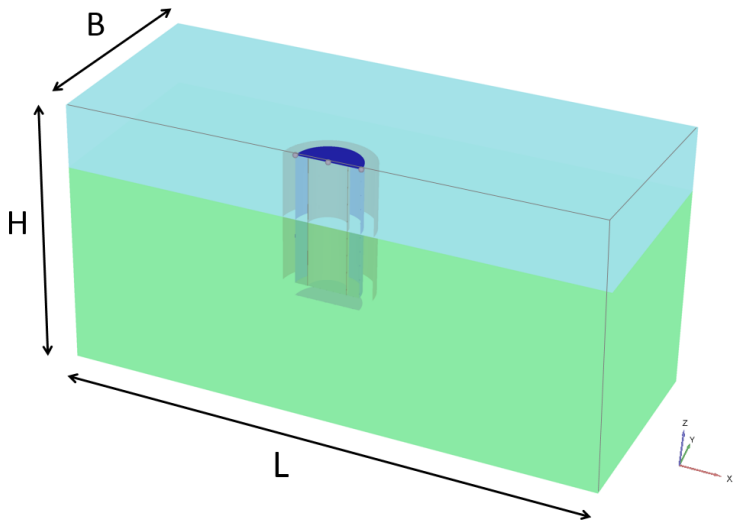

Figure 7.11: *Geometry of the static finite element model used in Step 2 of the multistep analysis. Dimensions are L=100 m, H=50 m and B=30 m.*

7.5.3 Step 3: Inertial Interaction

To evaluate inertial interaction and obtaining the seismic response of the superstructure in a simplified way, the eigenfrequencies of the structure will be found. When knowing the eigenfrequencies, the damping-dependent maximum acceleration of the structure can be found from the different response spectra obtained in Step 1. The following are to be obtained through Step 3:

- Eigenfrequencies (ω_1, ω_2) of superstructure
- Maximum horizontal response (a_x) of superstructure from response spectrum

To perform Step 3 analytically, the foundation-soil system is represented by springs and dashpots as shown in Figure 7.12.

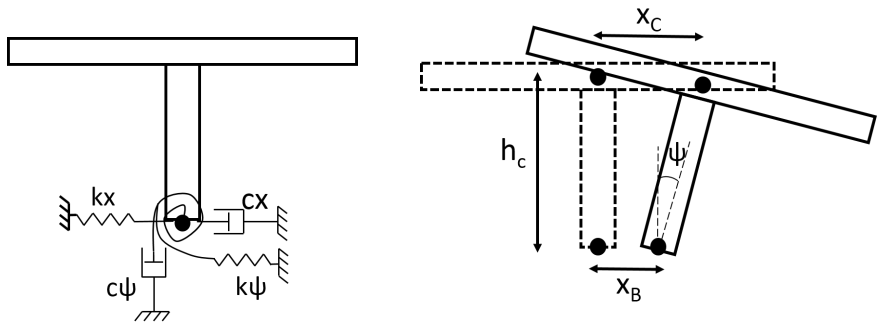

(a) *Simplified geometry* ***(b)*** *Dynamic deformation of system*

Figure 7.12: *Simplified system for calculation of the structure's eigenfrequencies.*

7.6 Mesh Sensitivity in Static Analysis

Finite element solutions are often mesh sensitive. Therefore is can be necessary to check for which degree of discretization the solution converges. The mesh at convergence should be used for analyses.

With a coarser mesh, a stiffer solution is expected. The discretized region should have increased ability to move with an increased number of elements, and should thus be more flexible with a mesh of high refinement.

A static sensitivity analysis is performed with three different mesh options in Plaxis 3D: *Coarse*, *Medium* and *Fine*. Table 7.5 displays the element discretization for the various analyses, and Figures 7.13 – 7.16 displays the corresponding mesh of foundation and soil. The analysis corresponds to Step 2 in the multi-step analysis, thus material properties and calculation scheme are exactly the same.

Table 7.5: *Mesh sensitivity study - Static analysis*

MESH SENSITIVITY STUDY			
Refinement	# of soil elements	# of nodes	Average element size
Coarse	11 449	17 836	4.18
Medium	85 638	123 164	1.53
Fine	253 185	356 124	0.89

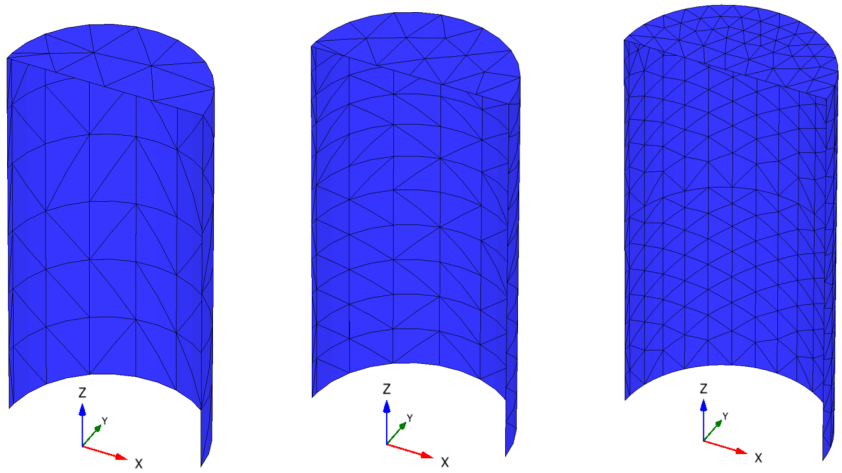

(a) Coarse mesh *(b) Medium Mesh* *(c) Fine mesh*

Figure 7.13: *Different element discretization of the suction caisson for sensitivity analysis.*

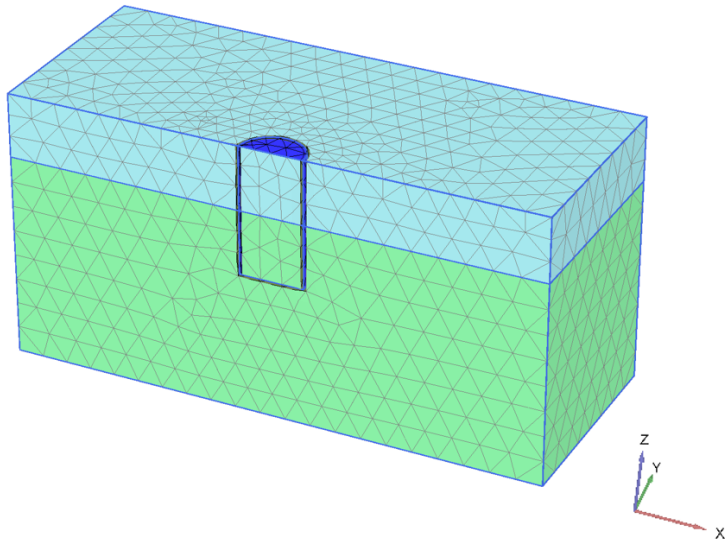

Figure 7.14: *Coarse element discretization of soil volume*

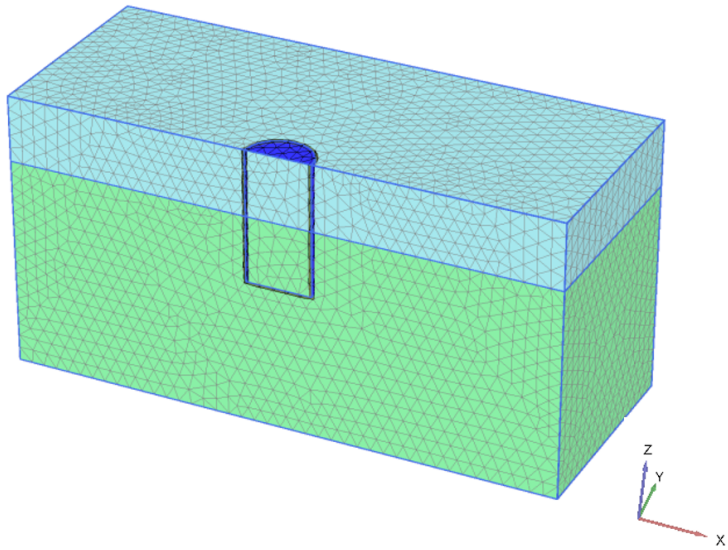

Figure 7.15: *Medium element discretization of soil volume*

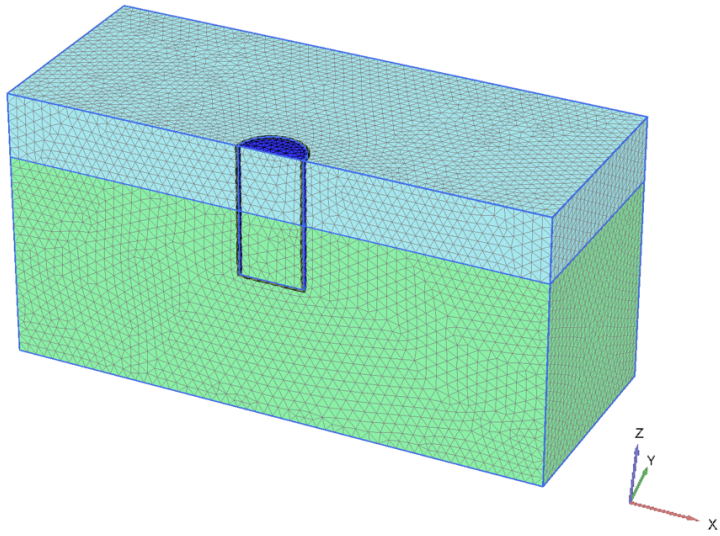

Figure 7.16: *Fine element discretization of soil volume*

Chapter 8

Results and Discussion of Analyses

In this chapter, results are presented for all the aforementioned analyses. There will be an ongoing discussion of the results for each analysis. An overall discussion with comparison of the soil-structure interaction analyses are presented at the end of the chapter.

8.1 Verification of Finite Element Models

In this section, the results from simple verification tests performed on the two modeling concepts are presented.

8.1.1 Initial Testing with Single Harmonic Signal

The soil layer's eigenfrequencies and theoretical amplification factors were calculated, and are indicated in Table 8.1. Results of the analyses are summarized in Figure 8.1, where response in the control point is plotted versus time.

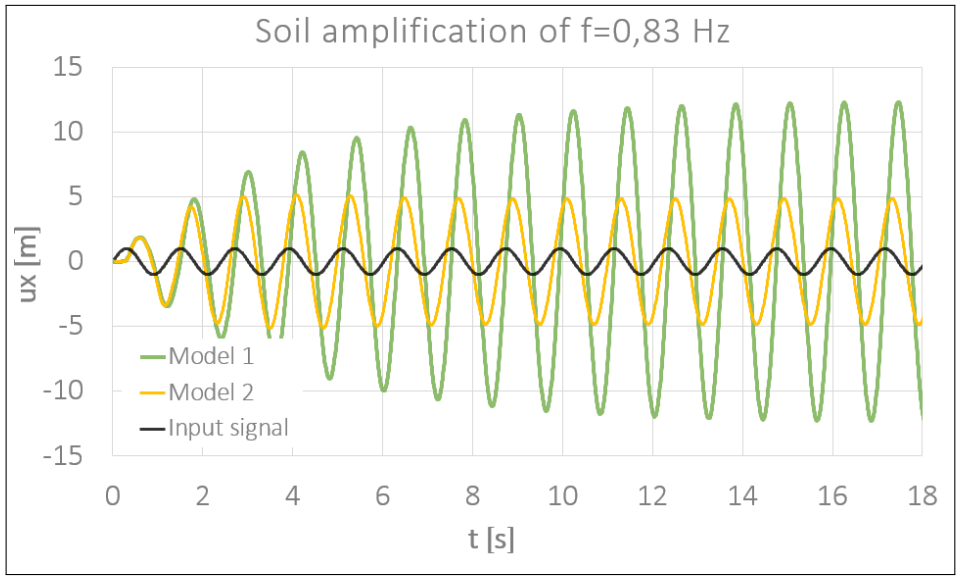

Figure 8.1: *Amplification of input signal in Plaxis 3D, using two different boundary conditions*

Table 8.1: *Theoretical amplification factors*

AMPLIFICATION FACTORS			
Mode, n	ω_n [rad/s]	f_n [Hz]	F(ω)
1	5.2	0.83	12.73
2	15.7	2.50	4.24
3	26.2	4.17	2.55
4	36.7	5.83	1.82
5	47.1	7.50	1.41
6	57.6	9.17	1.16

8.1.2 Soil Amplification Function

In Appendix I, the soil response in the control point is plotted for the first three eigenfrequencies using Model 1. The same procedure was performed to obtain the amplification at the intermediate frequencies. Figure 8.2 show the soil layer's eigenmodes as reproduced by Model 1. Steady-state amplification of the input signals through the soil layer was registered. The complete result from the analyses is presented in Figure 8.3.

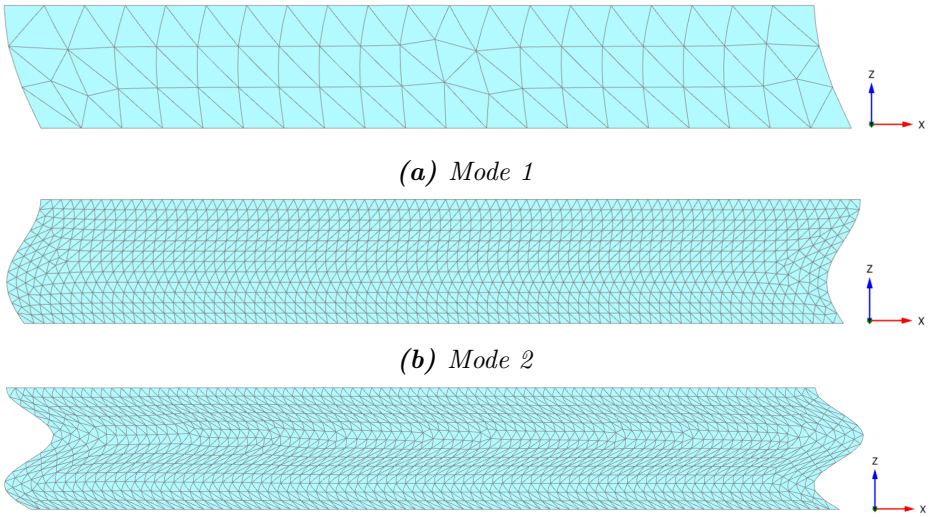

(a) Mode 1

(b) Mode 2

(c) Mode 3

Figure 8.2: *Soil layer's eigenmodes reproduced by Model 1*

8.1.3 Discussion of Result

Initial Testing with Single Harmonic Signal

As shown in Figure 8.1, Model 1 amplifies the 0.83 Hz-signal in a very satisfactory way compared to theory, obtaining a amplification factor of around 12.5. Model 2, however, produces quite an overdamped output signal, obtaining a factor of only 5.0. This should not be very surprising

regarding the nature of the vertically propagating SH wave. If the wave motion is restricted on the boundaries, the amplitude would simply not be able to develop in the same manner as for an unrestricted wave motion.

Soil Amplification Function

As indicated in Figure 8.3, the resulting soil amplification using Model 1 compares very well to the theoretical amplification function. The first three natural modes of the soil layer, was adequately reproduced by Model 1. As indicated in Figure 8.2, they correspond very well to the natural mode shapes presented in Section 3.4.2.

With basis in the results, the boundary concept of Model 1 seems to yield quite adequate results regarding reproduction of soil amplification function.

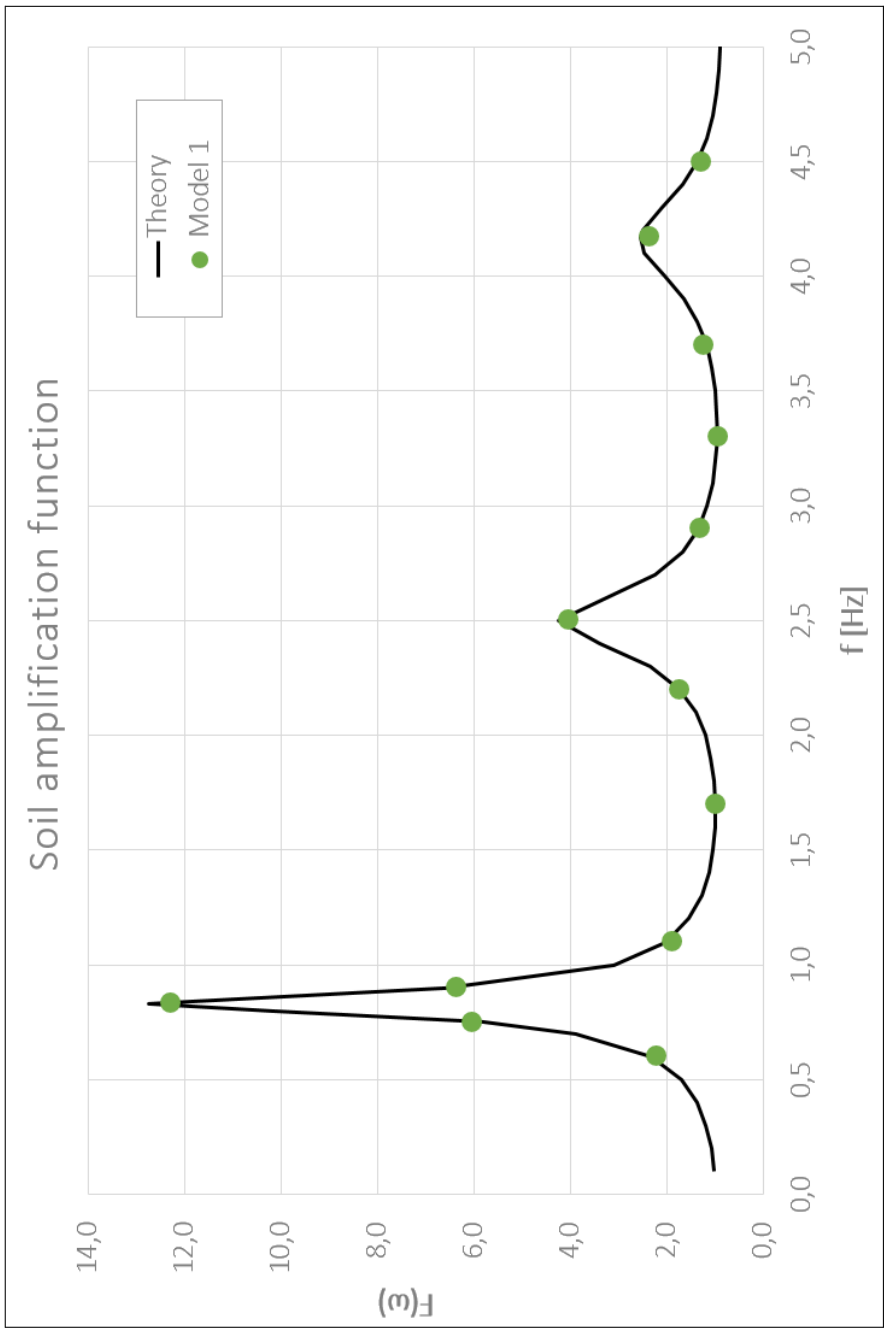

Figure 8.3: *Amplification function calculated in Excel and from Plaxis*

8.2 Free-Field Response Analysis

8.2.1 Model 1

The free-field response of the control point in Model 1 is plotted in Figure 8.4. Corresponding (exaggerated) deformation pattern of the soil slice is shown in Figure 8.5.

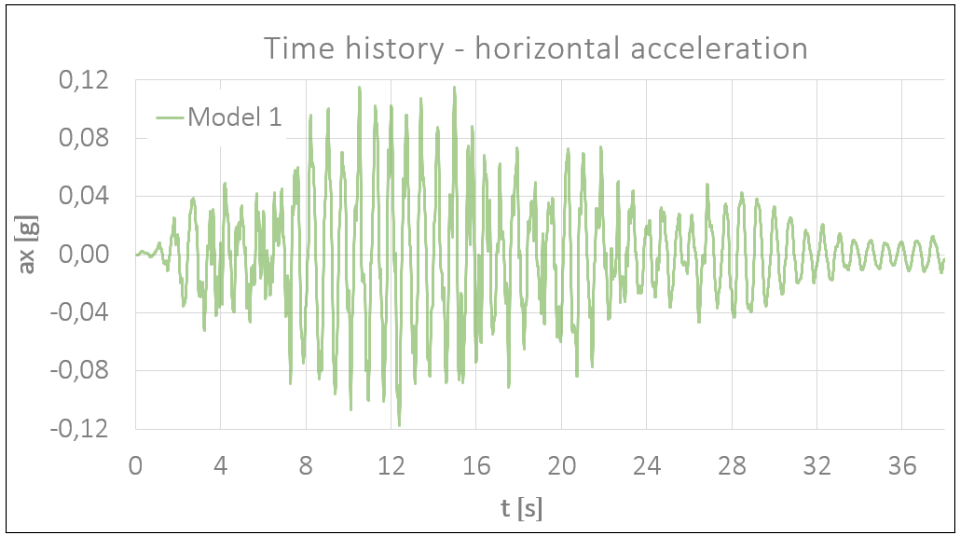

Figure 8.4: *Free-field response using Model 1*

8.2.2 Model 2

The free-field response of the control point in Model 2 is plotted in Figure 8.6. Corresponding (exaggerated) deformation pattern of the soil slice is shown in Figure 8.7.

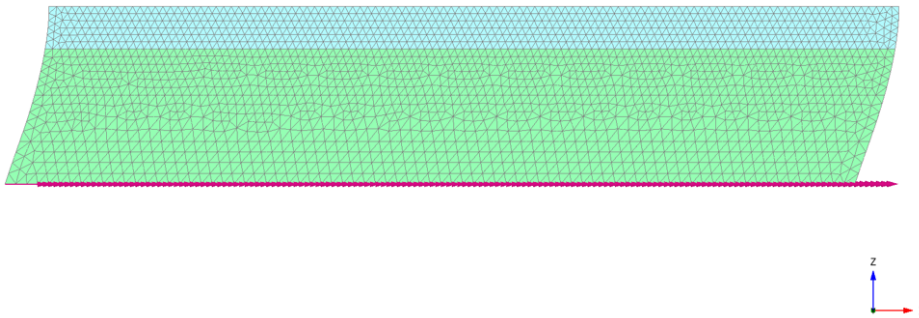

Figure 8.5: *Deformation pattern for free-field response using Model 1*

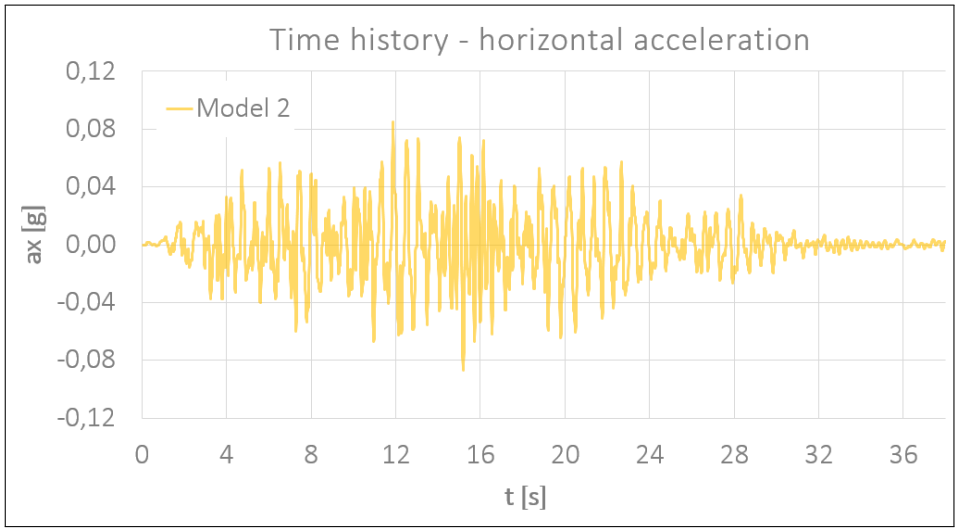

Figure 8.6: *Free-field response using Model 2*

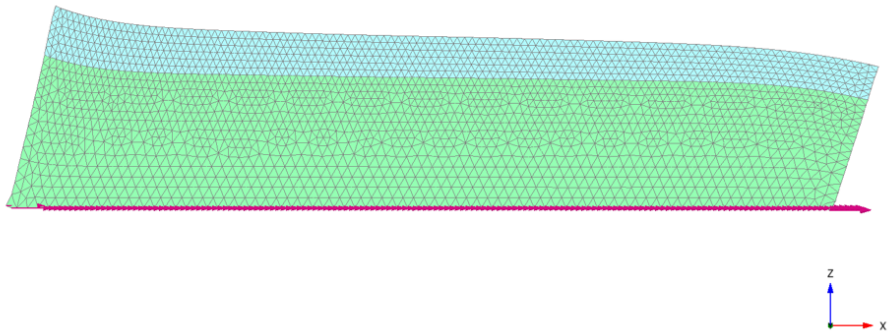

Figure 8.7: *Deformation pattern for free-field response using Model 2*

8.2.3 EERA

The free-field response obtained from EERA is plotted in Figure 8.8. The soil amplification function is plotted in Figure 8.9, indicating the soil layer's natural frequencies. Additional results from the analysis in EERA is gathered in Appendix J.1.

8.2.4 Comparison of Results

In Figure 8.10 the horizontal free-field response from Model 1 is compared to EERA. The same is done for Model 2 in Figure 8.11. In Figure 8.12, the response spectrum is plotted for the free-field response of the control point in Model 1, Model 2 and for EERA, using a damping ratio of 5 %. The response spectrum analysis was performed using the Matlab® script in Appendix K.

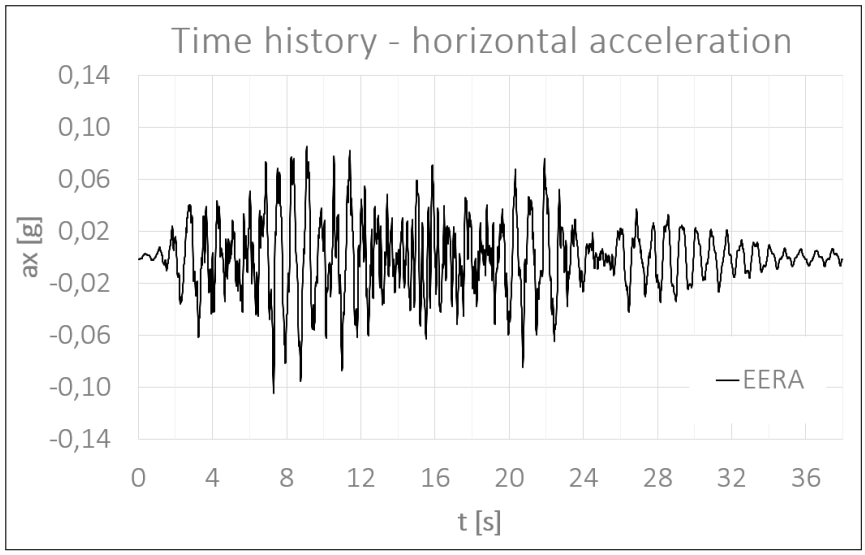

Figure 8.8: *Free-field response using EERA*

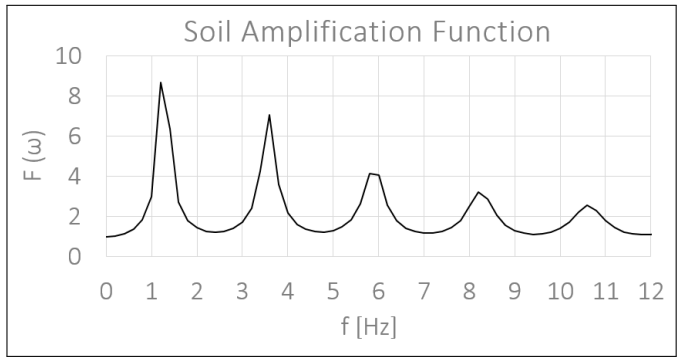

Figure 8.9: *Soil amplification function obtained from EERA*

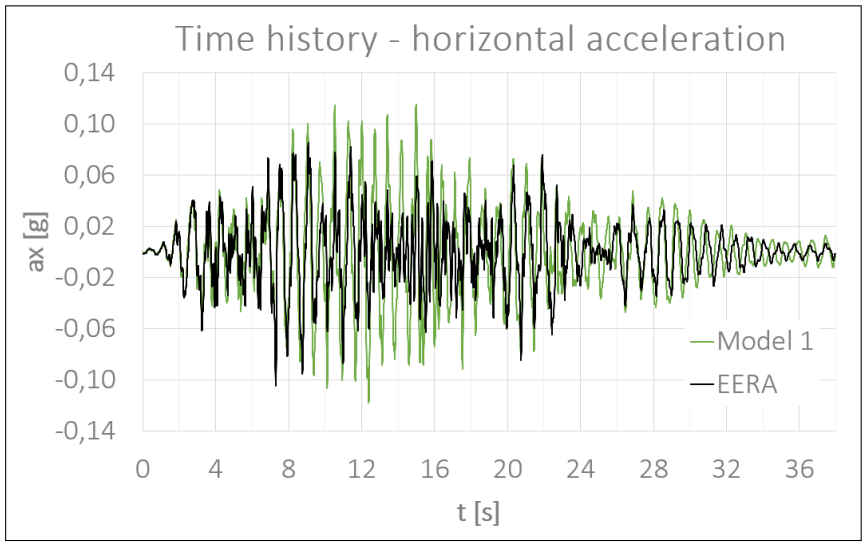

Figure 8.10: *Free-field response to seismic input signal in Model 1 and EERA*

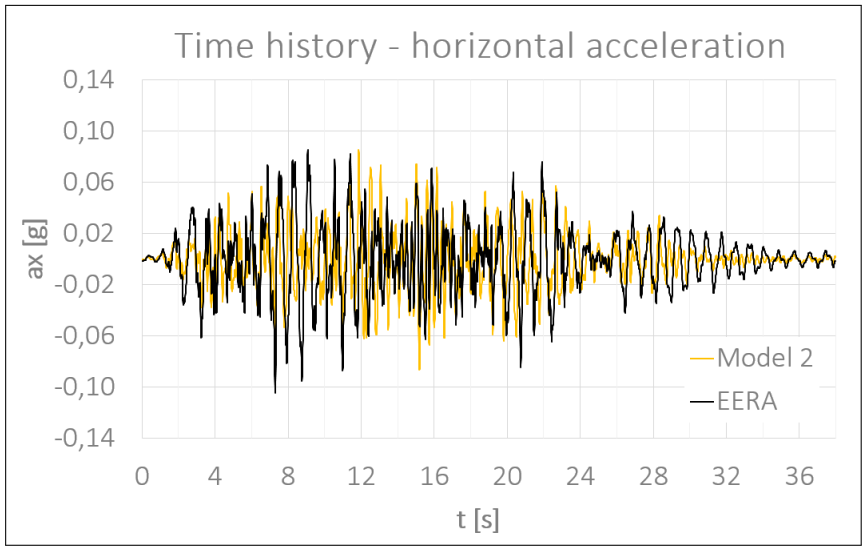

Figure 8.11: *Free-field response to seismic input signal in Model 2 and EERA*

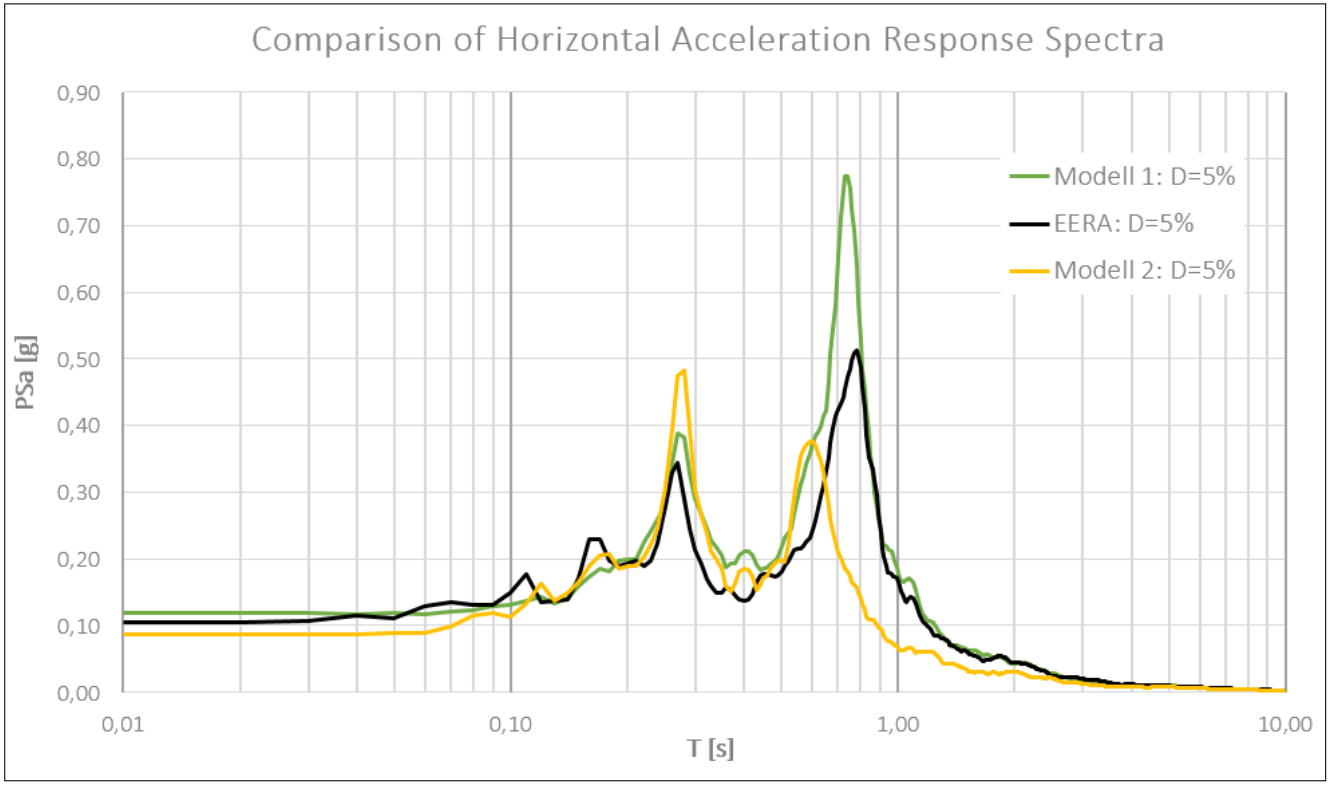

Figure 8.12: *Response Spectrum of free-field acceleration in Model 1, Model 2 and EERA*

8.2.5 Discussion of Results

In Figure 8.9, peaks indicate the soil layer's natural frequencies. It is expected that signals with these frequencies will be amplified the most through the soil layer. The fundamental period, i.e. the 1^{st} natural period, of the soil layer is T=0.8 s.

By comparing Figure 8.4 and Figure 8.6, it is evident that the two models respond quite differently to the input signal. Model 1 seem to be more dominated by longer periods, whereas Model 2 has a greater content of higher frequencies. This can be more easily demonstrated in the frequency domain, by regarding the response spectrum plotted in Figure 8.12. By considering the soil layer's fundamental period, T=0.8 s, Model 1 yields quite logical results, with evident amplification of periods around the fundamental. Model 2 seems to amplify mostly the second natural mode of the soil layer, which can be found at T=0.28 s. The difference in frequency content must be caused by the boundary conditions, being the only thing separating Model 1 from Model 2.

As discussed previously, the boundary conditions of Model 2 seem to inhibit proper simulation of the vertical SH-wave motion (Figure 8.1). The seismic input signal, being modeled as such a wave, will inevitably be restricted in to some extent at the boundaries. There is reason to believe that the boundary conditions, being modeled as viscous dampers, might generate counterwaves as a result of repressing the SH-wave motion. This could explain the difference in frequency content, with the higher frequencies in Model 2 solely being a side-effect of the input wave motion repression. By modifying relaxation coefficient C_1, governing the damping normal to the boundaries, the generation of these artificial stress waves could be avoided. However, by setting C_1=0, the viscous damper is practically removed, and would have no damping effect on other potential waves.

By considering the deformation patterns in Figures 8.5 and 8.7, Model 1 seems to describe the actual motion of a real soil under seismic loading more properly than Model 2. The soil slice obtains a free motion, but is simultaneously maintaining zero relative displacement between corresponding peripheral nodes. In Model 2, however, the soil slice take on

a quite non-physical shape, probably due to an attempt of relaxing the boundaries, while keeping the relative node displacements equal to zero.

As seen from the Figures 8.10 and 8.11, the free-field response obtained by the finite element models compares to some extent to the response obtained in EERA. However, a perfect match can never be expected. EERA performs calculations in the frequency domain, while Plaxis performs time-domain analyses. EERA uses iterative procedures to obtain an effective shear stiffness for each strain level, and considers strain-softening in the material through a predefined modulus reduction curve. For the finite element analyses, a constant strain-independent shear modulus is selected. The latter assumption is approximate, but valid for very small strains. By regarding the effective maximum shear strain profile obtained from EERA (see Appendix J.1, Figure J.4), it is evident that the shear strain is within the limits of the cyclic threshold shear strain (see Section 3.2). As indicated by the shear modulus reduction profile in Figure J.3, Appendix J.1, the modulus ratio is effectively above 90% for the whole profile. Thus, the assumption of a strain-independent shear modulus in Plaxis should be more or less valid.

Model 1, particularly, yields higher response than EERA. This could be caused by the defined Rayleigh damping ratio (see Section 6.2.4). The definition of the Rayleigh damping, will result in higher damping of the frequencies outside of the specified damping frequency range. Intermediate frequencies, on the other hand, will be less damped. Effective damping in Model 1, between the two specified Rayleigh damping frequencies (1 and 10 Hz), could be as low as 2%. With a closer look at the EERA calculations, the maximal damping of the soil layer was around 3.6% (Figure J.5, Appendix J.1).

Comment on Assumed Soil Properties

In Appendix J.2, results from EERA using the originally proposed (softer) soil properties are enclosed for comparison. However, it should be mentioned that the default shear modulus reduction curve for clay was used in EERA, not accounting for the high plasticity of the soil. Results show that the overall shear strain (Figure J.8) is somewhat higher than for

the adjusted soil profile, just exceeding the limit of the cyclic threshold shear strain. Thus, in potential analyses using the original soil profile, accounting for shear modulus reduction should be considered. A way of implementing this in Plaxis is using a strain-softening/hardening constitutive model for the soil. As commented in Section 6.2.4, Hardening Soil small or Soft Soil Creep material model could be used for this purpose. Using these models, material damping will be considered to some extent.

It can also be noted that the overall free-field response of the original soil profile (Figure J.10) was somewhat lower than for the adjusted soil profile. This has to do with the two profiles having different natural frequencies. They will therefore not amplify the same frequency with the same factor.

8.3 Direct Analysis (Linear)

8.3.1 Model 1

To assess the effect of soil-structure interaction, the structure's response is plotted together with the free-field response in Figure 8.13. An exaggerated deformation pattern during the earthquake is illustrated in Figure 8.14.

8.3.2 Model 2

The structure's response is plotted together with the free-field response in Figure 8.15. An exaggerated deformation pattern during the earthquake is illustrated in Figure 8.16.

8.3.3 Discussion of Results

Figure 8.17 shows the response of the superstructure in the time domain, using both Model 1 and Model 2 conditions. The maximum horizontal accelerations are summarized in Table 8.2. It is evident from these results,

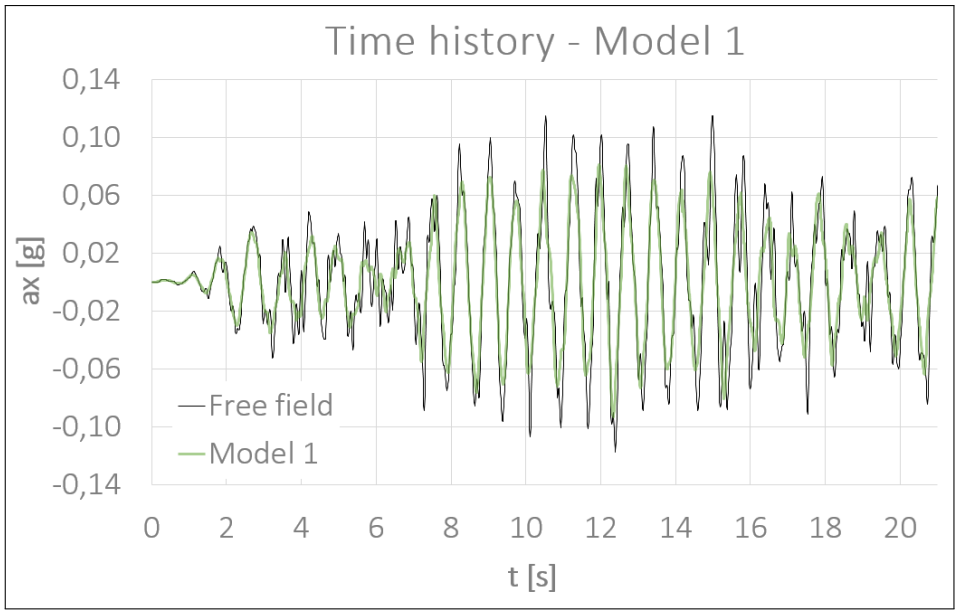

Figure 8.13: *Acceleration time history describing the response of the superstructure and free-field in the direct analysis. Model 1 conditions.*

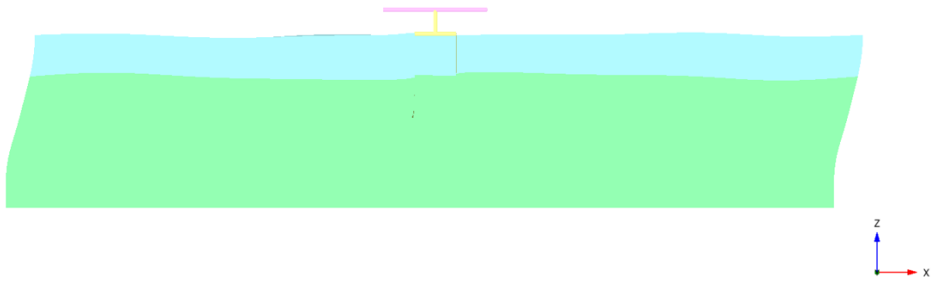

Figure 8.14: *Deformation pattern during earthquake simulation in Model 1.*

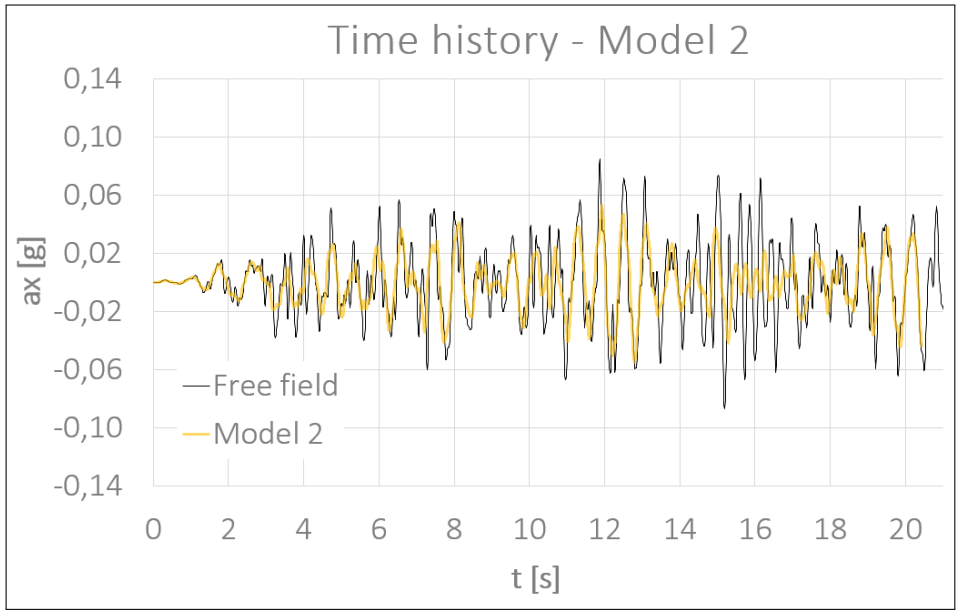

Figure 8.15: *Acceleration time history describing the response of the superstructure and free-field in the direct analysis. Model 2 conditions.*

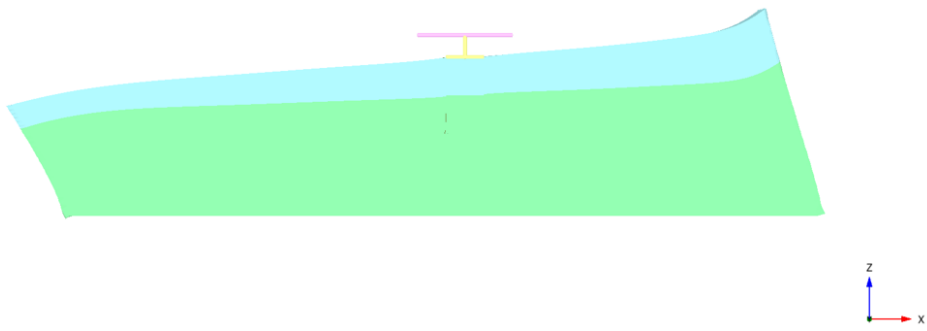

Figure 8.16: *Deformation pattern during earthquake simulation in Model 2.*

that Model 1 and Model 2 simulates the response to the earthquake quite differently.

Table 8.2: *Maximum acceleration of superstructure for Model 1 and Model 2*

MAX. ACCELERATION, a_x	
Model	a_x
Model 1	0.093g
Model 2	0.055g

Figure 8.13 show that the structure follows the horizontal motion of the free-field almost perfectly in Model 1. However, a slight decrease in amplitude is noted. Rocking of the structure and foundation was found to be negligible (not shown). This implies that the foundation-structure component move together with the soil, vibrating back and forth with a strictly horizontal motion as illustrated in Figure 8.18. With reference to Figure 5.2, it is noted that excitation modes depend on the wavelength of the signal, compared to the geometry and stiffness of the foundation. The *adjusted*, relatively stiff soil profile, repress the rocking excitation, which corresponds to Figure 5.2b. By considering the soil amplification function for the *original* soil profile (Figure J.6), it is clear that more of the lower frequencies will be amplified compared to the adjusted soil profile. Thus, seismic excitation of the original soil profile might lead to additional modes of excitation, such as rocking (Figure 5.2a) because of induced moments from the propagating wave. A more significant soil-structure interaction effect might therefore be expected.

The slightly lower response of the structure compared to free-field is likely due to the foundation-structure system not being able to transfer some of the frequencies properly. They are in stead filtered out, with a resulting "cut"of the peaks. This filtering phenomena is even more evident in Model 2 (Figure 8.15), especially around the high-frequency part of the response (14-17 s).

The deformation pattern for Model 1 seems quite more realistic than that of Model 2, as previously noted in the free-field analysis.

A comment to the shortened time history: The *input* time history (Figure

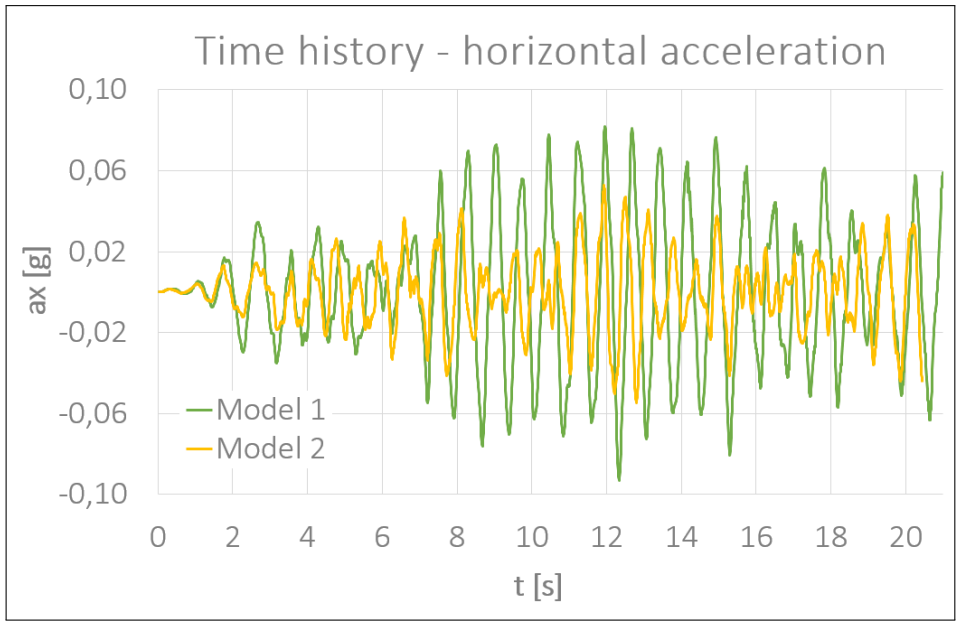

Figure 8.17: *Horizontal response of superstructure, results from Model 1 and Model 2*

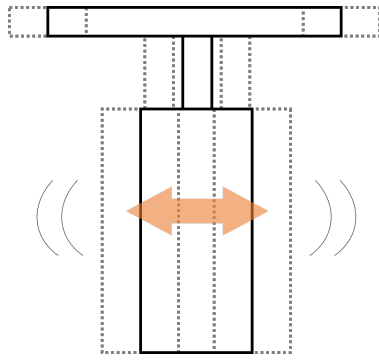

Figure 8.18: *Illustration of the strictly horizontal response of suction caisson and structure.*

6.3) lasts for approximately 38 seconds. Unfortunately, the analysis had to be stopped after 21 seconds, due to lack in computer capacity (disk space). The analysis should ideally have run for a minimum of 23 seconds, being the point where the earthquake starts decreasing in intensity. However, the results will still be used.

8.4 Direct Analysis (Non-Linear)

In Figure 8.19, the structure's response in the nonlinear analysis is plotted. Results from the linear analysis are included for comparison. The (exaggerated) deformation of the model is illustrated in Figure 8.20. Incremental deviatoric strain is plotted in Figure 8.21 and plastic points are shown in Figure 8.22.

8.4.1 Discussion of Results

As indicated in Figure 8.21 and Figure 8.22 there are local nonlinearities in vicinity of the foundation top during the earthquake. In Figure 8.22, the plastic points are plotted (red) together with tension cut-off points (white). The high concentration of these plastic points around the foundation top implies gapping between soil and foundation. This is not surprising, considering the strength of the soil surface being relatively low. As indicated by Figure 8.21, shear strains in the same order of magnitude are present at the bottom edges of the foundation. However, these strains are purely elastic, which is indicated by the lack of plastic points. This is explained by the somewhat higher shear strength at this level.

Considering Figure 8.19, the non-linear analysis seem to yield approximately the same response as the linear analysis for this case. Often, inclusion of non-linearity will have a *softening* effect, making the system more dynamic, thus including more effect from damping. This could be seen as reduction of the peaks. However, this is not very clearly demonstrated through the results of this analysis. Using the original soil profile, as discussed in Section 8.2.5, would probably yield more evident discrep-

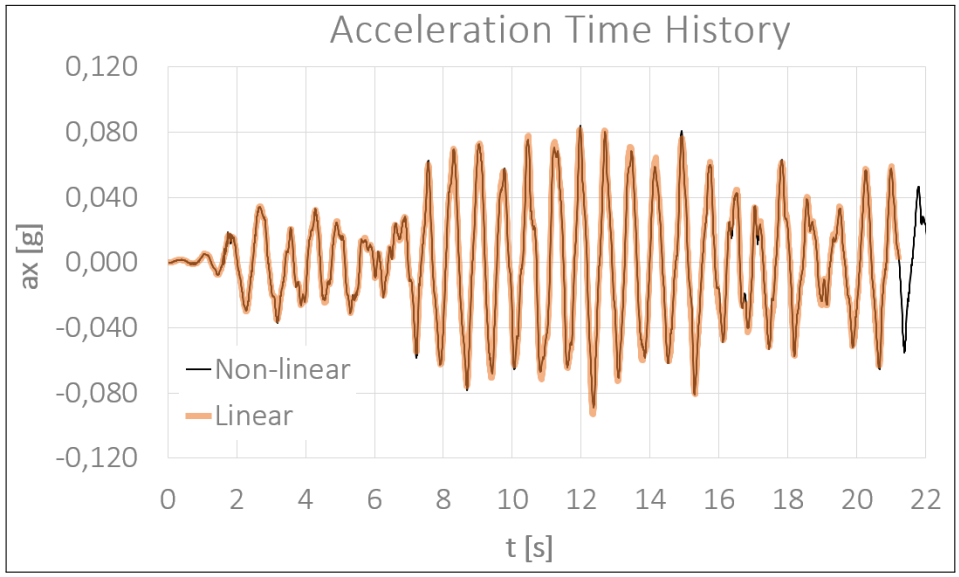

Figure 8.19: *Horizontal acceleration of structure in nonlinear and linear analysis.*

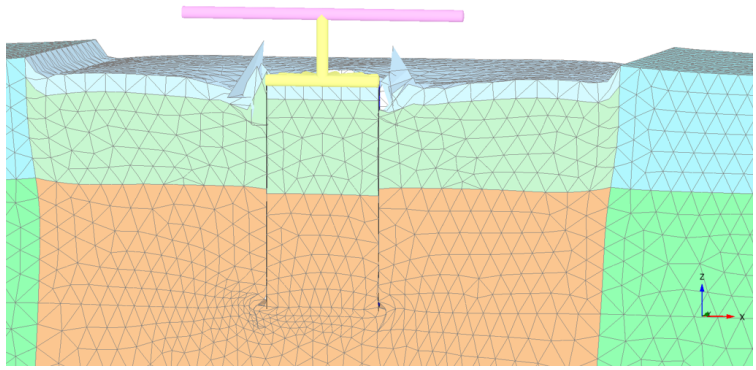

Figure 8.20: *Deformed mesh in non-linear analysis. Exaggerated for illustrative purposes.*

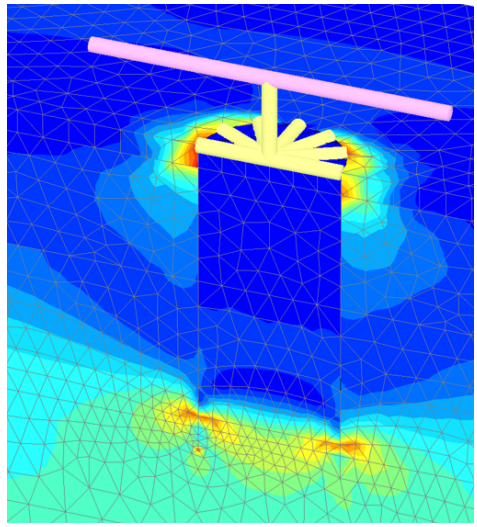

Figure 8.21: *Plot of incremental deviatoric shear strain indicating nonlinearities around the foundation.*

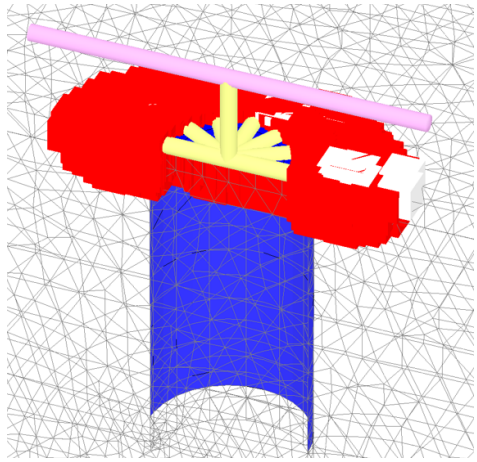

Figure 8.22: *Plot of plastic points indicating nonlinearities around the top of the foundation.*

ancies between linear and nonlinear analyses, with the likely introduction of additional modes of excitation, such as rocking.

8.5 Multi-Step Analysis

To maintain a straightforward and clean result chapter, all calculations are gathered in appendices. Relevant, corresponding appendices are commented upon for each step.

8.5.1 Step 1: Kinematic Interaction

Model 1

The time history for translative acceleration was found directly from a specified node at the center of the caisson lid. Response of the caisson is plotted together with the free-field response in Figure 8.23.

Time history for rocking acceleration was obtained by combining the time history of two specified nodes located at each side of the caisson lid. The result is plotted in Figure 8.24.

Response spectrum analysis was performed on the horizontal acceleration time history, and the result is shown in Figure 8.25.

Model 2

Step 1 was only performed for Model 1. However, the free-field motion from Model 2 has been used as reference, and as input for response spectrum analysis. The result is shown in Figure 8.26.

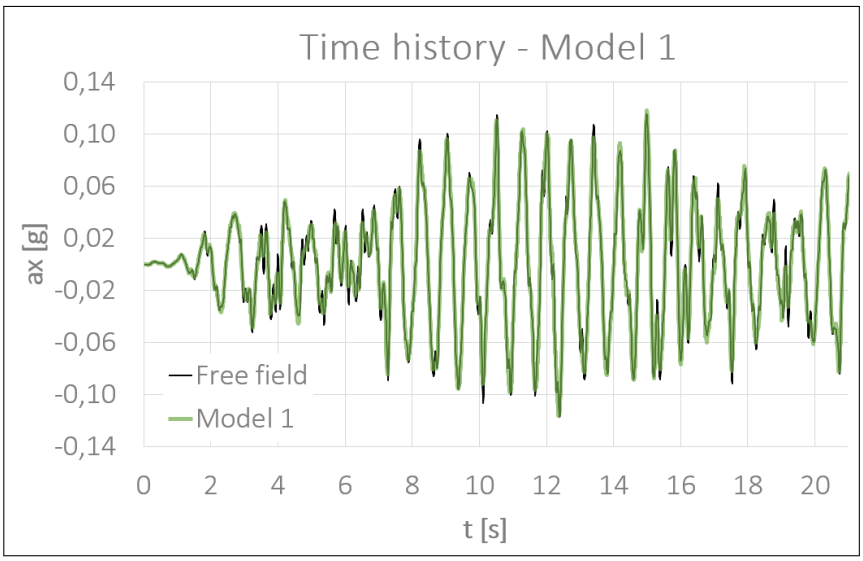

Figure 8.23: *Acceleration time history of horizontal caisson response using Model 1.*

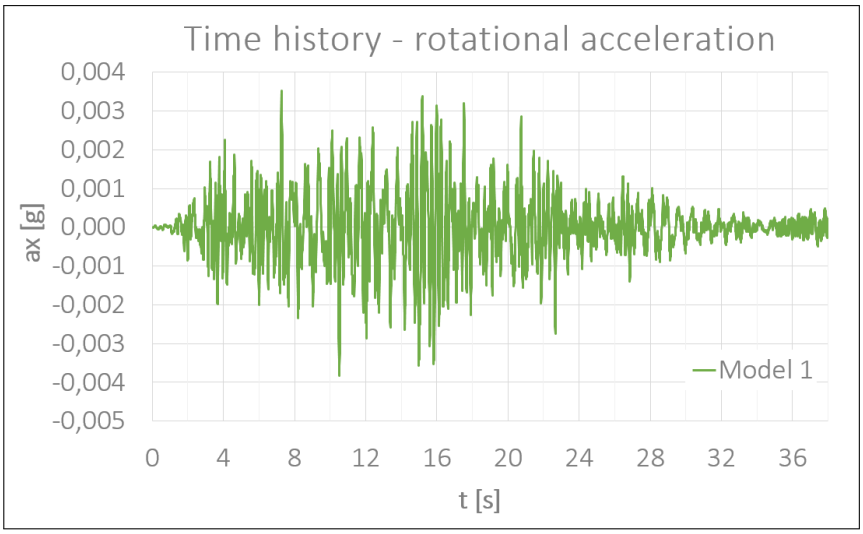

Figure 8.24: *Acceleration time history of rotational caisson response using Model 1.*

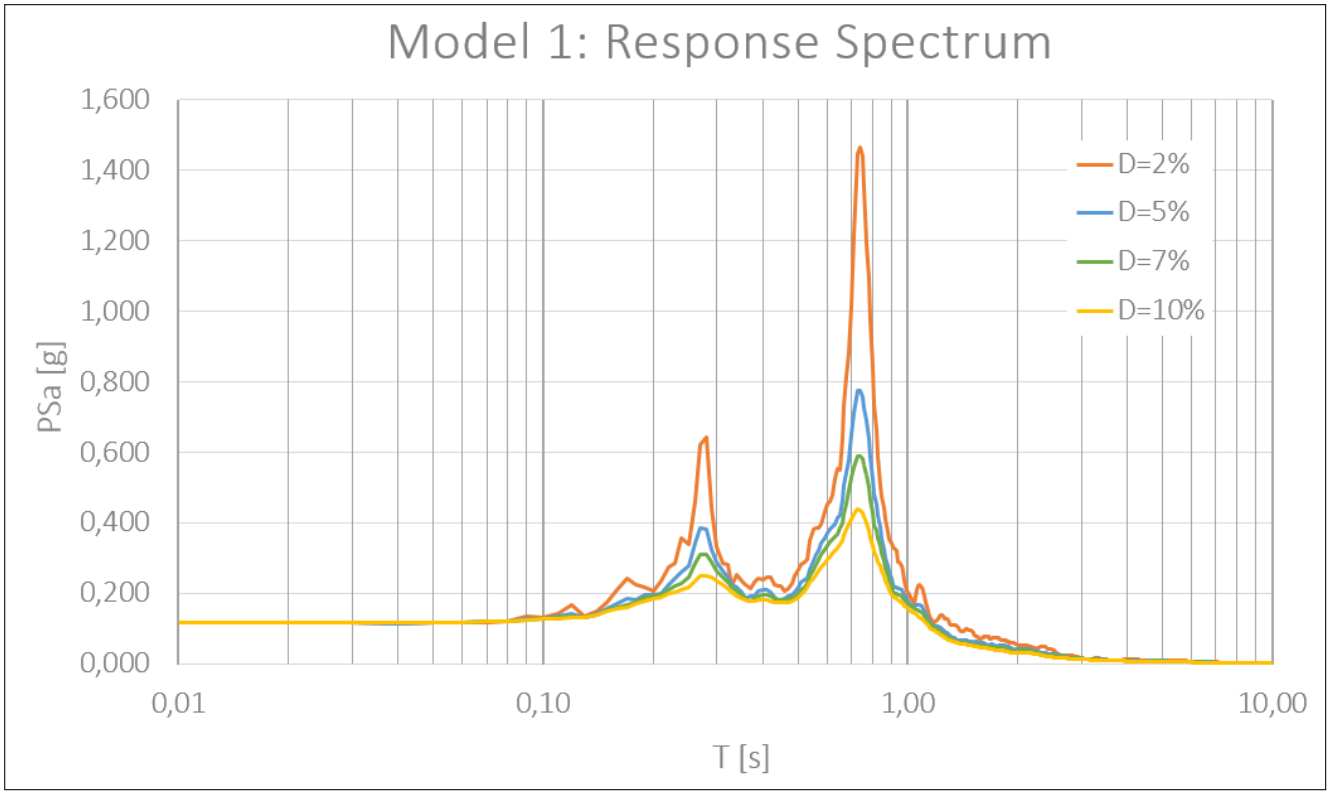

Figure 8.25: *Model 1: Response spectrum for horizontal acceleration of caisson top*

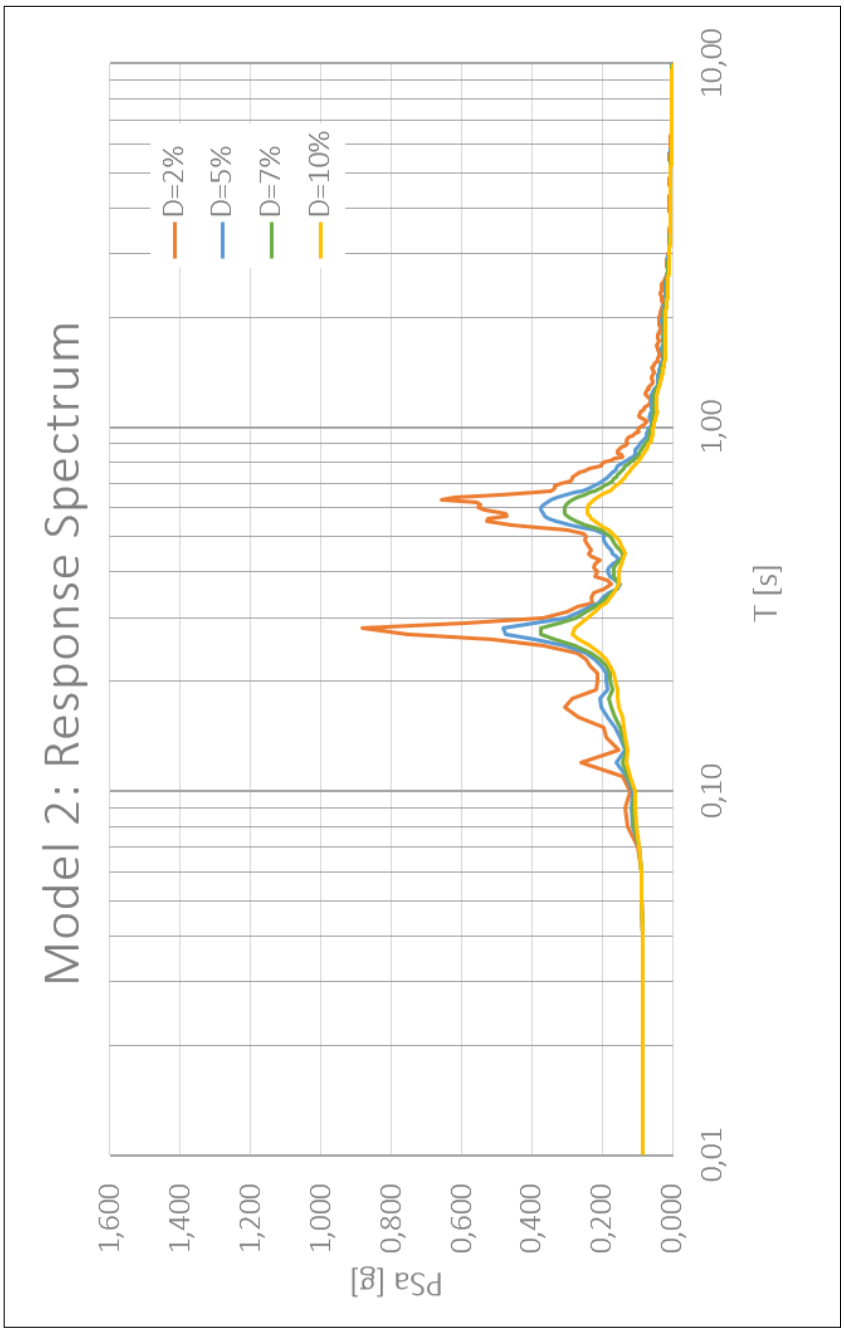

Figure 8.26: *Model 2: Response spectrum for horizontal free-field acceleration*

8.5.2 Step 2: Foundation Stiffness

Foundation Stiffness from Finite Element Analysis

This step is the same for both Model 1 and Model 2.

The stiffness matrix coefficients obtained from numerical solutions are shown in Table 8.3, together with results using closed-form solutions. The calculation procedure is shown in Appendix F. Figure 8.27 indicate the deformation patterns corresponding to the different load sets.

Table 8.3: *Static stiffness coefficients obtained from numerical analyses and closed-form solutions*

STATIC STIFFNESS COEFFICIENTS				
Coefficient	Unit	FEM	Emb. found.	Shaft in rock
K_{HH}	MN/m	6 907	11 722	4 668
$K_{H\theta} = K_{\theta H}$	MN/rad	102 234	393 848	62 913
$K_{\theta\theta}$	MNm/rad	2 214 092	12 979 765	2 133 046

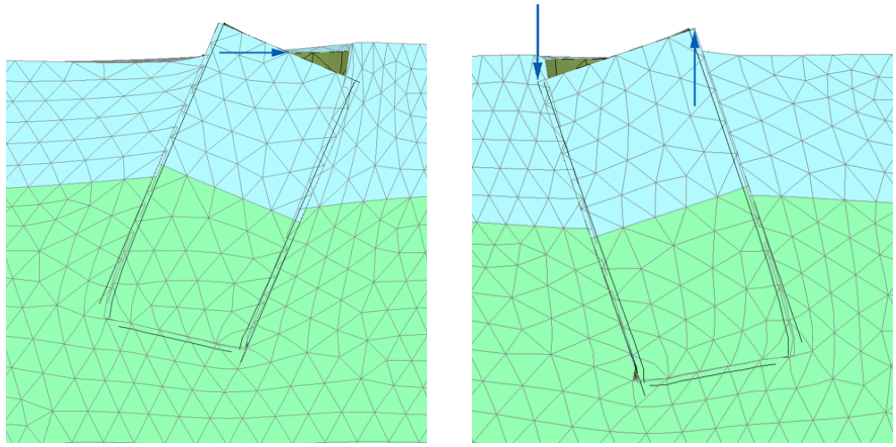

(a) *Deformation from load set 1* ***(b)*** *Deformation from load set 2*

Figure 8.27: *Deformation patterns in static analysis*

Foundation Stiffness from Closed-form Solutions

For full calculation procedure of closed-form solutions, the reader is referred to Appendix G. Stiffnesses from both numerical and closed-form solutions are summarized in Table 8.3.

8.5.3 Step 3: Inertial Interaction and Seismic Response

The eigenfrequencies of the superstructure, founded on springs representing the soil-foundation system, are calculated in Appendix H. The following eigenfrequencies and natural periods were obtained using stiffnesses found through the numerical analysis in Step 2:

$$\omega_1 = 329 \text{ s}^{-1} \Rightarrow \underline{\text{T}_1 = 0.02 \text{ s}}$$

$$\omega_2 = 134 \text{ s}^{-1} \Rightarrow \underline{\text{T}_2 = 0.05 \text{ s}}$$

With the natural periods of the superstructure available, maximum acceleration can be obtained from the response spectra from Step 1 (Figures 8.25-8.26). The structure's maximum acceleration amplitude for the two natural periods are presented in Table 8.4 for Model 1 and Model 2. Due to the structure having such low natural periods, the response is equal no matter which damping ratio is used for the soil, thus only one value is presented per period.

Table 8.4: *Maximum acceleration of superstructure for different natural periods*

MAX. ACCELERATION, $\mathbf{a}_x$		
	$\text{T}_1 = 0.02$ s	$\text{T}_2 = 0.05$ s
Model 1	0.119g	0.120g
Model 2	0.087g	0.090g

Natural mode shapes, corresponding to the calculated eigenfrequencies, are illustrated in Figure 8.28. Calculations are shown in Appendix H.

(a) 1^{st} *natural mode shape* *(b)* 2^{nd} *natural mode shape*

Figure 8.28: *The natural mode shapes of the superstructure. Illustrations are only indicative, as deformations are exaggerated.*

8.5.4 Discussion of Results

Step 1

As shown in Figure 8.23, the free-field and caisson responses are practically the same for Model 1. Figure 8.24 show that the caisson rotation is negligible, which together with Figure 8.23, implies that there is little kinematic interaction between foundation and soil. These results indicate that the caisson moves together with the soil, vibrating back and forth with a strictly horizontal motion. This is likely due to the relatively high shear modulus for the soil, resulting in vibration which do not transfer moments to the foundation (illustrated in Figure 5.2b).

Step 2

Numerical solution. The stiffness obtained from the finite element analysis is inevitably influenced by the assumption of a completely rigid foundation. This increases the overall stiffness of the foundation-soil system. The assumed soil profile is relatively stiff compared to the originally proposed material properties for the case study. Using the original soil profile would yield lower stiffness.

Closed-form solution for embedded foundation. As evident from the results presented in Table 8.3, the finite element solution does not correspond well to the closed-form solution for an embedded foundation. The latter clearly overestimates the stiffness of the caisson-soil interaction.

A reason for this is the validity of the closed-form solution being limited by a maximum depth-to-radii ratio of less than 2. With a depth-to-radii ratio of 4 in the case study, it becomes apparent that the closed-form solution is not applicable. Rotational stiffness is especially overestimated. This closed-form solution assumes a perfectly welded soil-foundation interface, which in most cases is unrealistic (see for example Gazetas (1991)). Closed-form solutions are available for *partially* embedded foundations, accounting for the limited interface strength and stiffness by reducing the contact area between soil and foundation. Effects from partial embedment are well illustrated by Gazetas (1991), and are significant for the rotational stiffness. By considering this, the predicted static stiffness would be lower. However, it would still gravely overestimate the rotational stiffness.

Closed-form solution for rigid shaft in rock. The closed-form solution for a rigid shaft in weaker rock yields lower stiffness than the numerical solution, yet in the same order of magnitude. The rotational stiffness is almost spot-on. The underestimated translation stiffness could be explained by the use of the shear modulus at soil surface for calculations.

Gazetas (1991) presents solutions for taking into account the effect of increasing shear modulus with depth. Simple formulas for surface foundations with various stiffness profiles are proposed. In this thesis, soil inhomogeneity was not taken into account when using the closed-form solutions. The shear modulus at the surface was used directly. By accounting for the increasing shear stiffness, using a shear modulus more representative for the soil layer, the closed-form solutions would yield higher foundation stiffness coefficients.

Step 3

The structure has very low natural periods, which can be explained by the very high foundation impedances compared to the structure's mass. Using the response spectrum, the acceleration can not possibly attain a lower value than the peak ground motion with such low natural periods.

General Discussion on Multi-step Approach

The multi-step analysis could be further simplified, being a sought feature in engineering, to comprise of only analytical solutions. The caisson response from Step 1 could be found through analytical solutions as explained in Section 5.3.1, using frequency-dependent transfer functions. However, this is not commonly practiced in geotechnical engineering due to the use of frequency-domain. In this specific case, the horizontal free-field acceleration could have been used directly, because of the negligible difference between suction caisson and free-field response. Step 1 could now potentially consist of a simple EERA calculation, saving a great amount of time. However, kinematic interaction could be more significant for a softer site. The evaluation should thus be included, especially when dealing with embedded foundations where rocking excitation can occur.

Step 2 could also be further simplified, by skipping the numerical solution, and using the closed-form solutions directly. However, caution should be exerted when doing this, because they are obviously not applicable in all situations. Their parameters have been fitted through parametric studies using numerical modeling, and certain validity limits exist. Alternatively for Step 2, simple lumped-parameter models could be implemented, as discussed in Wolf (1995). These simple physical models can be used for almost any case, yielding approximate solutions. Stiffness coefficients would have to be calibrated, for example through numerical modeling, in order of implementing the lumped-parameter model for Step 3. For properly dealing with nonlinearities in soil and interface, numerical methods are the best solution. However, this demands expert knowledge regarding the understanding of how to discrete the physical situation properly.

8.6 Mesh Sensitivity in Static Analysis

Figure 8.29 displays the variation in stiffness coefficients plotted versus mesh refinement.

8.6.1 Discussion of Results

Contrary to the aforementioned hypothesis, the stiffness coefficients seem to increase with mesh refinement. However, as shown in Figure 8.29 neither the horizontal static stiffness nor the coupled stiffness coefficient change significantly. The rotational stiffness coefficient, on the other hand, show a clear increase with finer mesh. The solution seem to converge, indicated by the reduction of the curve, between *Medium* and *Fine* mesh. As a compromise between calculation efficiency and accuracy, the *Medium* mesh refinement could be considered adequate.

A possible source of error, contributing to the stiffer solution with increased refinement, could be the use of interfaces. The virtual thickness of the interfaces is mesh-dependent (Plaxis 2013*a*), and a finer mesh will yield a (virtually) thinner interface. The shear deformation of a (virtually) thicker interface element, when subjected to a fixed force, will be larger than for a corresponding thinner element. As explained in Plaxis (2013*a*, Ch. 5), the virtual thickness of the interface is calculated as a factor multiplied with the global element size. Due to this, the virtual thickness will increase with coarser element discretization. Plaxis (2013*a*) also states that generation of elastic deformations increase with the virtual thickness of the interface. This means that a coarser mesh, with a corresponding thicker interface, could potentially yield larger deformations than a finer mesh, and thus larger values for the flexibility coefficients.

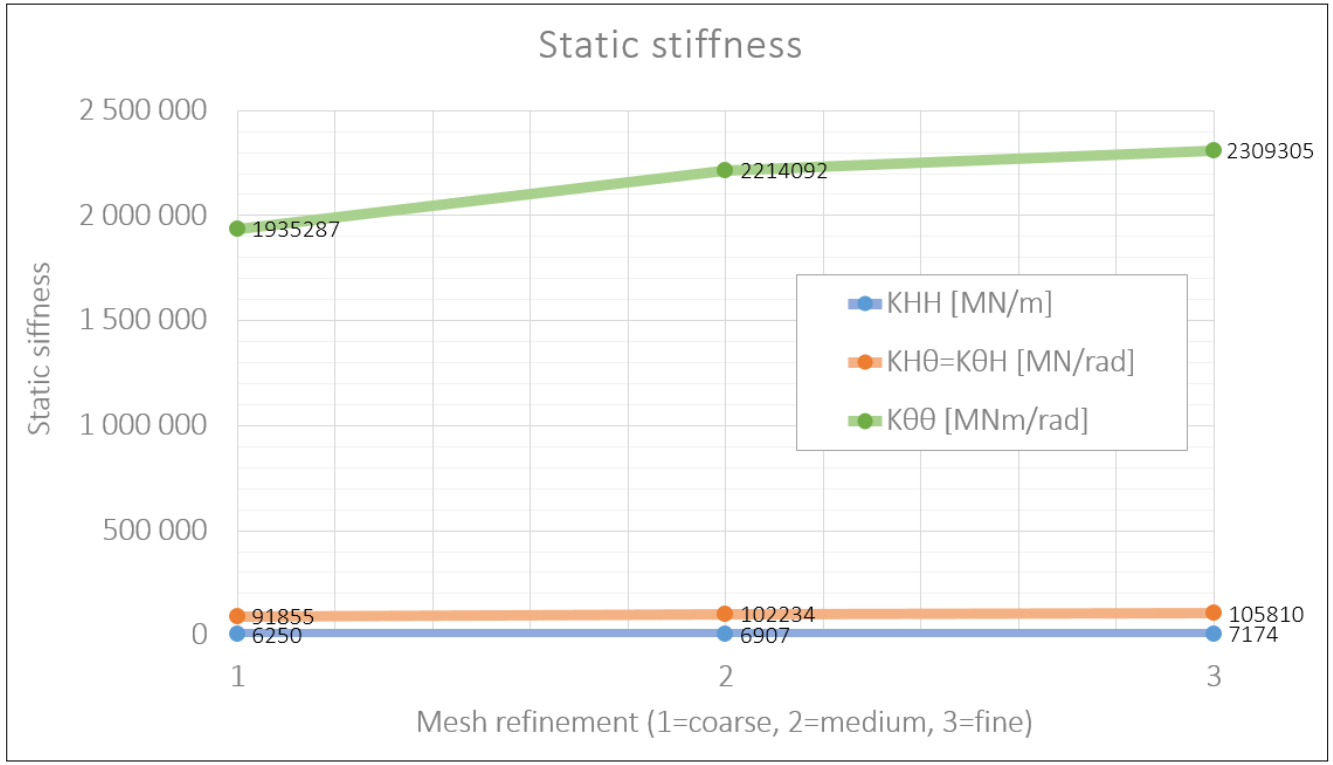

Figure 8.29: *Mesh dependency of static stiffnesses calculated in Excel*

8.7 Comparison and Discussion of SSI Analyses

The maximum horizontal accelerations obtained from direct analysis and multi-step analysis are tabulated in Table 8.5 for both Model 1 and Model 2. Maximum free-field acceleration is included for comparison. Deviations of results from multi-step analysis to direct analysis, are tabulated for each model.

Table 8.5: *Maximum acceleration of superstructure and free-field from SSI analyses. Deviation between multi-step and direct analyses are indicated in the rightmost column.*

	MAX. ACCELERATION, $\mathbf{a}_x$			
	Free-field	Direct	Multi-step (T_1/T_2)	Deviation
Model 1	0.117g	0.093g	0.119g/0.120g	28-29%
Model 2	0.087g	0.055g	0.087g/0.090g [1]	58-64%

[1] Based on the use of free-field response as input to RSA.

First of all, it must be noted that the structure response obtained from the multi-step analysis, coincides almost perfectly with the free-field motion. This is likely due to the structure's calculated eigenfrequency being so high, resulting in no amplification of it's response. Using a response spectrum in Step 3 will thus result in the response coinciding with the peak ground motion.

Further, it can be mentioned that the two methods of SSI analysis yields relatively different responses for the structure. Least deviation is obtained through the use of Model 1, where the multi-step analysis yields almost 30% higher response than the direct analysis. For Model 2, the deviations are as high as 58-64%. These results indicate that the multi-step analysis might be too simplified. On a general basis, the main reason for discrepancies between direct and the multi-step approach stem from the modeling of damping, which is not properly addressed using multi-step methods. In this case, the deviation is likely due to the response spectrum not being able to yield a lower maximum response than the peak ground motion for very small periods. In contrast to this, the direct analysis is able to capture the minor soil-foundation-structure interaction, leading to a slight

de-amplification of the response. With a less simplified multi-step analysis, particularly regarding Step 3, this de-amplification could be captured and less deviation is likely to be experienced. Through modeling the structure on springs and applying the foundation input motion, the response time history for the structure could be obtained also in the multi-step analysis. The maximum response would then be able to have a lower value than the free-field, in contrast to what is possible to obtain through a response spectrum analysis.

Compared to Model 1, Model 2 yields lower response for both the direct analysis and multi-step analysis. An apparent reason for this is the difference in boundary conditions, with the viscous boundaries in Model 2 restricting the seismic input motion. This was discussed more in-depth earlier in Section 8.2.5.

The imposed earthquake acceleration will propagate as vertical shear waves through the soil deposit, because of input definitions. Meanwhile, the foundation-structure component will start vibrating, acting as a source for body and surface stress waves propagating in various directions. These waves will be reflected at the boundaries. Due to this, Model 2 should be used in order to simulate radiation damping of these secondary waves. However, Model 1 is necessary for appropriately describing the seismic wave propagation through the layer in the first place, as discussed in Section 8.2.5. The two wave problems thus require contradictory boundary conditions. With basis in the gathered results from the analyses, Model 1 seems to be the most appropriate modeling concept of the two. However, it is clear that both models have their disadvantages.

8.7.1 Discussion of General Assumptions

Assumptions regarding Element Discretization

By meshing the finite element model according to a selected minimum wave length, the frequencies corresponding to shorter wavelengths than this, will be filtered. However, the selected limit frequency of 10 Hz is considered a valid assumption, being in the upper range of the general

frequency content of the design earthquake. In addition, by considering the soil layer's amplification function from EERA (Figure 8.9), it is evident that frequencies above 10 Hz will not be significantly amplified through the soil layer.

Assumptions regarding Structure and Foundation

The assumption of a completely rigid caisson foundation, was unnecessary, but was initially chosen to more easily compare the results to closed-form solutions. Because of the use of a soil profile of relatively high shear stiffness, it is assumed that the rigidity of the caisson does not influence the solution significantly.

The structure was modeled as an infinitely stiff beam with uniform distributed mass. In reality the structure consists of a manifold with various pipe connections, with a total geometry very different from a beam. However, the assumptions regarding the superstructure is likely not the main source of error introduced in these analyses.

Connection and support beams were assigned unrealistically high values for second moments of area and cross-sectional area. This was done in order to make sure they acted completely rigid. This might have introduced some minor errors in the finite element model, however it is not believed that it had significant influence on the solution.

Assumptions Regarding Soil Properties

The increase of the overall shear stiffness was necessary due to calculation efficiency, however, it resulted in an analysis yielding only minor SSI effects. As previously discussed in Section 8.2.5, the use of the original soil profile would probably yield more ˜interesting˝results, with more significant soil-structure interaction.

Assumptions regarding Foundation Stiffness

In reality, the foundation stiffness is frequency dependent, as discussed in numerous publications (see for example Gazetas (1983)). The assumption of a static stiffness, will be valid for a low frequency range, before damping and inertia have significant influence. However, the analyses show that the foundation-structure system vibrates with relatively high frequency, thus implying a need for frequency-dependent springs.

Chapter 9

Observations and Further Work

9.1 Observations and Conclusive Remarks

In this thesis, soil-structure interaction has been evaluated through the use of both a direct and a multi-step method. Plaxis 3D 2012 was used for numerical modeling, implementing two different modeling concepts with different boundary conditions.

Limitations of Plaxis 3D have been experienced, and knowledge about the influence of boundary conditions in dynamic analyses, has been gained. Results show that it is not possible to model a vertically propagating shear wave, while simultaneously simulating radiation damping of waves from other sources in Plaxis 3D 2012.

The best solution was found to be the use of the Model 1 concept, with lateral boundaries free in the horizontal direction, without the use of viscous dampers. These boundary conditions will not enable absorption of incoming stress waves generated by the vibrating caisson foundation, which will inevitably result in reflection of these back into the system. For this purpose, Model 2 conditions are necessary. However, the two wave prob-

lems demand contradictory boundary conditions, and the Model 1 concept seems to introduce least errors in the analysis. Default settings for dynamic analyses in Plaxis 3D (Model 2) were found to yield strange results, and are not recommended for seismic analyses.

Results using a multi-step approach yielded 30-60% higher maximum response compared to a direct approach. This indicates that the use of simplified analyses, approximating the soil-foundation-structure system with the use of dynamic springs, introduces uncertainty. Less simplified analyses, particularly regarding Step 3 in the multi-step approach, would probably yield less deviation between the two methods of analyses, by allowing the structure to actually obtain a response lower than the free-field response. With the response spectrum, this is not possible for such low natural periods, and the response will inevitably coincide with the peak ground motion.

The implemented soil properties were adjusted, by raising the overall stiffness, in order to perform the analyses capacity. Use of the original soil profile would require a much finer element discretization, with correspondingly longer computational time. However, using the original soil profile would likely lead to more significant soil-structure interaction.

Direct analysis, with dynamic modeling in finite element programs, is not straightforward and demands quite a lot of knowledge about the various considerations that must be made. The computational time is very long, and the analysis requires computers with relatively high capacities (both disk-space and RAM). A multi-step analysis generally takes less time; however, this also depends on the selected approach in dealing with the various steps of the analysis. Direct methods will enable the possibility of considering material and geometric non-linearities. Strain-dependent stiffness and gapping can then be accounted for. However, non-linear finite element analyses are even more time consuming than the linear analyses.

Observations using Plaxis 3D 2013

Plaxis 3D *2012* was used for numerical analyses in this thesis. However, Plaxis 3D *2013* was used for a while, until the author realized it was

not applicable for her purpose. Implementation of Model 1 conditions in Plaxis 3D version *2013*, was not possible. It seemed as though the use of lateral boundaries, free in the horizontal direction, was not allowed in the Dynamics module of that version. Testing resulted in what looked more like Model 2 conditions, however, with huge stress increments at the lateral boundaries. This was a major drawback, resulting in many days of wasted efforts having to redo multiple numerical analyses.

The author urges Plaxis to further develop the 3D Dynamics module in their software, in order to perform seismic analyses with more appropriate boundary conditions.

9.2 Recommendations for Further Work

An apparent next step in this thesis would, first of all, be to use the original soil profile for similar SSI analyses. It is expected that the softer soil will yield more significant SSI effects. Next, it would be interesting to account for the frequency-dependence of the foundation impedances. This could be done in the frequency-domain for equivalent linear problems, through Fourier transforms and superposition of harmonic signals, or using a simple physical model (lumped parameter) in the time-domain as the ones described by Wolf (1995). Doing this, results using strictly static springs could be compared to results using dynamic springs, which would be an interesting task.

Another exercise, as originally proposed by Multiconsult AS, could be to develop a type of *p-y curves* for large diameter caissons in clay. Static non-linear spring stiffness could be evaluated through numerical analyses, and parametric studies could reveal governing relationships. This could enable the possibility of developing generalized solutions applicable for certain foundation geometries and soil conditions.

As a comment to the mesh sensitivity analysis, the influence of interface (virtual) thickness on the solution should be investigated further.

Bibliography

American Petroleum Institute (2010), *Recommended Practice for Planning, Designing and Constructing Fixed Offshore Platforms — Working Stress Design / American Petroleum Institute*, American Petroleum Institute.

Athanasiu, C. (2014), 'Soil parameters (in norwegian)', Accessed 13 February 2014. [e-mail] Message to M.Brandt from C. Athanasiu. Thursday 13 February 2014: 12:38.

Aubeny, C., Murff, J. & Moon, S. (2001), 'Lateral undrained resistance of suction caisson anchors', *International Journal of Offshore and Polar Engineering* **11**(3), 211 – 219.

Bao, H., Bielak, J., Ghattas, O., Kallivokas, L. F., O'Hallaron, D. R., Shewchuk, J. R. & Xu, J. (1998), 'Large-scale Simulation of Elastic Wave Propagation in Heterogeneous Media on Parallel computers', *Computer Methods in Applied Mechanics and Engineering* **152**, 85 – 102.

Barbosa, L. V. (2013), 'Fourier transform', [online] Available at: <`http://en.wikipedia.org/wiki/Fourier_transform`>. [Accessed 01.05.2014].

Bardet, J., Ichii, K. & Lin, C. (2000), 'Eera - a computer program for equivalent-linear earthquake site response analysis of layered soil deposits'.

Byrne, B., Houlsby, G., Martin, C. & Fish, P. (2001), 'Suction caisson foundations for offshore wind turbines', *Wind Engineering* **26**(3), 145 – 155.

Carter, J. P. & Kulhawy, F. H. (1988), 'Analysis and design of drilled shaft foundations socketed into rock'. Report EL-5918.

Carter, J. P. & Kulhawy, F. H. (1992), 'Analysis of laterally loaded shafts in rock', *Journal of Geotechnical Engineering* **118**(6), 839 – 855.

Chopra, A. K. (1995), *Dynamics of Structures: Theory and Applications to Earthquake Engineering*, Prentice Hall.

Christian, J. T., Roësset, J. M. & Desai, C. S. (1977), Two- and three-dimensional dynamic analyses, *in* C. S. Desai & J. T. Christian, eds, 'Numerical Methods in Geotechnical Engineering', McGraw-Hill Book Company, pp. 683–718.

Cook, R. D., Malkus, D. S., Plesha, M. E. & Witt, R. J. (2002), *Concepts and Applications of Finite Element Analysis*, 4th ed. edn, WILEY.

Elsabee, F. (1973), 'Static stiffness coefficients for circular foundations embedded in an elastic medium', MSc in Civil Engineering at Massachusetts Institute of Technology.

Emdal, A., Grande, L. & Nordal, S. (2006), *Geotechnics, calculation methods (in norwegian)*, Department of Civil and Transport Engineering, NTNU. Lecture Notes in course TBA4105, spring 2010, The Norwegian University of Science and Technology.

Gazetas, G. (1983), 'Analysis of machine foundation vibrations: State of the art', *International Journal of Soil Dynamics and Earthquake Engineering* **2**(1), 2 – 42.

Gazetas, G. (1991), Foundation vibrations, *in* H.-Y. Fang, ed., 'Foundation Engineering Handbook', Springer US, pp. 553–593.

Gazetas, G. (1995), Surface and embedded foundations, *in* 'Course Material from Civil Engineering European Courses "Applications of Soil Dynamics: Dynamic Soil - Foundation - Structure Interaction"'. Originally printed in Corps of Engineers WES Manual on "Seismic Stability of Earth Structures", Chapter 4.

Gerolymos, N. & Gazetas, G. (2006*a*), 'Development of Winkler Model for Static and Dynamic Response of Caisson Foundations with Soil and Interface Nonlinearities', *Soil Dynamics and Earthquake Engineering* **26**(5), 363–376.

Gerolymos, N. & Gazetas, G. (2006*b*), 'Static and Dynamic Response of Massive Caisson Foundations with Soil and Interface Nonlinearities – Validation and Results', *Soil Dynamics and Earthquake Engineering* **26**(5), 377–394.

Gerolymos, N. & Gazetas, G. (2006*c*), 'Winkler model for lateral response of rigid caisson foundations in linear soil', *Soil Dynamics and Earthquake Engineering* **26**(5), 347–361.

Haigh, S., Ghosh, B. & Madabhushi, S. (2005), 'Importance of time step discretisation for nonlinear dynamic finite element analysis', *Canadian Geotechnical Journal* **42**(3), 957 – 963.

Houlsby, G. & Byrne, B. (2000), 'Suction caisson foundations for offshore wind turbines and anemometer masts', *Wind Engineering* **24**(4), 249 – 255.

Houlsby, G., Ibsen, L. B. & Byrne, B. (2005), Suction caissons for wind turbines, *in* 'Proceedings of International Symposium on Frontiers in Offshore Geotechnical Engineering'.

Ibsen, L. B., Liingaard, M. & Andersen, L. (2006), 'Dynamic stiffness of suction caissons – torsion, sliding and rocking', [Technical report] Department of Civil Engineering, Aalborg University.

Jeanjean, P. (2009), Re-assessment of p-y curves for soft clays from centrifuge testing and finite element modeling, *in* 'Proceedings of the 2009 Offshore Technology Conference', number OTC 20158.

Kausel, E. A. (1974), 'Forced vibrations of circular foundations on layered media', [PhD Thesis] Massachusetts Institute of Technology.

Kaynia, A. (2014), 'Discussion on the use of static stiffness as alternative to dynamic impedance functions', [Conversation] Personal communication, 2 June 2014.

Kramer, S. L. (2014), *Geotechnical Earthquake Engineering*, Pearson Education Limited. Pearson New Internation Edition.

Liingaard, M. (2006), 'Dynamic Behaviour of Suction Caissons', [PhD Thesis] Department of Civil Engineering, Aalborg University.

Lysmer, J. & Kuhlemeyer, R. (1969), 'Finite Dynamic Model for Infinite Media', *Journal of Engineering and Mechanical Division,* **95**, 859 – 877.

Matlock, H. (1970), Correlations for design of laterally loaded piles in soft clay, *in* 'Proceedings of the 1970 Offshore Technology Conference', number OTC 20197.

Mylonakis, G. & Gazetas, G. (2000), 'Seismic soil-structure interaction: Beneficial or detrimental?', *Journal of Earthquake Engineering* **4**(3), 277–301.

NGI (2011), 'Skirted caisson foundations for offshore structures', [online] Available at: <`http://www.ngi.no/en/Contentboxes-and-structures/Reference-Projects/Reference-projects/Skirted-Caisson-Foundations-for-Offshore-Structures/`>. [Accessed 07.04.2014].

Nordal, S. (2013), *Geotechnical Engineering, Advanced Course*, Akademika Forlag. Lecture Notes and Background Material in course TBA4116, autumn 2013, The Norwegian University of Science and Technology.

Olivadoti, G. (2001), 'Sensing, analyzing, and acting in the first moments of an earthquake', *Analog Dialogue* **35**(1), 1 – 3.

Pecker, A. (2007), *Advanced Earthquake Engineering Analysis*, SpringerWien New York. International Centre for Mechanical Sciences (CISM).

Plaxis (2012), *Plaxis 2D 2012*, Plaxis bv.

Plaxis (2013*a*), *Plaxis 3D Reference Manual*, Plaxis bv. [Accessed 15.01.2014].

Plaxis (2013*b*), *Plaxis 3D Scientific Manual*, Plaxis bv. [Accessed 15.01.2014].

Plaxis (2013*c*), *Plaxis 3D Tutorial Manual*, Plaxis bv. [Accessed 15.01.2014].

Plaxis Support (2014), 'Re: [4516] Help a student with modelling in Plaxis 3D', Accessed 27 March 2014. [e-mail] Message to M.Brandt from Plaxis Support(support@plaxis.com). Thursday 27 March 2014: 10:59.

Stevens, J. & Audibert, J. (1979), Re-examination of p-y curve formulations, *in* 'Proceedings of the 1979 Offshore Technology Conference', number OTC 3402.

The Norwegian Pile Commitee (2012), *Pile Guide 2012 / The Norwegian Pile Commitee (in Norwegian: Peleveiledningen 2012 / utarbeidet av Den Norske Pelekomité*, [Oslo] : Norsk Geoteknisk Forening.

Tjelta, T. I. (2001), Suction piles: Their position and application today, *in* 'The Eleventh International Offshore and Polar Engineering Conference'.

Varun, Assimaki, D. & Gazetas, G. (2009), 'A simplified model for lateral response of large diameter ciasson foundations - linear elastic formulation', *Soil Dynamics and Earthquake Engineering* **1**(29), 268–291.

Veletsos, A. S. & Wei, Y. T. (1971), 'Lateral and rocking vibrations of footings', *Journal of the Soil Mechanics and Foundations Division* **97**(9), 1227 – 1248.

Vucetic, M. & Dobry, R. (1991), 'Effect of soil plasticity on cyclic response', *Journal of Geotechnical Engineering* **117**(1), 89 – 107.

Whitman, R. V. (1976), Soil-platform interaction, *in* 'Proceedings of the International Conference on the Behaviour of Off-Shore Structures', Vol. 1, pp. 817 – 829.

Wolf, J. P. (1985), *Dynamic Soil-Structure Interaction*, New Jersey: Prentice-Hall.

Wolf, J. P. (1995), Foundation Vibration Analysis usin Simple Physical Models for Foundations Dynamics - State of the Art Paper, *in* 'Proceedings of the Third International Conference on Recent Advances in Geotechnical Earthquake Engineering and Soil Dynamics'.

Nomenclature

LATIN SYMBOLS

a	Attraction
a_0	Dimensionless frequency factor
a	acceleration
B	Width
C	Damping matrix
c	Cohesion
C_1	Viscosity coefficient
C_2	Viscosity coefficient
E	Young's modulus/elasticity modulus
$F(\omega)$	Amplification factor
f	Frequency
f	Flexibility coefficient
f	Flexibility matrix
G	Shear modulus
G_max	Maximum shear modulus
$H(\omega)$	Amplification factor
H	Height
h	Height
I	Second moment of area
K	Stiffness coefficient
k	Stiffness coefficient
K	Stiffness matrix
L	Length
M	Oedometer/constrained modulus
M	Mass
M	Mass matrix
R_{inter}	Interface reduction factor
s_u	Undrained shear strength
T	Period
u	Displacement
$\dot{u}$	Velocity
$\ddot{u}$	Acceleration
V_p	Compression wave velocity
V_s	Shear wave velocity
W_D	Energy dissipation
W_S	Peak strain energy

GREEK SYMBOLS

α	Rayleigh damping coefficient
β	Rayleigh damping coefficient
δt	Critical time step
Δt	Total dynamic time
λ	Wave length
σ	Normal stress
ρ	Mass density
γ	Shear strain, unit weight
η	Viscosity
τ	Shear stress
ν	Poisson's ratio
ξ	Damping ratio
ω	Angular frequency/eigenfrequency
Φ_n	Mode shape
ϕ	Friction angle
ψ	Angle
θ	Angle

ABBREVIATIONS

BE	Boundary Element
DOF	Degree of freedom
EERA	Equivalent-linear Earthquake Response Analysis
FE	Finite Element
FEA	Finite Element Analysis
FEM	Finite Element Method/Model
MDOF	Multiple-Degree-of-Freedom
RSA	Response Spectrum Analysis
SDOF	Single-Degree-of-Freedom
SSI	Soil-structure Interaction

List of Figures

List of Tables

Appendix A

Task Description

NTNU
Faculty of Engineering Science and Technology
Institute of Civil and Transport Engineering

MASTER DEGREE THESIS

Spring 2014
for

Student: Madeleine Brandt

Earthquake Analysis of Subsea Structure on Caisson Foundation using 3D Finite Element Solution

BACKGROUND

One of the challenging problems in geotechnical design of caisson foundations of subsea structures is the evaluation of the soil-structure interaction during earthquakes. Depending on the soil conditions and properties, and also on site seismicity, the frequency-dependent stiffness of the soil response to caisson movements must sometimes be included in the analyses, for a realistic design. Common methods for evaluating the foundation stiffness is currently based on closed-form solutions for shallow embedded foundations or piles, lumped-parameter models or finite element modeling. The choice of method depends on the importance of the project. In some cases, the use of approximate solutions with frequency-independent stiffness is adequate. However, in critical projects, the frequency-dependence must also be considered.

TASK

The scope of the work for the Master Thesis is to evaluate soil-structure interaction using direct and multi-step methods. The thesis will evaluate dynamic modeling in Plaxis 3D with regards to seismic loading.

Task description

The study shall include:

- A description of Plaxis 3D and considerations for dynamic finite element modeling.
- Earthquake analysis of caisson foundation, using direct approach and a practical multi-step approach.
- Dynamic 3D finite element analyses in Plaxis 3D, and evaluation of different techniques for handling boundary conditions in Plaxis 3D for site response analyses.
- If the time permits, a brief study of non-linear behavior during earthquake loading.

General about content, work and presentation

The text for the master thesis is meant as a framework for the work of the candidate. Adjustments might be done as the work progresses. Tentative changes must be done in cooperation and agreement with the professor in charge at the Department.

In the evaluation thoroughness in the work will be emphasized, as will be documentation of independence in assessments and conclusions. Furthermore the presentation (report) should be well organized and edited; providing clear, precise and orderly descriptions without being unnecessary voluminous.

The report shall include:

- Standard report front page (from DAIM, http://daim.idi.ntnu.no/)
- Title page with abstract and keywords.(template on: http://www.ntnu.no/bat/skjemabank)
- Preface
- Summary and acknowledgement. The summary shall include the objectives of the work, explain how the work has been conducted, present the main results achieved and give the main conclusions of the work.
- The main text.
- Text of the Thesis (these pages) signed by professor in charge as Attachment 1.

The thesis can as an alternative be made as a scientific article for international publication, when this is agreed upon by the Professor in charge. Such a report will include the same points as given above, but where the main text includes both the scientific article and a process report.

Advice and guidelines for writing of the report is given in "Writing Reports" by Oivind Arntsen, and in the departments "Råd og retningslinjer for rapportskriving ved prosjekt og masteroppgave" (In Norwegian) located at http://www.ntnu.no/bat/studier/oppgaver.

Submission procedure
Procedures relating to the submission of the thesis are described in DAIM (http://daim.idi.ntnu.no/). Printing of the thesis is ordered through DAIM directly to Skipnes Printing delivering the printed paper to the department office 2-4 days later. The department will pay for 3 copies, of which the institute retains two copies. Additional copies must be paid for by the candidate / external partner.

On submission of the thesis the candidate shall submit a CD with the paper in digital form in pdf and Word version, the underlying material (such as data collection) in digital form (e.g. Excel). Students must submit the submission form (from DAIM) where both the Ark-Bibl in SBI and Public Services (Building Safety) of SB II has signed the form. The submission form including the appropriate signatures must be signed by the department office before the form is delivered Faculty Office.

Documentation collected during the work, with support from the Department, shall be handed in to the Department together with the report.

According to the current laws and regulations at NTNU, the report is the property of NTNU. The report and associated results can only be used following approval from NTNU (and external cooperation partner if applicable). The Department has the right to make use of the results from the work as if conducted by a Department employee, as long as other arrangements are not agreed upon beforehand.

Tentative agreement on external supervision, work outside NTNU, economic support etc.
Separate description is to be developed, if and when applicable. See
http://www.ntnu.no/bat/skjemabank for agreement forms.

Health, environment and safety (HSE) http://www.ntnu.edu/hse
NTNU emphasizes the safety for the individual employee and student. The individual safety shall be in the forefront and no one shall take unnecessary chances in carrying out the work. In particular, if the student is to participate in field work, visits, field courses, excursions etc. during the Master Thesis work, he/she shall make himself/herself familiar with "Fieldwork HSE Guidelines". The document is found on the NTNU HMS-pages at
http://www.ntnu.no/hms/retningslinjer/HMSR07E.pdf

The students do not have a full insurance coverage as a student at NTNU. If you as a student want the same insurance coverage as the employees at the university, you must take out individual travel and personal injury insurance.

Startup and submission deadlines
Startup and submission deadlines are according to information found in DAIM.

Professor in charge: Amir M. Kaynia and Gudmund R. Eiksund

Other supervisors: Steinar Nordal

Department of Civil and Transport Engineering, NTNU
Date: 07.06.2014

Gudmund Eiksund

Professor in charge (signature)

Appendix B

Wave Behavior at Boundaries

An initial harmonic wave (the incident wave) is propagating along the longitudinal axis of a constrained rod. It is propagating in "material 1" towards a boundary to "material 2". The wave energy of the incident wave will partially be transmitted from material 1 to material 2, and partially be reflected back to material 1. The wave length of the stress wave is $\lambda_1 = 2\pi/k1$ for material 1, and $\lambda_2 = 2\pi/k2$ for material 2. Thus, the stress solution for the incident, reflected and transmitted wave can be described by Eq. (B.1a), Eq. (B.1b) and Eq. (B.1c), respectively.

$$\sigma_i(x,t) = \sigma_i e^{i(\omega t - k_1 x)} \tag{B.1a}$$

$$\sigma_r(x,t) = \sigma_r e^{i(\omega t + k_1 x)} \tag{B.1b}$$

$$\sigma_t(x,t) = \sigma_t e^{i(\omega t - k_2 x)} \tag{B.1c}$$

The corresponding displacements are assumed to have the same harmonic form as the stress waves, and are thus described by:

$$u_i(x,t) = A_i e^{i(\omega t - k_1 x)} \tag{B.2a}$$
$$u_r(x,t) = A_r e^{i(\omega t + k_1 x)} \tag{B.2b}$$
$$u_t(x,t) = A_t e^{i(\omega t - k_2 x)} \tag{B.2c}$$

The stress waves can be related to the displacement waves via strain ($\delta u/\delta x$):

$$\sigma_i(x,t) = M_1 \frac{\delta u_i(x,t)}{\delta x} = -ik_1 M_1 A_i e^{i(\omega t - k_1 x)} \tag{B.3a}$$
$$\sigma_r(x,t) = M_1 \frac{\delta u_r(x,t)}{\delta x} = +ik_1 M_1 A_r e^{i(\omega t + k_1 x)} \tag{B.3b}$$
$$\sigma_t(x,t) = M_2 \frac{\delta u_t(x,t)}{\delta x} = -ik_2 M_2 A_t e^{i(\omega t - k_2 x)} \tag{B.3c}$$

Which shows that the stress amplitudes are given by:

$$\sigma_i = -ik_1 M_1 A_i \tag{B.4a}$$
$$\sigma_r = +ik_1 M_1 A_r \tag{B.4b}$$
$$\sigma_t = -ik_2 M_2 A_t \tag{B.4c}$$

Requirements of compatibility of displacements and stresses at the boundary, yields:

$$u_i(0,t) + u_r(0,t) = u_t(0,t) \tag{B.5a}$$
$$\Rightarrow A_i e^{i\omega t} + A_r e^{i\omega t} = A_t e^{i\omega t} \tag{B.5b}$$
$$\Rightarrow A_i + A_r = A_t \tag{B.5c}$$

for the displacements, and the following for stresses at the interface:

$$\sigma_i(0,t) + \sigma_r(0,t) = \sigma_t(0,t) \tag{B.6a}$$
$$\Rightarrow \sigma_i e^{i\omega t} + \sigma_r e^{i\omega t} = \sigma_t e^{i\omega t} \tag{B.6b}$$
$$\Rightarrow \sigma_i + \sigma_r = \sigma_t \tag{B.6c}$$

By introducing the relationship $kM = \omega\rho v$ from:

$$k = \frac{2\pi}{\lambda} = \frac{2\pi}{V_p(2\pi/\omega)} = \frac{\omega}{V_p}$$
$$M = V_p^2\rho$$
$$\Rightarrow kM = \omega V_p\rho$$

And combining Eq. (B.4), (B.5c) and (B.6c), the following equation is obtained:

$$-\rho_1 V_1 A_i + \rho_1 V_1 A_r = \rho_2 V_2 A_t = \rho_2 V_2 (A_i + A_r) \tag{B.7}$$

This equation can be rearranged with respect to the reflected displacement amplitude:

$$A_r = \frac{\rho_1 V_1 - \rho_2 V_2}{\rho_1 V_1 + \rho_2 V_2} A_i = \frac{1 - \rho_2 V_2/\rho_1 V_1}{1 + \rho_2 V_2/\rho_1 V_1} A_i = \frac{1-\alpha}{1+\alpha} A_i \tag{B.8}$$

And by combination with Eq. (B.5c), the transmitted displacement amplitude can be expressed by:

$$A_t = \frac{2\rho_1 V_1}{\rho_1 V_1 + \rho_2 V_2} A_i = \frac{2}{1 + \rho_2 V_2/\rho_1 V_1} A_i = \frac{2}{1+\alpha} A_i \tag{B.9}$$

α is defined as the *impedance ratio* between the materials.

By rearranging Eq. (B.4) with respect to the displacement amplitude, and substituting into Eq. (B.8) and (B.9), the stress amplitudes can be expressed as functions of impedance ratio:

$$\sigma_r = \frac{\alpha - 1}{1+\alpha}\sigma_i \tag{B.10a}$$
$$\sigma_t = \frac{2\alpha}{1+\alpha}\sigma_i \tag{B.10b}$$

Thus, it is clearly seen that the impedance ratio is the governing parameter for definition of the behavior at the interface between two materials. In the following sections, three special situations are discussed, being of great relevance to ground response problems.

B.0.1 Impedance Ratio = 1

With an impedance ratio equal to unity, it's clear that material 1 is the same as material 2. This implies that the rod is infinite. From Eq. (B.10), (B.8) and (B.9), the reflected and transmitted stresses and displacements are calculated:

$$\sigma_r = \frac{1-1}{1+1}\sigma_i = 0 \tag{B.11a}$$

$$\sigma_t = \frac{2}{1+1}\sigma_i = \sigma_i \tag{B.11b}$$

$$A_t = \frac{1-1}{1+1}A_i = 0 \tag{B.11c}$$

$$A_t = \frac{2}{1+1}A_i = A_i \tag{B.11d}$$

With an impedance ratio equal to unity, all the wave energy is thus transmitted, leaving no reflection of either stress nor displacement.

B.0.2 Impedance Ratio = 0

With an impedance ratio equal to zero, material 1 is infinitely much stiffer than material 2. This can be translated to the rod having a *free end*. From Eq. (B.10), (B.8) and (B.9), the reflected and transmitted stresses and displacements are calculated:

$$\sigma_r = \frac{1-0}{1+0}\sigma_i = \sigma_i \tag{B.12a}$$

$$\sigma_t = \frac{2\times 0}{1+0}\sigma_i = 0 \tag{B.12b}$$

$$A_t = \frac{1-0}{1+0}A_i = A_i \tag{B.12c}$$

$$A_t = \frac{2}{1+0}A_i = 2A_i \tag{B.12d}$$

B.0.3 Impedance Ratio = ∞

With an impedance ratio equal to infinity, material 2 is infinitely much stiffer than material 1. This can be translated to the rod having a *fixed end*. From Eq. (B.10), (B.8) and (B.9), the reflected and transmitted stresses and displacements are calculated:

$$\sigma_r = \frac{\infty - 1}{1 + \infty}\sigma_i = \sigma_i \tag{B.13a}$$

$$\sigma_t = \frac{2 \times \infty}{1 + \infty}\sigma_i = 2\sigma_i \tag{B.13b}$$

$$A_t = \frac{1 - \infty}{1 + \infty}A_i = A_i \tag{B.13c}$$

$$A_t = \frac{2}{1 + \infty}A_i = 0 \tag{B.13d}$$

Appendix C

Soil Profile

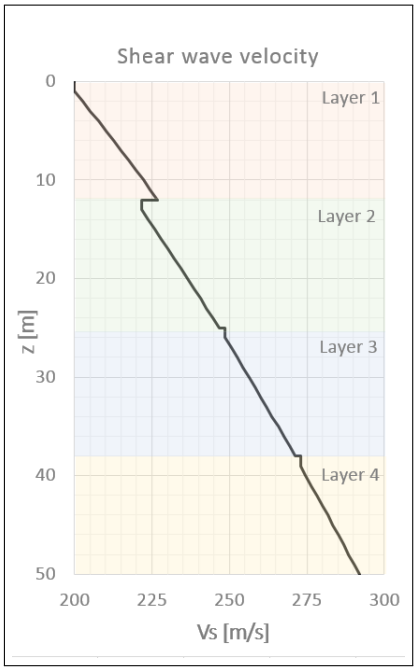

Figure C.1: *Shear wave velocity profile. Soil layers are indicated. The jump in velocity between Layer 1 and Layer 2 is caused by an increase of the unit weight.*

Appendix D

Calculation of Maximum Element Dimension

To be able to vary the element dimension, it was decided to divide the model into 4 layers. In Figure D.1, the calculated maximum element dimension is found for each layer by using average values for the layers. This is calculated by the following equation:

$$L_{max} = \frac{1}{8}\lambda_{min} = \frac{1}{8}V_s T_{min} = \frac{1}{8}\frac{V_s}{f_{max}} \tag{D.1}$$

MAXIMUM ELEMENT DIMENSION								
Layer	z0	Δz	γ	V_s	G_max	f_max	λ_min	L_max
-	m	m	kN/m3	m/s	Mpa	Hz	m	m
1	0	12	14,5	213,7	67,5	10	21,37	2,67
2	12	13	15,5	234,3	86,7	10	23,43	2,93
3	25	13	15,5	260,0	106,8	10	26,00	3,25
4	38	12	15,5	282,5	126,1	10	28,25	3,53

Figure D.1: *Calculation of maximum element dimension for a maximum frequency of 10 Hz.*

Appendix E

Calculation Phases in Plaxis 3D

Table E.1: *Calculation phases - Direct analysis and multi-step (Step 1)*

CALCULATION PHASES - DIRECT & MULTI-STEP (STEP 1) ANALYSIS				
Phase	Start from	Calculation type	Loading type	Comment
Initial phase	–	Plastic	Staged construction	Initial stress generation
Foundation	Initial phase	Plastic	Staged construction	Activate foundation geometry
Structure [1]	Foundation	Plastic	Staged construction	Activate structure geometry
Boundaries [2]	Structure	Plastic	Staged construction	Activate boundaries
Earthquake [3]	Boundaries	Dynamic	Staged construction	T=38 s (m=3800, n=1)

Table E.2: *Calculation phases - Multi-step analysis (Step 2)*

CALCULATION PHASES - MULTI-STEP ANALYSIS (STEP 2)				
Phase	Start from	Calculation type	Loading type	Comment
Initial phase	–	Plastic	Staged construction	Initial stress generation
Foundation	Initial phase	Plastic	Staged construction	Activate geometry
→ Load set 1	Foundation	Plastic	Staged construction	Horizontal point load, F_x=1 kN
→ Load set 2	Foundation	Plastic	Staged construction	Vertical point loads, F_z=1 kN

[1] Only in direct analysis.
[2] Both models: Activate prescribed displacements at bottom boundary with zero value. Model 1: Activate prescribed displacements at vertical boundaries.
[3] Total simulation time is set to 38 s. Total steps = 3800. Model 2: Viscous boundaries are defined.

Appendix F

Static Stiffness from Numerical Solution

The stiffness matrix from a FE solution is found by inverting the flexibility matrix. The flexibility matrix can be obtained by finding the displacements and rotations corresponding to given translational and moment loads. With basis in the following load-displacement relation, expressions for the flexibility coefficients can be found:

$$\begin{bmatrix} F_H \\ M_\theta \end{bmatrix} = \begin{bmatrix} K_{HH} & K_{H\theta} \\ K_{\theta H} & K_{\theta\theta} \end{bmatrix} \begin{bmatrix} u_H \\ u_\theta \end{bmatrix} \tag{F.1}$$

$$\begin{gathered} \mathbf{F} = \mathbf{K}\mathbf{u} \\ (\mathbf{K})^{-1}\mathbf{F} = (\mathbf{K})^{-1}\mathbf{K}\mathbf{u} \\ \mathbf{f}\mathbf{F}{=}\mathbf{u} \end{gathered}$$

$$\Downarrow$$

$$\begin{bmatrix} f_1 & f_2 \\ f_3 & f_4 \end{bmatrix} \begin{bmatrix} F_H \\ M_\theta \end{bmatrix} = \begin{bmatrix} u_H \\ u_\theta \end{bmatrix} \tag{F.2}$$

$$\Downarrow$$

$$f_1\ F_H + f_2\ M_\theta = u_H = u_{HH} + u_{H\theta}$$

$$f_3\ F_H + f_4\ M_\theta = u_\theta = u_{\theta H} + u_{\theta\theta}$$

$$\Downarrow$$

$$f_1 = u_{HH}/F_H$$

$$f_2 = u_{H\theta}/M_\theta$$

$$f_3 = u_{\theta H}/F_H$$

$$f_4 = u_{\theta\theta}/M_\theta$$

By inverting the flexibility matrix, the stiffness matrix is obtained:

$$\begin{bmatrix} K_{HH} & K_{H\theta} \\ K_{H\theta} & K_{\theta\theta} \end{bmatrix} = \frac{1}{f_1 f_4 - f_2 f_3} \begin{bmatrix} f_4 & -f_2 \\ -f_3 & f_1 \end{bmatrix} \tag{F.3}$$

Calculations performed in Excel

Flexibility coefficients related to horizontal load, F=1kN		
ux	0,00000045734 m	(uHH)
delta_ux	0,00000050744 m	
theta	-0,00000002114 rad	(uθH)
f1	0,00000045734 -	(uHH)
f3	-0,00000002114 -	(uθH)

Figure F.1: *Flexibility coefficients related to translation. Calculations performed in Excel.*

Flexibility coefficients related to rotational load, M=12kNm		
ux	-0,000000253 m	(uHθ)
deltaX	0,0000004109 m	
theta	0,000000017 rad	(uθθ)
f4	0,0000000014 -	uθθ/12kNm
f2	-0,000000021 -	uHθ/12kNm

Figure F.2: *Flexibility coefficients related to rotation. Calculations performed in Excel.*

CALCULATION OF STIFFNESS MATRIX

f1	0,00000045734	0,00000045734	>>	1/det= 4,8412E+15
f2	-0,00000002109	-0,00000002112		
f3	-0,00000002114	-0,00000002112		
f4	0,00000000143	0,00000000143		

KHH	6907095 kN/m	>>	KHH= 6907 MN/m
KHθ	102233739 kN/rad		KHθ= 102234 MN/rad
KθH	102233739 kNm/m		KθH= 102234 MNm/m
Kθθ	2214092131 kNm/rad		Kθθ= 2214092 MNm/rad

Figure F.3: *Stiffness coefficients from FE analyses. Calculations performed in Excel.*

Appendix G

Static Stiffness from Closed-form Solutions

G.1 Embedded Foundation on Homogeneous Stratum-over-Bedrock

The static stiffness coefficients for an embedded foundation on a homogeneous stratum-over-bedrock was calculated from Eq. 5.9 – 5.11, using G=G_0=59 MPa, ν=0,5, R=6 m, D=24 m and H=50 m.

$$K_{HH} = \frac{8 \times 59 \times 6}{2 - 0,5} \left(1 + \frac{1}{2} \times \frac{6}{50}\right) \left(1 + \frac{2}{3} \times \frac{24}{6}\right) \left(1 + \frac{5}{4} \times \frac{24}{50}\right)$$

$$\Downarrow$$

$$K_{HH} = 11722 \text{ MN/m}$$

$$K_{\theta\theta} = \frac{8 \times 59 \times 6^3}{3(1 - 0,5)} \left(1 + \frac{1}{6} \times \frac{6}{50}\right) \left(1 + 2 \times \frac{24}{6}\right) \left(1 + 0,7 \times \frac{24}{50}\right)$$

$$\Downarrow$$

$$K_{\theta\theta} = 826738 \text{ MNm/rad}$$

$$K_{H\theta} = 0,4 \times 11722 \times 24$$

$$\Downarrow$$

$$K_{H\theta} = 112528 \text{ MN}$$

However, for comparison with the finite element solution the stiffness terms must be translated from the bottom to the top of the foundation. A new set of equations, describing the stiffness at the top of the caisson, are obtained by translation of the center of stiffness the distance D (24 m) in the following manner:

$$K_{HH,T} = K_{HH} = \underline{11722 \text{ MN/m}}$$

$$K_{\theta\theta,T} = K_{\theta\theta} + 2DK_{\theta H} + D^2K_{HH} = \underline{12979765 \text{ MNm/rad}}$$

$$K_{H\theta,T} = DK_{HH} + K_{H\theta} = \underline{393848 \text{ MN}}$$

G.1.1 Obtaining the Expressions for Translation Terms

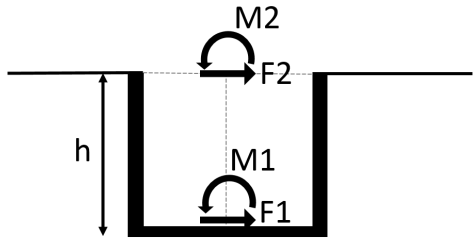

Figure G.1: *Translation of center of stiffness from bottom (1) to top (2) of foundation*

Original equation of motion:

$$\begin{bmatrix} F_1 \\ M_1 \end{bmatrix} = \begin{bmatrix} k_{xx} & k_{x\theta} \\ k_{\theta x} & k_{\theta\theta} \end{bmatrix} \begin{bmatrix} u_1 \\ \theta_1 \end{bmatrix} \tag{G.1}$$

which yields:

$$F_1 = k_{xx}u_1 + k_{x\theta}\theta_1 \tag{G.2}$$

$$M_1 = k_{\theta x}u_1 + k_{\theta\theta}\theta_1 \tag{G.3}$$

Must define the relations between F_1, M_1 and F_2, M_2:

$$F_1 = F_2 = k_{xx}u_1 + k_{x\theta}\theta_1 \tag{G.4}$$

$$M_1 = M_2 - F_2 h \tag{G.5}$$

$$\Downarrow$$

$$\begin{aligned} M_2 &= (k_{\theta x}u_1 + k_{\theta\theta}\theta_1) + (k_{xx}u_1 + k_{x\theta}\theta_1)h \\ &= (hk_{xx} + k_{\theta x})u_1 + (k_{\theta\theta} + hk_{x\theta})\theta_1 \end{aligned} \tag{G.6}$$

Must define relation between u_1, θ_1 and u_2 and θ_2:

$$\theta_1 = \theta_2 \tag{G.7}$$

$$u_1 = u_2 + \theta_1 h = u_2 + \theta_2 h \tag{G.8}$$

Insert for u_1 and θ_1 in equations for F_2 and M_2:

$$\begin{aligned} F_2 &= k_{xx}(u_2 + \theta_2 h) + k_{x\theta}\theta_2 \\ &= k_{xx}u_2 + (hk_{xx} + k_{x\theta})\theta_2 \end{aligned} \tag{G.9}$$

$$\begin{aligned} M_2 &= (hk_{xx} + k_{\theta x})(u_2 + \theta_2 h) + (k_{\theta\theta} + hk_{x\theta})\theta_2 \\ &= (hk_{xx} + k_{\theta x})u_2 + (h^2 k_{xx} + 2hk_{x\theta} + k_{\theta\theta})\theta_2 \end{aligned} \tag{G.10}$$

This yields the force-displacement relation at the top of the foundation:

$$\begin{bmatrix} F_2 \\ M_2 \end{bmatrix} = \begin{bmatrix} k_{xx} & hk_{xx} + k_{x\theta} \\ hk_{xx} + k_{\theta x} & h^2 k_{xx} + 2hk_{x\theta} + k_{\theta\theta} \end{bmatrix} \begin{bmatrix} u_2 \\ \theta_2 \end{bmatrix} \tag{G.11}$$

G.2 Shafts Socketed in Weaker Rock

The static stiffnesses for a short, rigid shaft socketed in weaker rock were obtained by inverting the flexibility matrix. The flexibility coefficients were found from Eq. 5.18 – 5.20 using G=G$_0$=59 MPa, ν=0,5, B=12 m, D=24 m and H=50 m.

$$f_{xx} = \left(\frac{0,4}{59 \times 12}\right)\left(\frac{2 \times 24}{6}\right)^{-1/3} = 0,000356 \text{ m/MN}$$

$$f_{x\theta} = f_{\theta x} = \left(\frac{0,3}{59 \times 12^2}\right)\left(\frac{2 \times 24}{12}\right)^{-7/8} = 0,0000105 \text{ –/MN}$$

$$f_{\theta\theta} = \left(\frac{0,8}{59 \times 6^3}\right)\left(\frac{2 \times 24}{6}\right)^{-5/3} = 0,00000079 \text{ rad/MNm}$$

By inverting the flexibility matrix, the stiffness matrix is obtained:

$$\begin{bmatrix} K_{HH,shaft} & K_{H\theta,shaft} \\ K_{\theta H,shaft} & K_{\theta\theta,shaft} \end{bmatrix} = \frac{1}{f_{xx}f_{\theta\theta} - f_{\theta x}f_{x\theta}} \begin{bmatrix} f_{\theta\theta} & -f_{x\theta} \\ -f_{\theta x} & f_{xx} \end{bmatrix} \tag{G.12}$$

$$K_{HH,shaft} = 4668 \text{ MN/m}$$

$$K_{\theta\theta,shaft} = 2133046 \text{ MNm/rad}$$

$$K_{H\theta,shaft} = K_{\theta H,shaft} = 62913 \text{ MN}$$

However, for comparison with the numerical solution the stiffness terms must be translated. In the solution for shafts in rock the defined positive direction of rotation is clockwise, in contrast to the counterclockwise definition of rotation in the numerical model. A slight translation of the

stiffnesses must therefore be made, resulting in the following coefficients:

$$K_{HH} = K_{HH,shaft} = \underline{4668 \text{ MN/m}}$$

$$K_{\theta\theta} = K_{\theta\theta,shaft} = \underline{2133046 \text{ MNm/rad}}$$

$$K_{H\theta} = K_{\theta H} = -K_{H\theta,shaft} = \underline{62913 \text{ MN}}$$

G.2.1 Obtaining the Expressions for Translation Terms

Original equation of motion:

$$\begin{bmatrix} F_1 \\ M_1 \end{bmatrix} = \begin{bmatrix} k_{xx} & k_{x\theta} \\ k_{\theta x} & k_{\theta\theta} \end{bmatrix} \begin{bmatrix} u_1 \\ \theta_1 \end{bmatrix}$$

which yields:

$$F_1 = k_{xx}u_1 + k_{x\theta}\theta_1$$

$$M_1 = k_{\theta x}u_1 + k_{\theta\theta}\theta_1$$

Must define the relations between F_1, M_1 and F_2, M_2:

$$F_2 = F_1 = k_{xx}u_1 + k_{x\theta}\theta_1$$

$$M_2 = -M_1 = -(k_{\theta x}u_1 + k_{\theta\theta}\theta_1)$$

Must define the relations between u_1, θ_1 and u_2 and θ_2:

$$\theta_1 = -\theta_2$$

$$u_1 = u_2$$

Insert for u_1 and θ_1 in equations for F_2 and M_2:

$$F_2 = k_{xx}u_2 - k_{x\theta}\theta_2$$

$$M_2 = -(k_{\theta x}u_2 - k_{\theta\theta}\theta_2) = -k_{\theta x}u_2 + k_{\theta\theta}\theta_2$$

For comparison with the numerical solution, the stiffness terms must be translated. In the solution for shafts in rock the defined positive direction of rotation is clockwise, in contrast to the counterclockwise definition of rotation in the numerical model. A slight translation of the stiffnesses must therefore be made:

$$K_{HH} = K_{HH,shaft}$$

$$K_{\theta\theta} = K_{\theta\theta,shaft}$$

$$K_{H\theta} = K_{\theta H} = -K_{H\theta,shaft} = -K_{\theta H,shaft}$$

Appendix H

Step 3 - Calculations

H.1 Equations of Motion

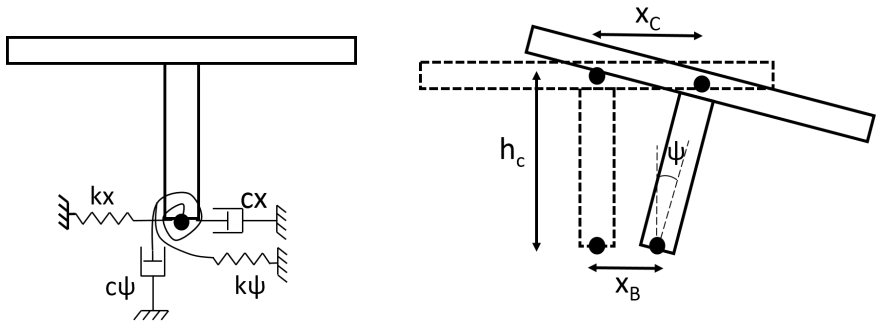

(a) Simplified geometry *(b) Dynamic deformation of system*

Figure H.1: *Simplified system for calculation of the structure's eigenfrequencies.*

To obtain the stiffness and mass matrices of the structure shown in Figure H.1a, some assumptions are necessary:

- The vertical and horizontal beams are assumed infinitely stiff (EI=∞)
- The mass of the lateral beam is zero

- The horizontal beam has a uniform distributed mass (M_{tot}=mL).

By dynamic force and moment equilibrium of the system (see Figure H.1b), and knowing the relation $x_C = x_B + \psi h_C$, the equations of motion can be found:

$$\sum F_X = M\ddot{x}_C + c_x\dot{x}_B + k_x x_B \tag{H.1}$$

$$\Downarrow$$

$$\sum F_X = M(\ddot{x}_B + \ddot{\psi}h_C) + c_x\dot{x}_B + k_x x_B \tag{H.2}$$

and

$$\sum M_B = Mh_C\ddot{x}_B + \left(\frac{ML^2}{12} + Mh_C^2\right)\ddot{\psi} + c_\psi\dot{\psi} + k_\psi\psi \tag{H.3}$$

Note that the inertial moment contribution from the horizontal beam, is as for the inertia around the midpoint of the rod in Figure H.2, though with an additional contribution because of translation of center of gravity.

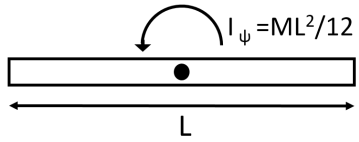

Figure H.2: *Moment of inertia around midpoint of a rod*

The dynamic equilibrium equations presented above can be systematized in the following matrices:

$$\begin{bmatrix} M & Mh_C \\ Mh_C & \frac{1}{12}ML^2 + Mh_C^2 \end{bmatrix}\begin{bmatrix}\ddot{x}_B \\ \ddot{\psi}\end{bmatrix} + \begin{bmatrix} c_x & 0 \\ 0 & c_\psi \end{bmatrix}\begin{bmatrix}\dot{x}_B \\ \dot{\psi}\end{bmatrix} + \begin{bmatrix} k_x & 0 \\ 0 & k_\psi \end{bmatrix}\begin{bmatrix}x_B \\ \psi\end{bmatrix} = \begin{bmatrix}0 \\ 0\end{bmatrix} \tag{H.4}$$

H.2 Calculation of Mass Matrix

With M=325 tons, h_C=7 m and L=30 m, the mass matrix is calculated as follows:

$$\begin{bmatrix} M & Mh_C \\ Mh_C & \frac{1}{12}ML^2 + Mh_C^2 \end{bmatrix} = \begin{bmatrix} 1 & 7\text{ m} \\ 7\text{ m} & 124\text{ kgm}^2 \end{bmatrix} 325 \cdot 10^3\text{ kg} \tag{H.5}$$

H.3 Stiffness Matrix

Table H.1: *Static stiffness coefficients obtained from numerical analyses and closed-form solutions*

STATIC STIFFNESS COEFFICIENTS				
Coefficient	Unit	FEM	Emb. found.	Shaft in rock
K_{HH}	MN/m	6 907	11 722	4 668
$K_{H\theta}$	MN/rad	102 234	393 848	62 913
$K_{\theta H}$	MNm/m	102 234	393 848	62 913
$K_{\theta\theta}$	MNm/rad	2 214 092	12 979 765	2 133 046

H.4 Eigenfrequency of MDOF System

The following derivations are well-known from dynamics and can be found in Chopra (1995, Ch. 10), amongst others.

The equations of motions for free vibration of an undamped MDOF system are given by:

$$\boldsymbol{M\ddot{u} + Ku = 0} \tag{H.6}$$

For a two DOF system, this can be written in matrix notation:

$$\begin{bmatrix} M_1 & M_2 \\ M_3 & M_4 \end{bmatrix} \begin{bmatrix} \ddot{u_1} \\ \ddot{u_2} \end{bmatrix} + \begin{bmatrix} K_1 & K_2 \\ K_4 & K_3 \end{bmatrix} \begin{bmatrix} u_1 \\ u_2 \end{bmatrix} = \begin{bmatrix} 0 \\ 0 \end{bmatrix} \tag{H.7}$$

The free vibration of this system can be described mathematically by Eq. (H.8):

$$\mathbf{u} = \mathbf{\Phi_n q_n(t)} \tag{H.8}$$

which in matrix form is written:

$$\begin{bmatrix} u_1 \\ u_2 \end{bmatrix} = \begin{bmatrix} \Phi_{11} & \Phi_{12} \\ \Phi_{21} & \Phi_{22} \end{bmatrix} \begin{bmatrix} q_1(t) \\ q_2(t) \end{bmatrix} \tag{H.9}$$

In the above equations, $\mathbf{q}_n\mathbf{(t)}$ describes the simple harmonic functions accounting for the time variation of the vibration:

$$q_n(t) = A_n \cos(\omega_n t) + B_n \sin(\omega_n t) \tag{H.10}$$

and $\mathbf{\Phi_n}$ describes the natural deflection shapes of the free vibration system. By double derivation of the harmonic function, it is apparent that the double derivative of $\mathbf{u}$ can be described by $(-\omega^2\mathbf{u})$.

By substituting for $\ddot{\mathbf{u}}$ in Eq. (H.6), the following equation is obtained:

$$[\mathbf{M}(-\omega^2)\mathbf{\Phi_n} + \mathbf{K}\mathbf{\Phi_n}]q_n(t) = \mathbf{0}$$

$$\Rightarrow (\mathbf{K} - \omega^2\mathbf{M})\mathbf{\Phi_n} = \mathbf{0} \tag{H.11}$$

For non-trivial solutions, the determinant of the expression in the parenthesis must be equal to zero:

$$det[\mathbf{K} - \omega^2\mathbf{M}] = 0 \tag{H.12}$$

Which yields the following expressions:

$$det\left|\begin{bmatrix} K_1 & K_2 \\ K_3 & K_4 \end{bmatrix} - \omega^2 \begin{bmatrix} M_1 & M_2 \\ M_3 & M_4 \end{bmatrix}\right| = \begin{bmatrix} 0 \\ 0 \end{bmatrix} \tag{H.13}$$

With the determinant of a two-by-two matrix being $det(A) = a_{11}a_{22} - a_{21}a_{12}$, we have:

$$(K_1 - \omega^2 M_1)(K_4 - \omega^2 M_4) - (K_2 - \omega^2 M_2)(K_3 - \omega^2 M_3) = 0$$

$$\Downarrow$$

$$\begin{aligned}(K_1K_4 - K_2K_3) - \omega^2(K_1M_4 + K_4M_1 - K_2M_3 - K_3M_2) \\ +(\omega^2)^2(M_4M_1 - M_3M_2) = 0\end{aligned} \tag{H.14}$$

By solution of the quadratic equation (H.14) with respect to ω^2, the following expressions for the two eigenfrequencies of the system are obtained:

$$\omega_{1,2} = \sqrt{\frac{-b \pm \sqrt{b^2 - 4ac}}{2a}} \tag{H.15}$$

where

$$a = 1$$

$$b = \frac{-(K_1M_4 + K_4M_1 - K_2M_3 - K_3M_2)}{M_4M_1 - M_3M_2}$$

$$c = \frac{K_1K_4 - K_2K_3}{M_4M_1 - M_3M_2}$$

H.4.1 Natural Periods

Corresponding natural periods are found from:

$$T_{1,2} = 2\pi/\omega_{1,2} \tag{H.16}$$

H.4.2 Natural Mode Shapes

The natural mode shapes of the superstructure can be found with basis in Eq. (H.11):

$$(\mathbf{K} - \omega^2\mathbf{M})\mathbf{\Phi_n} = \mathbf{0} \tag{H.17}$$

$$\Downarrow$$

$$(K_1 - \omega^2M_1)\Phi_{11} + (K_2 - \omega^2M_2)\Phi_{21} = 0 \tag{H.18a}$$

$$(K_3 - \omega^2M_3)\Phi_{12} + (K_4 - \omega^2M_4)\Phi_{22} = 0 \tag{H.18b}$$

Define $\mathbf{\Phi_{2n}}$=1 for both mode shapes:

$$\mathbf{\Phi_{1n}} = \frac{(K_2 - \omega^2 M_2)}{(K_1 - \omega^2 M_1)} \tag{H.19}$$

Insert for the two eigenfrequencies obtained from Eq. (H.15) to obtain the mode shape matrix:

$$\begin{bmatrix} \Phi_{11} & \Phi_{12} \\ \Phi_{21} & \Phi_{22} \end{bmatrix} = \begin{bmatrix} \Phi_{11} & \Phi_{12} \\ 1 & 1 \end{bmatrix} \tag{H.20}$$

H.5 Eigenfrequencies of the Superstructure

For a system without coupled horizontal-rotational terms, such as the superstructure system, the equations simplify:

$$\omega_{1,2} = \sqrt{\frac{-b \pm \sqrt{b^2 - 4ac}}{2a}} \tag{H.21}$$

where

$$a = 1$$

$$b = \frac{-(K_1 M_4 + K_4 M_1)}{M_4 M_1 - M_3 M_2}$$

$$c = \frac{K_1 K_4}{M_4 M_1 - M_3 M_2}$$

H.5.1 Calculations of Natural Frequencies and Periods in Excel

Calculations were performed in Excel using stiffness coefficients found from numerical and closed-form solutions.

CALCULATION OF EIGENFREQUENCY - FEM		
K1	6,9071E+09	N/m
K2	0	N/rad
K3	0	Nm/m
K4	2,2141E+12	Nm/rad
M1	3,250E+05	kg
M2	2,275E+06	kgm
M3	2,275E+06	kgm
M4	4,030E+07	kgm2
a	1	-
b	-1,2597E+05	rad/s^2
c	1,9305E+09	rad/s^4
w1^2	1,081E+05	rad/s^2
w2^2	1,786E+04	rad/s^2
w1	329	rad/s
w2	134	rad/s
T1	**0,019**	**s**
T2	**0,047**	**s**

(a) Numerical solution

CALCULATION OF EIGENFREQUENCY - SHAFT		
K1	4,6680E+09	N/m
K2	0	N/rad
K3	0	Nm/m
K4	2,1330E+12	Nm/rad
M1	3,250E+05	kg
M2	2,275E+06	kgm
M3	2,275E+06	kgm
M4	4,030E+07	kgm2
a	1	-
b	-1,1126E+05	rad/s^2
c	1,2569E+09	rad/s^4
w1^2	9,850E+04	rad/s^2
w2^2	1,276E+04	rad/s^2
w1	314	rad/s
w2	113	rad/s
T1	**0,020**	**s**
T2	**0,056**	**s**

(b) "Shaft in rock" solution

CALCULATION OF EIGENFREQUENCY - EMBEDDED		
K1	1,1722E+04	N/m
K2	0	N/rad
K3	0	Nm/m
K4	1,2980E+13	Nm/rad
M1	3,250E+05	kg
M2	2,275E+06	kgm
M3	2,275E+06	kgm
M4	4,030E+07	kgm2
a	1	-
b	-5,3250E+05	rad/s^2
c	1,9206E+04	rad/s^4
w1^2	5,325E+05	rad/s^2
w2^2	3,607E-02	rad/s^2
w1	730	rad/s
w2	0,190	rad/s
T1	**0,009**	**s**
T2	**33,084**	**s**

(c) "Embedded foundation" solution

Figure H.3: *Calculation of natural frequencies and natural periods in Excel*

H.5.2 Natural Mode Shapes

Natural mode shapes were calculated from the results of the numerical analysis.

MODE SHAPE 1		MODE SHAPE 2	
ϕ_11	-0,11	ϕ_12	0,027
ϕ_21	1	ϕ_22	1

Figure H.4: *Mode shapes of superstructure. Calculations performed in Excel.*

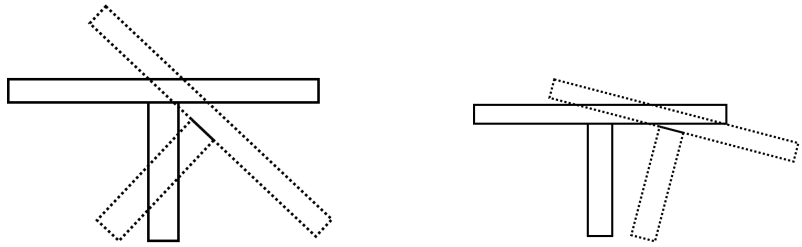

(a) *Eigenmode 1* ***(b)*** *Load set 2*

Figure H.5: *The eigenmodes of the superstructure*

Appendix I

Amplification of Harmonic Signals in Plaxis 3D

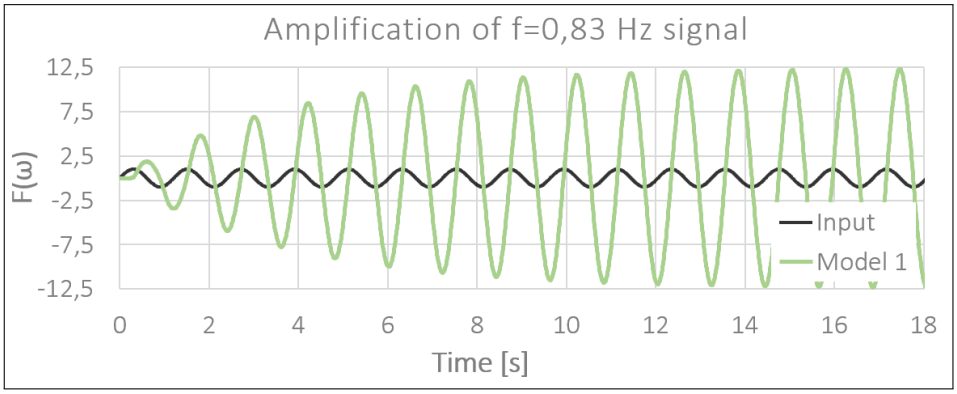

Figure I.1: *Amplification of signal corresponding to soil deposit's 1st eigenfrequency*

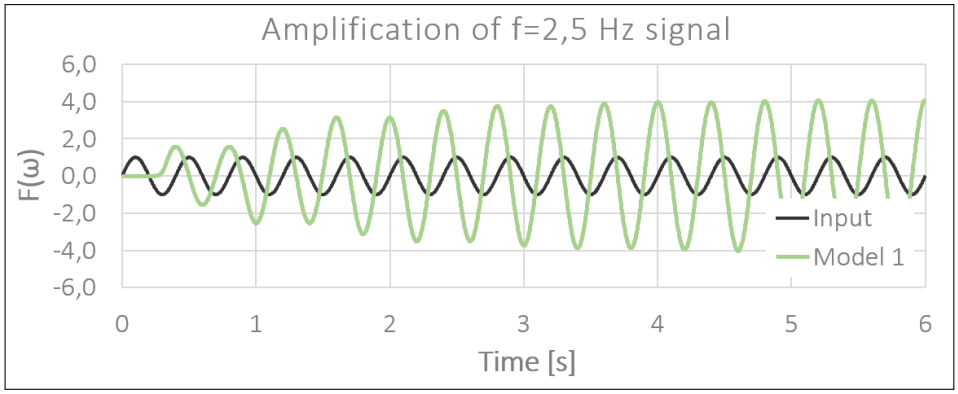

Figure I.2: *Amplification of signal corresponding to the soil deposit's second eigenfrequency*

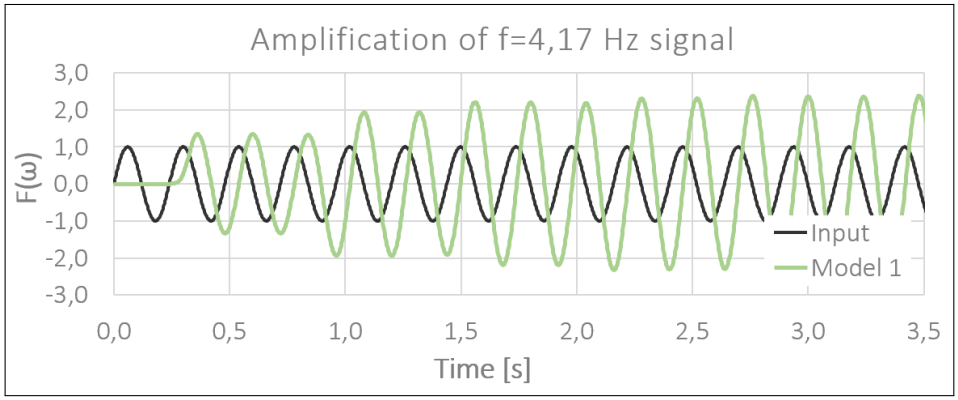

Figure I.3: *Amplification of signal corresponding to the soil deposit's third eigenfrequency*

Appendix J

Results from EERA

J.1 Results from EERA - Adjusted Soil Profile

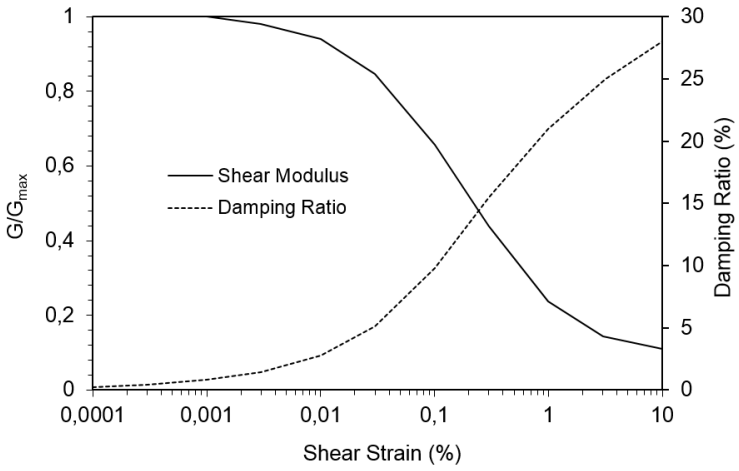

Figure J.1: *Damping and shear modulus reduction curves used in EERA - Adjusted soil profile*

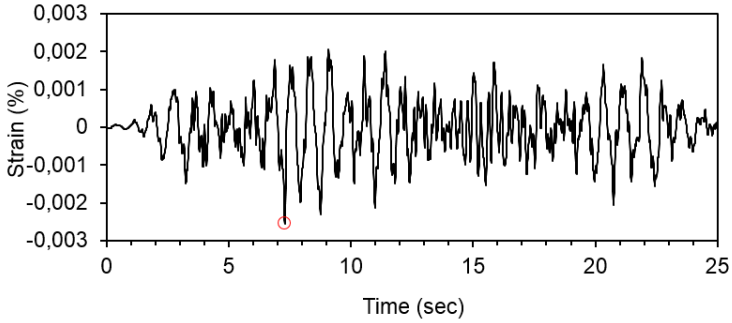

Figure J.2: *Strain time history in EERA*

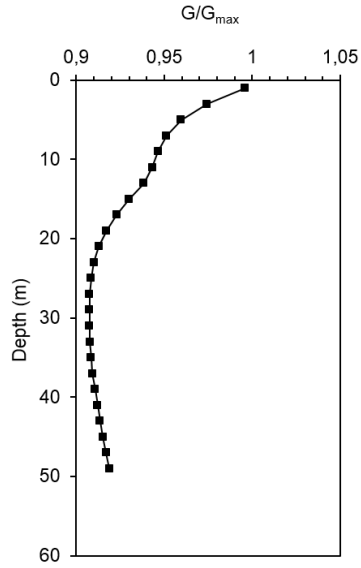

Figure J.3: *Shear modulus ratio over depth of soil layer - Adjusted soil profile*

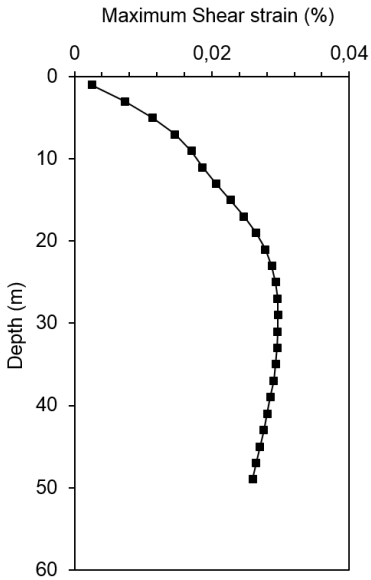

Figure J.4: *Maximum shear strain over depth of soil layer - Adjusted soil profile*

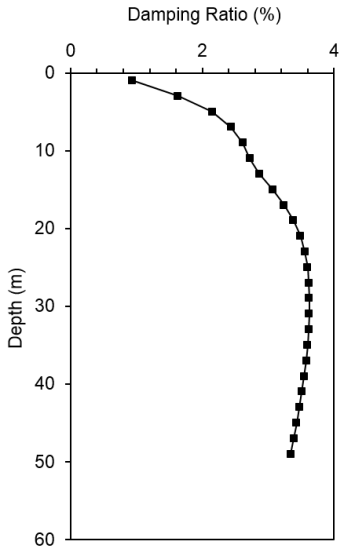

Figure J.5: *Effective damping ratio over depth of soil layer - Adjusted soil profile*

J.2 Results from EERA - Original Soil Profile

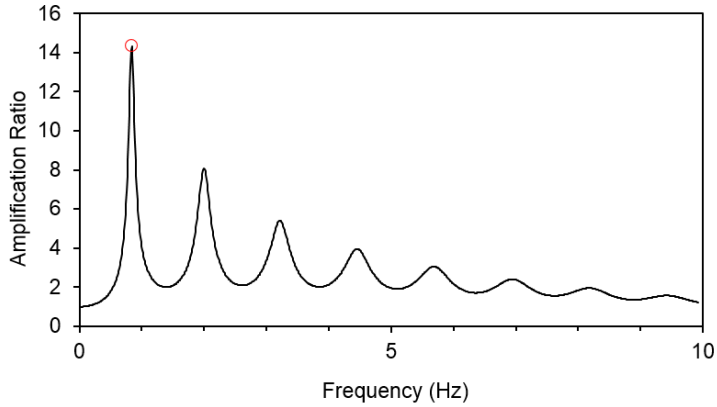

Figure J.6: *Soil amplification function - Original soil profile*

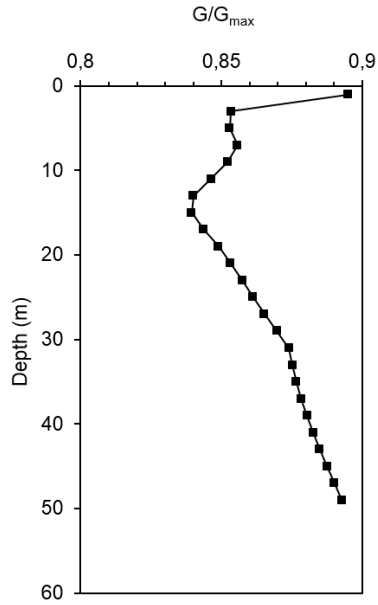

Figure J.7: *Shear modulus ratio over depth of soil layer - Original soil profile*

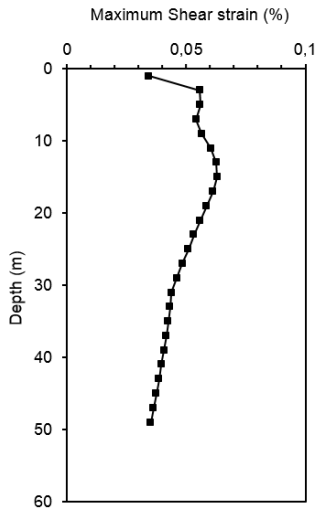

Figure J.8: *Maximum shear strain over depth of soil layer - Original soil profile*

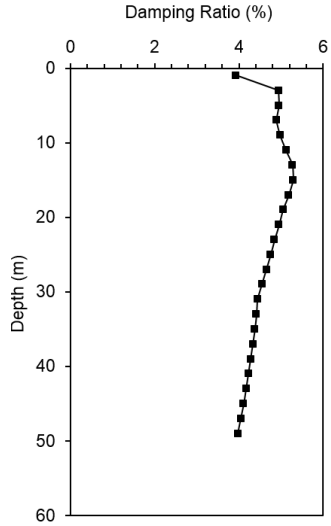

Figure J.9: *Effective damping ratio over depth of soil layer - Original soil profile*

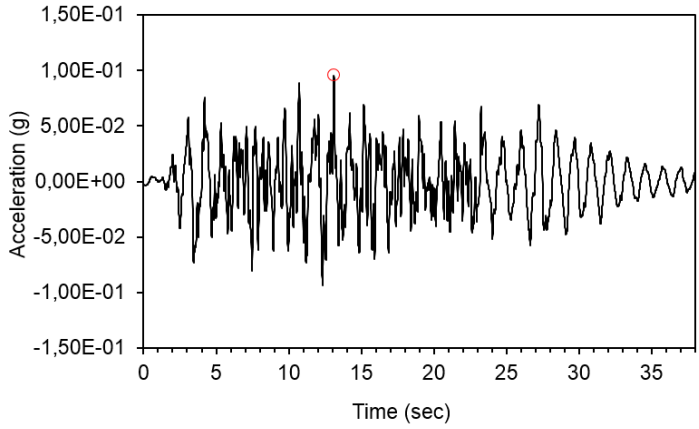

Figure J.10: *Acceleration time history - Original soil profile*

Appendix K

Matlab® Script

```
%% Elastisk respons-spektrum
% Beregner og plotter respons-spektrum til akselerasjons-tidserier
% sammen med tilsvarende EC8 spektrum
%%
clc
clear all
close all

load acc_responseX.txt

t = acc_responseX(:,1) ;  % tidsintervall
ag = acc_responseX(:,2) ;  % grunn-akselerasjon


%% Newmarks lineare metode (gamma=1/2, beta=1/6)

gamma=0.5; beta=1/6; % Newmarks lineare metode
zet=0.05; % dempningsgrad
Tend=10; % hoeyeste periode

dt=t(2)-t(1);

u=zeros(size(ag));
v=u;
```

```
ac=u;
T(1,1)=0;

for j=1:round(Tend/dt)
    omega(j,1)=2*pi*(1/T(j,1));
    m=1;
    k=(omega(j))^2*m;
    c=2*zet*omega(j)*m;
    keff=k+(gamma/(beta*dt))*c+(1/(beta*dt^2))*m;
    a=(1/(beta*dt))*m+(gamma/beta)*c;
    b=(1/(2*beta))*m+dt*((gamma/(2*beta))-1)*c;
for i=1:length(u)-1
     dR=-(ag(i+1)-ag(i))+a*v(i,1)+b*ac(i,1);
     du=dR/keff;
     dv=(gamma/beta)*du/dt-(gamma/beta)*v(i,1)+(1-(gamma/(2*beta)))*dt*ac(i
         ,1);
     dac=(1/beta)*(du-dt*v(i,1))/(dt)^2-(1/(2*beta))*ac(i,1);
     u(i+1,1)=u(i,1)+du;
     v(i+1,1)=v(i,1)+dv;
     ac(i+1,1)=ac(i,1)+dac;
end
%
Sd(j,1)=max(abs(u));
%Sv(j,1)=max(abs(v));
%Sa(j,1)=max(abs(ac));
%PSv(j,1)=Sd(j)*omega(j);
PSa(j,1)=Sd(j,1)*(omega(j))^2;
T(j+1,1)=T(j)+dt;
end
ag(end)=[];
T(end)=[];
Sd(2,1)=0; PSv(1:2,1)=0; PSa(1:3,1)=max(abs(ag));

%Skriver ut verdiene av T til angitt fil
FileOut = ['C:\Users\madelebr\Copy\Masteroppgave\Matlab\rsa\5rsaT.txt'];
[fout,errmsg]=fopen(FileOut,'wt');

if(fout<0);
    sprintf('Filen er lukket');
    sprintf('Error. %s',errmsg);
end
```

```
65
66  if(fout>=0);
67      fprintf(fout,sprintf('%f \n', T));
68  end
69
70  %Skriver ut korresponderende verdier av PSa til angitt fil
71  FileOut1 = ['C:\Users\madelebr\Copy\Masteroppgave\Matlab\rsa\5rsaPSA.txt'];
72  [fout,errmsg]=fopen(FileOut1,'wt');
73
74  if(fout<0);
75      sprintf('Filen er lukket');
76      sprintf('Error. %s',errmsg);
77  end
78
79  if(fout>=0);
80      fprintf(fout,sprintf('%f \n',PSa));
81  end
```